National Technical University of Athens
School of Chemical Engineering
Department of Analysis, Design, and Development of Processes and Systems

Diploma Thesis

Chemical speciation and source apportionment of the atmospheric aerosol in Athens, Greece

Katsikari Stavroula
Head Professor: Kavousanakis Mihalis
Supervisor: Diapouli Evangelia

February 2023

Acknowledgments

This diploma thesis on the title "Chemical speciation and source apportionment of the atmospheric aerosol in Athens, Greece" was carried out in the Environmental Radioactivity Laboratory, Institute of Nuclear & Radiological Sciences & Technology, Energy & Safety N.C.S.R. "DEMOKRITOS".

At the end of this work, I would particularly like to thank the Head Professor, Prof. Kavousanaki Mihali, that throughout this time was beside me by providing his undivided assistance, knowledge and time spent in solving any of the problems that during this thesis.

In addition, I would like to thank Dr. Diapouli Evangelia from the National Centre of Scientific Research "Demokritos" who has provided me this opportunity to work in the field of experimental air quality research. Her contribution to the preparation of the diploma thesis, from the experimental part (proper handling of scientific instruments), to the processing of experimental measurements, analysis and evaluation of results, as well as the resolution of arising issues was of paramount importance and proved valuable with a direct impact on work.

In addition, I would like to refer to the staff of the NCSR "Demokritos" laboratory and to thank them for the support and help they have given me, and especially PhD Student Papagiannis Stefanos a member of the Demokritos who, with his experience in this field, has helped in the chemical composition analysis of the aerosol.

Of course all the professors of the School of Chemical Engineering of had an important role in this final step of my undergraduate studies; their way of teaching led me to show even greater zeal for the completion of this work, but also to maintain a steady and upward course throughout my curriculum.

Finally, I would like to thank my family and people close to me who have been beside me constantly and I owe them great gratitude.

Abstract

Athens is a European city with high burden by particle pollution. For addressing health concerns and undertaking mitigation measures, the aerosol composition and sources should be identified. In this study, samples $PM_{2.5}$ were collected at two sites, a traffic site (Aristotelous street, city center) and an urban background site (station at NCSR "Demokritos"), during 2019-2020 and analyzed using thermal-optical and XRF analysis. The results showed that the mean $PM_{2.5}$ concentration was higher at the traffic site compared to the urban background site. Carbonaceous matter (organic and elemental) was the most abundant species in the total PM mass. The differences between the chemical profiles of the major anthropogenic and natural particulate matter sources in the two areas, with different levels of urbanization and traffic density within the same urban agglomeration, was obtained by Positive Matrix Factorization analysis. For both sites, seven sources were identified (Mineral dust, Traffic exhaust emissions, Traffic non-exhaust emissions, Biomass burning, Secondary sulphate and organics, Heavy oil combustion and Sea salt). The variation between the source profiles for each site was observed through comparison with the final solution, which corresponds to a PMF analysis of the combined database obtained by both urban background and traffic site. Traffic exhaust emissions was the major contributing source at the traffic site (46.9%), while the major contributor at the urban background site was secondary sulphate and organics (49.3%). Biomass burning influenced both sites, especially during the cold period, mainly due to residential heating. The peaks of daily soil dust contribution were used to identify potential African dust events at each site, using 5-day backward air mass trajectories by the Hybrid Single Particle Lagrangian Integrated Trajectory (HYSPLIT) Model.

Περίληψη

Η Αθήνα χαρακτηρίζεται ως μία Ευρωπαϊκή χώρα με υψηλά επίπεδα σωματιδιακής ρύπανσης, με συνέπεια την πρόκληση σοβαρών προβλημάτων τόσο στον άνθρωπο όσο και στο περιβάλλον. Για την ανάπτυξη αποτελεσματικών μέτρων ελέγχου για τον έλεγχο της σωματιδιακής ρύπανσης, είναι απαραίτητος ο προσδιορισμός της σύστασης του αερολύματος και η εύρεση των κύριων πηγών εκπομπής του. Για τον ανωτέρω σκοπό, στην παρούσα διπλωματική εργασία, λήφθηκαν 24ωρα δείγματα ΑΣ$_{2.5}$ (αιωρούμενων σωματιδίων διαμέτρου έως και 2.5 um) από δύο σταθμούς στην Αθήνα. Ο ένας σταθμός αφορά στο αστικό υπόβαθρο και στεγάζεται στις εγκαταστάσεις του Εθνικού Κέντρου Έρευνας Φυσικών Επιστημών "Δημόκριτος", ενώ ο δεύτερος αναφέρεται σε σταθμό κυκλοφορίας και βρίσκεται στο κέντρο της Αθήνας επί της οδού Αριστοτέλους. Χρησιμοποιήθηκε θερμο-οπτική ανάλυση και φθορισμός ακτινών Χ, ώστε να καταγραφεί η χημική σύσταση των σωματιδίων. Τα αποτελέσματα έδειξαν πως στο σταθμό υψηλής κυκλοφορίας η συγκέντρωση αιωρούμενων σωματιδίων ήταν πολύ υψηλότερη συγκριτικά με εκείνη που βρέθηκε για τον σταθμό υποβάθρου. Επιπλέον, βρέθηκε πως ο οργανικός και στοιχειακός άνθρακας είναι τα συστατικά με την υψηλότερη συνεισφορά στην συνολική μάζα των αιωρούμενων σωματιδίων. Τα δεδομένα χημικής σύστασης χρησιμοποιήθηκαν περαιτέρω για την εύρεση των κύριων πηγών εκπομπής σωματιδιακών ρύπων, με εφαρμογή μεθοδολογίας επιμερισμού πηγών, και συγκεκριμένα με την μέθοδο θετικής παραγοντοποίησης μητρών (Positive Matrix Factorization analysis, PMF). Η μέθοδος εφαρμόστηκε για τρείς περιπτώσεις, τα δεδομένα από τον σταθμό αστικού υποβάθρου και από τον σταθμό κυκλοφορίας ξεχωριστά, και από την συνολική βάση δεδομένων και από τους δύο σταθμούς. Η βάση δεδομένων που αντιστοιχεί στην τελική λύση επιμερισμού πηγών αφορά στην κοινή βάση και των δύο σταθμών. Οι δύο επιμέρους λύσεις για κάθε σταθμό ξεχωριστά αξιοποιήθηκαν για την μελέτη της διαφοροποίησης των χημικών προφίλ των πηγών, ανάλογα με τα χαρακτηριστικά του κάθε σταθμού μέτρησης. Τα αποτελέσματα της ανάλυσης οδήγησαν στην εύρεση επτά πηγών εκπομπής, που περιλαμβάνουν την σκόνη του εδάφους, το αλάτι της θάλασσας, την καύση βιομάζας, την καύση βαρέων κλασμάτων πετρελαίου, τις εκπομπές των αυτοκινήτων, τον σχηματισμό δευτερογενών θειικών και οργανικών ενώσεων και τις εκπομπές που προκαλούνται λόγω της κίνησης των οχημάτων. Οι εκπομπές των αυτοκινήτων είναι ο κύριος παράγοντας που συνεισφέρει στη μάζα των σωματιδίων όσον αφορά στον σταθμό κυκλοφορίας (46.9%), ενώ ο σχηματισμός δευτερογενών θειικών και οργανικών ενώσεων αποτελεί την κύρια πηγή συνεισφοράς στον σταθμό αστικού υποβάθρου (49.3%). Η καύση βιομάζας συνεισφέρει σημαντικά και στις δύο περιοχές και παρουσιάζει ιδιαίτερη αύξηση τους χειμερινούς μήνες, πιθανόν λόγω της αυξημένης χρήσης ξύλου ως καύσιμο στην οικιακή θέρμανση. Παρατηρώντας την χρονοσειρά της συγκέντρωσης της πηγής της σκόνης εδάφους, διαπιστώνονται ορισμένα μέγιστα, τα οποία στη συνέχεια χρησιμοποιούνται για τυχόν ανίχνευση φαινομένων μεταφοράς σκόνης από χώρες της Αφρικής (Sahara dust events).

Contents

1. Atmosphere

1.1. The layers of atmosphere

The atmosphere includes five major and many secondary layers, based on its temperature. Troposphere, stratosphere, mesosphere, thermosphere and exosphere are the primary layers of Earth's atmosphere. In addition, atmosphere is divided into two regions, upper and lower. The lower atmosphere is usually considered to extend to the top of the stratosphere.

The Earth's lowest layer extends from the Earth's surface up to the tropopause. Its altitude is approximately 12 km and it depends on latitude and time of the year. In detail, its height is lower at Earth's poles and higher at the equator. The top of the troposphere is called the tropopause and its lowest part is called the boundary layer. In this lowest part, the air motions are defined by the properties of the Earth's surface. Since the wind blows over the surface and thermals rise from the land, turbulence is generated. So, this turbulence lead to redistribution of temperature, moisture, pollutants and other constituents within the boundary layer. Earth's troposphere is characterized by decreasing temperature with altitude, by about 6.5°C per kilometer (*NIWA Taihoro Nukurangi*). The closer you go to the Earth's surface, the temperature is getting higher because of the energy transfer that is taking place. This affects the pressure, which decreases with height. So a parcel of air is cooler in higher altitude. Most of weather phenomena take place in the troposphere and most of the clouds which are formed by weather are placed here. The whole region of troposphere and the transition region between the troposphere and stratosphere are characterized by rapid vertical mixing.

1.2. Air pollution

The term of "air pollution" is referred to the situation in which concentration of either noxious or benign substances are significantly higher in comparison with the normal ambient levels, due mainly to anthropogenic activities. This condition affects people, animals, vegetation and materials with undesirable consequences. Air pollution is distinguished into two major categories. The first one is related to high concentrations of sulphur compounds and particles. The main sources of emissions are combustion of coal and fuels which contain sulphur, so this type of air pollution can be observed in cities with cold climates. The second type of air pollution was recorded by the widespread use of gasoline as a motor fuel. Although it is called "photochemical smog", this type of pollution is not smog, but contains a number of compounds of complex chemistry that exist when an atmosphere filled with organic gases and oxides of nitrogen are being radiated by the sunlight. These procedures occur in regions with high temperature and bright sunlight. Nitric oxide and organic compounds are the primary products of these processes. But these compounds are rapidly converted to secondary pollutants, such as ozone.

1.3. Atmospheric residence times

Each substance which is emitted into the atmosphere will be removed either close to their point of emission or in a large distance from it. Atmospheric residence time refers to the average lifetime of a representative molecule of the substance, before it is totally removed. Dry deposition and wet deposition are two major removal processes. Dry deposition is the process by which atmospheric trace gases and particulate matter are directly transferred to the Earth's surface. On the other hand, wet deposition is referred as the procedure in which atmospheric gases and particles mix with suspended water and fall to the Earth's surface in aqueous form – such as rain, snow or fog. In the lower atmosphere, residence time of particles does not usually exceed several weeks. The main removal mechanisms take place close to the surface – such as dry deposition. For altitudes above about 100 meters, the dominant removal mechanism is the precipitation scavenging (*World Meteorological Organization*).

2. Atmospheric aerosol

2.1. General

Particulate matter consists one of the complex pollutant categories and is characterized by its size, chemical composition and atmospheric concentration. Aerosol includes any kind of scattered liquid or solid substances that exists in atmosphere under normal conditions. Its size belongs on microscopic or submicroscopic scale, but particulate matter is larger than molecular dimensions. Because of its complexity, complete research of atmospheric particle requires determining its concentration, size distribution, chemical composition, phase and morphology. Several other terms are used for the classification of particulate matter based on its size and phase. For example, dust refers to the solid particulates that are formed by processes of crushing, grinding and blasting. Fume is defined as the solid particles who are generated by condensation from the vapor state. Liquid particles are usually called mist or fog. The terms of smog and soot are used for substances which are produced by incomplete combustion of carbonaceous materials. Particles' size, number and chemical composition depend on several mechanisms which take place in the atmosphere, before they are removed. Airborne particles come from both direct emissions and emissions of certain gases – which either condense as particles directly or undergo chemical transformation processes to a species which eventually condenses as a particle.

2.2. Sizes of atmospheric particles

Atmospheric particles are divided into two main categories based on their size. The first group consists of particles with diameter less than 2.5 μm ($PM_{2.5}$) and are called "fine", whereas those with diameter greater than 2.5 μm are referred as "coarse". The distinction between fine and coarse mode is a principal process because of differentiation of their origin, transformation procedures, removal mechanisms, chemical composition, optical properties and deposition patterns in the respiratory tract. It has been considered that coarse mode tends to quickly precipitate, so the consequences are observed in regions near to its emission sources; in addition, this size fraction may be retained in the upper respiratory tract and, thus, does not impact the lower respiratory system. In contrast, fine particles have greater atmospheric residence time and cover long distances. For example, a strong dust storm travels from the desert Gobi in East Asia to the east regions and after a week affects the measurements of $PM_{2.5}$ concentration in west coast of USA (*Masters et al., 2018*). Fine particles are more harmful to human's health, because this small size fraction enters the lower respiratory system.

The coarse mode is mainly formed by mechanical processes or from Earth's crust, sea salt sprays, pollen, dust from roads. The super-coarse particles with diameter bigger than 10 μm may affect the environment. Fine particles are divided into nuclei and accumulation mode. The first one has diameter about 0.005 to 0.1 μm and is originated from condensation of hot vapors during combustion processes and from the nucleation of atmospheric species to form other particles. The nuclei mode does not contribute significantly to the total mass of airborne particles, due to its extremely small size; it is dominant, though, in terms of particle number concentration. The main loss mechanism for this mode is the coagulation with larger particles. Particles in the accumulation mode have diameter about 0.1 to 2.5 μm and are mainly formed from the coagulation of particles in the nuclei mode and from the condensation of vapors

onto existing particles. Accumulation mode constitutes a considerable part of the aerosol mass, and displays the highest atmospheric residence time because the removal processes are inefficient in this system.

2.3. Chemical composition

The chemical composition of tropospheric aerosol at a particulate site depends on the time of the year, location and distance from the emission sources. Because of the fact that fine particles are mainly produced by combustion and chemical reaction, an important fraction of tropospheric particles is man-made in origin. According to a study which was conducted in the Eastern Mediterranean, natural sources, such as sea salt and dust, accounts only about 40% of the fine mode, whereas coarse mode's origin is mainly natural (*Koulouri et al., 2008*). *Figure 1* shows that elements of a major anthropogenic origin, such as Ni, V and Cr are found both in coarse and fine fraction. In addition, coarse mode is related to natural sources, due to the high contribution of elements, such as Na, Cl, Ti (*Koçak et al., 2007*).
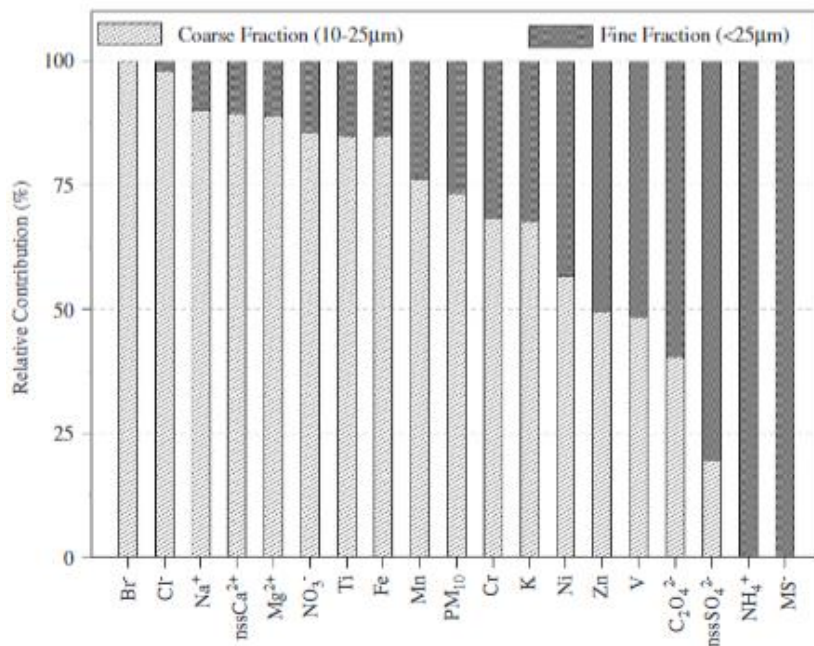
Figure 1: Relative contributions of PM_{10} and aerosol species in the fine and coarse fraction (Koçak et al., 2007).

The main chemical components of tropospheric aerosol are sulphate, ammonium, nitrate, sodium, chloride, trace elements, carbonaceous materials, crustal elements and water. Carbonaceous materials are divided into organic and elemental carbon. In the last decades, the levels of aerosol which is formed by anthropogenic activities, have dramatically increased. This phenomenon has influenced human health, visibility, acid deposition and Earth's radiation balance. In recent years, great progress has been made with respect to air quality management, through the adoption of stricter air pollution mitigation strategies and the development of cleaner technologies, especially in Europe and U.S.A.; nonetheless, particulate pollution remains a major environmental problem, with significant implications

for public health and climate change. *Figure 2* shows the typical mass proportions of chemical components in two different sites (*Pöschl et al., 2005*).

.
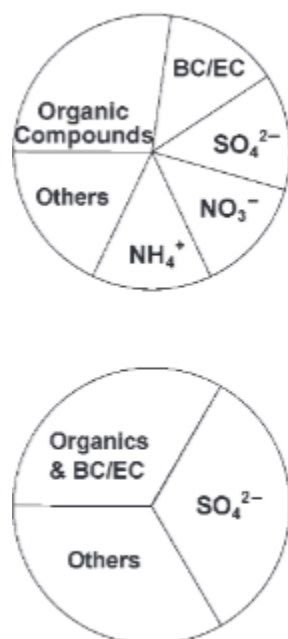
Figure 2: Typical mass proportions of chemical components in urban area (top) and high alpine air region (bottom) (Pöschl et al., 2005).

.

2.4. Sources of atmospheric aerosol

Particulate matter can be natural or anthropogenic based on their origin. This variety produce particulates with very different size, chemical composition, and reactivity. In urban and industrial areas, anthropogenic aerosols are mainly emitted by traffic, industrial activities, building activities and emissions from households. In rural regions, the basic anthropogenic sources are both biomass burning and emissions from farming activities. In addition, natural particles can be emitted by seas and oceans, deserts, soil, volcanoes, vegetation, wildfires, and lightning.

2.4.1. Anthropogenic sources

2.4.1.1. Traffic

Primary and secondary anthropogenic particulate matter are released to the atmosphere by road traffic. Depending on their formation mechanisms, their size and chemical composition vary. The emissions of traffic are divided into two main categories. The first one involves the gases and ultrafine primary carbon particles which are directly released through exhaust pipes of road vehicles. *Figure 3* shows that engine exhaust particles typically consisting of sulphuric acid and particles, hydrocarbon – sulphate particles and solid carbonaceous particles with adsorbed hydrocarbon – sulphate layer (*Kittelson et al., 1998*).
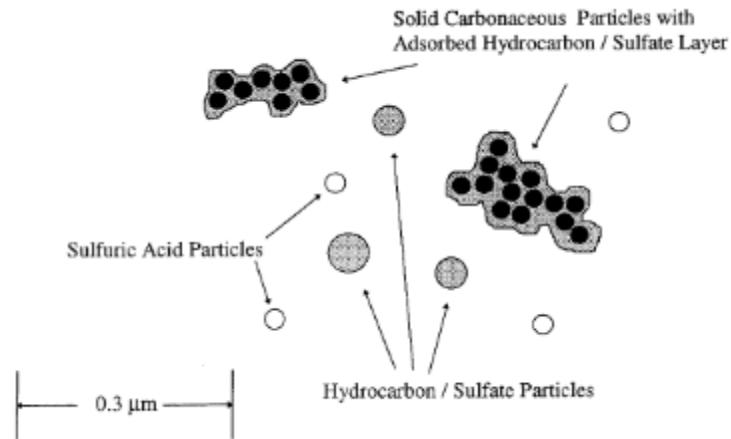
Figure 3: Typical composition and structure of engine exhaust particles (Kittelson et al., 1998).

The second one includes all the non-exhaust emissions from road vehicles. This involves particles from brake wear, tire wear, road surface abrasion and resuspension in the wake of traffic. For example, particles with traces of elements such as strodium, copper, molybdenum, barium, chromium, and manganese are emitted due to brake and tire wear. Traffic is a main source of trace elements and nitrogen oxides, mainly in urban areas. Small concentrations of metals, such as copper, zinc and cadmium are released by road vehicles, whereas platinum, palladium and rhodium come from the vehicle catalytic converters. Furthermore, motors emit elements, such as potassium, bromine, and chlorine. It has been observed that concentrations and sources of lead have been changed due to the ban of leaded gasoline worldwide. The diesel-powered vehicles PM emissions are 10-100 times higher in comparison with those from gasoline-powered vehicles. These aerosols contain toxic chemicals, such as PAHs, which is harmful for people's health (*Calvo et al. 2013*).

The emissions of railway, air and maritime traffic influence the atmospheric aerosol, too. According to a study, iron particles emissions of railway lines contribute 67% to the railway related PM_{10} (particles with diameters up to 10 um). Also, the percentages of aluminum and calcium contribution are 23% and 10% respectively (*Lorenzo et al., 2006*). As far as air traffic, several metal particles are emitted, including aluminum, chromium, barium, nickel, titanium and iron (*Starik, 2008*). Furthermore, ship emissions include carbonaceous particulate matter and SO_2 and NO_x (*Corbett, J.J. and Fischbeck, P., 1997*).

2.4.1.2. Industrial activities

Industrial activities release a large amount of a variety of particles and gases. The type of production process, the technology and the raw material used influence the type of pollutants. Huge amounts of primary particulate matter are mainly emitted from the industries – related to the production of ceramics, bricks and cement – foundries, mining and quarrying. These pollutants are related with both the production processes and manipulation of raw materials employed. Mining processes release toxic metals and metalloids such as arsenic, cadmium and lead which are associated to smelting processes and wind erosion of mine tailings and fugitive emissions. Elements such as nickel, vanadium, manganese, and copper are commonly released in foundries, whereas vanadium and nickel are mainly emitted in the combustion of fuel–oil. Furthermore, the process of energy production from fossil fuels

release gases which are precursors of secondary aerosols. Primary particulate matter formed by coal waste products and unburnt coal, or char are generated by coal burning in power plants. It is very interesting that recycling plants and composting plants release bacteria and fungi to the atmosphere (*Tohka et al., 2006*).

2.4.1.3. Coal burning

Coal is an abundant fuel source which is used to produce electricity and heat. The type and amount of pollutants released depend on coal maturity, coal combustors and burning conditions. Emissions of fine aerosol include toxic chemicals (PAHs) and elements, such as arsenic, selenium, mercury, chromium, cadmium, lead, antimony, and zinc (*Liu et al., 2008; Xu et al., 2011*).

2.4.1.4. Biomass burning

Biomass burning is a major source of both natural and anthropogenic particulate matter and gases. It includes wildfires, burning of agricultural land and residue after harvesting activities and biomass combustion occurring in household stoves. This type of source affects not only close-to-close sited but also regions thousands of kilometers away (*Alves et al., 2011b*). Biomass burning emissions consist of carbonaceous compounds, mainly of organic carbon, and of inorganic components in low concentrations. The organic fraction includes 40-80% water soluble compounds and a percentage of acids (*Reid et al., 2005b*). The inorganic fraction contains insoluble dust and ashes. Biomass burning emits particles mainly in the accumulation mode and a smaller fraction in the coarse mode, which includes dust, carbon aggregates ash and unburnt parts of fuel (*Badarinath et al., 2009; Formenti et al., 2003*).

2.4.1.5. Cooking

Cooking is a major source of fine particles in urban sites. Cooking method, cooking appliances and food ingredients influence these emissions. Also, a connection between temperature and emission factors has been observed, affecting chemical composition of aerosols and their physical characteristics. It has been found that palmitic, stearic and oleic acids and cholesterol are the basic compounds, identified in organic aerosol from meat cooking. Also, several other hazardous components are emitted when frying on a gas stove compared to frying on an electric stove. *Figure 4* shows the relative contribution of different PM components to total $PM_{2.5}$ mass emitted from different gas cooking methods are measured.
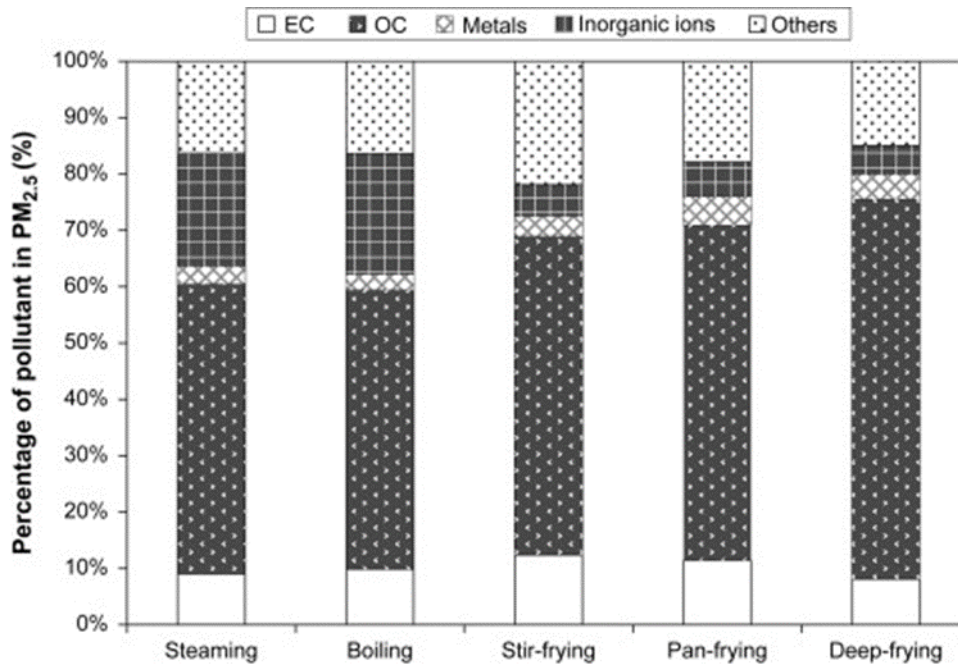
Figure 4: Relative contribution of different components to the total $PM_{2.5}$ emitted in gas cooking methods (See et al., 2008).

According to See et al. (2008), emissions of water-based cooking methods resulted in higher concentrations of water-soluble ions and inorganic ions including fluoride, chlorine, and sulphate. On the other hand, higher concentrations of organic matter and metals were observed when oil-based methods are applied. $PM_{2.5}$ and related chemical compounds' emissions varied depending on the cooking method, with deep-frying displaying the highest PM load, followed by pan-frying, stir-frying, boiling, and steaming.

2.4.1.6. Waste burning

Waste burning is a significant source of aerosol in urban and rural areas. According to Mohr et al. (2009), 500 $\frac{\text{Tg of C}}{\text{yr}}$ are released to the atmosphere from waste burning; about 50% of waste consists of carbon. Waste contains biomass, plastics, paper, and other material – for example textiles, rubber, glass, metals. Because of its heterogeneity, waste burning emissions are variable and are influenced by waste composition, fullness of the barrel and combustion conditions. It is interesting to note that high amounts of hydrochloric acid are measured in waste burning emissions, whereas this phenomenon is not observed in biomass burning emissions. This fact can be explained by the existence of large amounts of polyvinyl chloride in waste (*Akagi et al., 2011*).

2.4.2. Natural sources

2.4.2.1. Mineral dust

Mineral dust is a major source of natural primary particles, which are produced basically by wind erosion and resuspension of the Earth's surface (e.g., from deserts, dry lake beds and semi-arid surface). The global dust belt consists of a number of regions – the Sahara in the north Africa, the deserts in the Arabian Peninsula and Oman and Gobi and Taklimakan in China – which influence significantly the global aerosol loading. Mediterranean and northern European countries are mainly affected by African dust events. African dust event is characterized by the transportation of natural particulate matter from north Africa (Sahara and Sahel deserts) to southern Europe. Mediterranean cities are more affected by dust events, whereas northern countries are less affected due to the distance from the source and their climate. It has been observed that dust outbreaks over Europe more likely occur in February and March and it is possible to be monitored in summer. In the first case, dust particles come from Sahel deserts and are transported over the Atlantic Ocean, whereas in the second occasion dust comes from Sahara deserts and is transported over the Mediterranean basin. Equations have been developed, so mineral dust could be calculated through concentrations of silicon dioxide and aluminum – levels of these elements can be connected with African dust events.

$$\text{mineral dust} = Al \cdot 12.2 \, (\textit{Prospero et al., 1987}) \quad [\textbf{2.1a}] \text{ or}$$

$$\text{mineral dust} = SiO_2 \cdot 3.03 \, (\textit{Bowen, H.J.M., 1966}) \quad [\textbf{2.1b}]$$

Dry climate and the scarcity of precipitation in the Southern countries permit the long atmospheric residence time of particles and thus impact the air quality. North African dust is injected into the atmosphere and is transported over the Mediterranean and Southern Europe, North Europe, Canary Islands, North and South America, Cape Verde, and Barbados (*EC, 2004*).

The emissions of dust particles are influenced by wind speed and precipitation, as well as soil surface, soil moisture and vegetation cover. Mineral dust can be produced through two main ways. The first one is the saltation, which is referred to the move of layers of soil just above the surface with the existence of wind. The second one is called sandblasting and includes the emissions of dust aerosol duo to collides of saltating particles. It has been observed that dust particles rise from the surface to the atmosphere under a certain threshold speed. In this case, particles with diameter close to 100 μm are not able to remain for long time in the atmosphere due to their mass. Smaller particles, especially those between 0.1 and 5 μm, can remain for longer time in the atmosphere. It has been demonstrated that particles in this size range, emitted by arid and semi-arid regions, are able to travel up to 500 km. Furthermore, dust particles vary greatly in their characteristics and composition. Calcite, quartz, dolomite, clays, feldspar and smaller amounts of calcium sulphate and iron oxides are the main components of dust aerosol. However, the characteristics and the composition of the soil influence the chemical and mineralogical composition of dust particles. The presence of iron and titanium dioxide in mineral dust is an important parameter because these compounds participate in crucial environmental processes. In general, iron influence the marine ecosystem productivity

and radiative effects. Also, it impacts the global biogeochemical cycle. On the other hand, titanium dioxide is related to heterogeneous photoreactions. It is important to note that anthropogenic sources, such as farming, factories, roads, herding livestock and mining activities, also have a minor contribution to the dust aerosol. According to Mohowald et al. (2010), dust emissions have doubled over the past 100 years, while the authors suggest that anthropogenic activities play a key role in this increase.

2.4.2.2. Sea spray aerosols

Primary marine particles are produced during the eruption of rising bubbles through the sea-surface microlayer (SML). A single air bubble breaking up in the ocean can produce either up to ten particles of marine aerosol (with diameters between 2 and 4 μm) or several hundred particles (with diameter smaller than 1 μm). In the first case, particles are called jet drops and reach up to 15cm above to the surface. In the second case, film drops are found in higher altitudes where the water vapor evaporates completely or not due to the lower relative humidity (*Woodcock, 1972*). Sea spray aerosols can be found basically in the coarse fraction, but those which contribute to the sub-micron fraction are more interesting due to their direct and indirect impacts on radiative transfer. Marine aerosol consists of sodium, chloride and smaller concentrations of sulphate, potassium, magnesium, and calcium. In the presence of anthropogenic emissions, chloride may react with sulphuric acid and nitric acid and convert into a gaseous state in the atmosphere, as shown below (*White, 2008*):

$$\text{NaCl}_{(s)} + \text{HNO}_{3(g)} \rightarrow \text{HCl}_{(g)} + \text{NaNO}_{3(s)} \qquad [\textbf{2.2}]$$

$$2\text{NaCl}_{(s)} + \text{H}_2\text{SO}_{4(g+\,aq)} \rightarrow 2\text{HCl}_{(g)} + \text{Na}_2\text{SO}_{4(s)} \qquad [\textbf{2.3}]$$
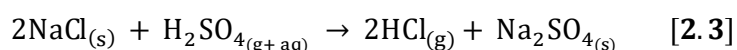
It is interesting to note that amounts of organic compounds have also been observed in sea spray aerosols emitted by phytoplankton. The main monitored compound is dimethyl-sulphide (DMS). The marine organic carbon emissions are estimated at about $8.2\,\frac{\text{Tg}}{\text{y}}$, when the total sea salt emissions are $24\,\frac{\text{Tg}}{\text{y}}$. The concentration of DMS is increased during the periods that planktons are blooming. The organic carbon concentration displays a correlation with chlorophyl, suggesting as common source a biological activity. A general belief is that marine organic carbon emissions are comparable or higher to those from fossil fuel and enhance the global organic carbon burden by about 20% (*O'Dowd et al., 2008*).

2.4.2.3. Biogenic emissions

Primary and secondary aerosols are formed by vegetation and several types of microorganisms. Pollen, fern spores and fungal spores are the main biogenic aerosol with diameters up to 100 μm. Small fragments and excretions from plants, animals, bacteria, viruses, carbohydrates, proteins, waxes, and ions are found in particles with diameters smaller than 10 μm. Several of these compounds are phospholipids, β-1,3-D-glucan, ergosterol, mannitol and arabitol. Secondary organic aerosol and ozone may be formed by biogenic volcanic organic compounds, including isoprene, alcohols, ketones, monoterpenes and

sesquiterpenes. It is estimated that emissions of biogenic volcanic organic compounds are ten times bigger than those of anthropogenic activities (*Atkinson, R. and Arey, J., 2003*).

2.4.2.4. Volcanic eruptions

Volcanic eruptions are a major source of tropospheric and stratospheric pollution. The main pollutants that are emitted are greenhouse gases, sulphur, and aerosols. Tropospheric particles have a lifetime of about 1 week, whereas stratospheric aerosols can remain approximately for 1 to 2 years (*Gao et al., 2007*). Volcanoes are responsible for both the emission of primary particles and the production of secondary aerosols. Sulphur dioxide, which is released to the atmosphere in large amounts during the eruptions, is oxidized to secondary sulphate aerosol. It is estimated that between 14 to 36% of this oxidized form originates from volcanic eruptions (*Chin, M. and Jacob, D.J., 1996*). Volcanic emissions include several elements in variable concentration – such as aluminium, silicon, sulphur, chlorine, potassium, calcium, titanium, manganese, iron, copper, and zinc. It is estimated that mercury emissions by volcanoes and geothermal activities reach about 90 $\frac{\text{Mg}}{\text{y}}$ (*Pirrone et al., 2010*).

According to Chin, M., Jacob, D.J. (1996), globally, anthropogenic, biogenic, and volcanic emissions account for about 70%, 23% and 7% of the global sulphur sources, respectively. However, they account for 37%, 42% and 18% of the global column of atmospheric SO_4^{2-} respectively.

2.4.2.5. Lightning

Lightning is a source of NO_x and secondary natural nitrate particles in the atmosphere. In the first step, an air channel is ionized and then the following reactions are taking place:

$$N_2 + O_2 \rightarrow 2NO \qquad [\mathbf{2.4}]$$

$$2NO + O_2 \rightarrow 2NO_2 \qquad [\mathbf{2.5}]$$
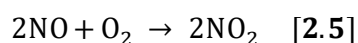
It is interesting to note that aerosols and lightning are tightly correlated, because of the ability of aerosols to affect lightning activity through modifications of cloud microphysics. It seems that they have a bidirectional relation, and for this reason an enhanced lightning activity is observed near urban sites. According to a study, a 60% increase in aerosol loading can cause more than 150% increase in lightning flashes (*Yuan et al., 2011*).

2.5. Effects of aerosol

2.5.1. Earth's climate

Anthropogenic aerosol can affect global climate through two effects. The first one, direct effect, is based on dispersion and absorption of the solar and thermal radiation from particles. As far as the other one, indirect effect, aerosol alters the microphysical and optical properties of cloud droplets. In the atmosphere, these cloud droplets are acting as cloud condensation nuclei (CCN). Cloud condensation nuclei are defined as particles which are able to be activated

to grow to fog or cloud droplets, in the condition of the existence of a supersaturation of water vapor (*Seinfeld, J.H. and Pandis, SP.N., 2006*). The last effect can be divided into two categories. In the first one, an increase of cloud albedo is observed. This happens because the effective radius of cloud droplets decreases when the particle number concentration increases. The second indirect effect is the impediment of precipitation and the rise of cloud water due to the increase of cloud droplets effective radius. Toshihiko et al. (2005) simulated, aerosol indirect and direct effects on climate through aerosol transport-radiation model, and calculated global mean radiative forcing. The value of global mean direct radiative forcing is about $-0.1 \frac{W}{m^2}$, whereas the value of global mean indirect radiative forcing is nearly $-0.9 \frac{W}{m^2}$. Due to indirect and direct effect of anthropogenic aerosol particles, changing ratios of clouds and precipitation parameters have higher values over land than above the ocean. Thus, the effective radius of cloud droplets is decreased about 10% due to the first indirect effect. Moreover, the aerosol direct effect and the first indirect effect cause changes in the liquid water and precipitation.

2.5.2. Natural and built environment

2.5.2.1. Visibility impairment

Fine particles ($PM_{2.5}$) are the main cause of reduced visibility (haze), due to their interaction with solar radiation. Because of the presence of pollution particles in the atmosphere, only a fraction of sunlight can penetrate, while the rest of solar radiation is diffused, reflected, or absorbed by particles. The reduced solar radiation leads to decreased visibility, clarity, and alteration of colors in the atmosphere. This phenomenon is more intense under humid conditions. It is mentioned that $PM_{2.5}$ concentration equal to 150 $\frac{ug}{m^3}$ corresponds to maximum visibility equal to 8 km (*Diapouli, E., 2008*).

2.5.2.2. Environmental damage

The effects of pollution particles settling depends on their chemical composition. Several of the most common consequences are change of the nutrient balance in coastal waters and large river basins, depletion of the nutrients in soil, damage of sensitive forests and farm crops and impact on ecosystems diversity. In addition, lakes and streams acidity is enhanced by particulate matter settling. Pollution particles contribute to acid rain effects, with several consequences for both the natural environment and materials (*US EPA*).

2.5.2.3. Materials damage

Particulate matter can damage materials, including objects and buildings of culture heritage, such as statues and monuments. Two main mechanisms of materials damage are erosion and accretion. The first mechanism reduces the lifetime of materials, while the second one decreases the time of beneficial use of surfaces (*Diapouli, E., 2008*).

2.5.3. Human health

Pollution exposure is linked to a variety of health problems, such as decreased lung function, aggravated asthma, irregular heartbeat, nonfatal heart attacks and premature death in people with heart or lung disease (*Figure 5*). As far as particle pollution exposure, the most sensitive population groups are children, elderly and people with heart or lung disease.
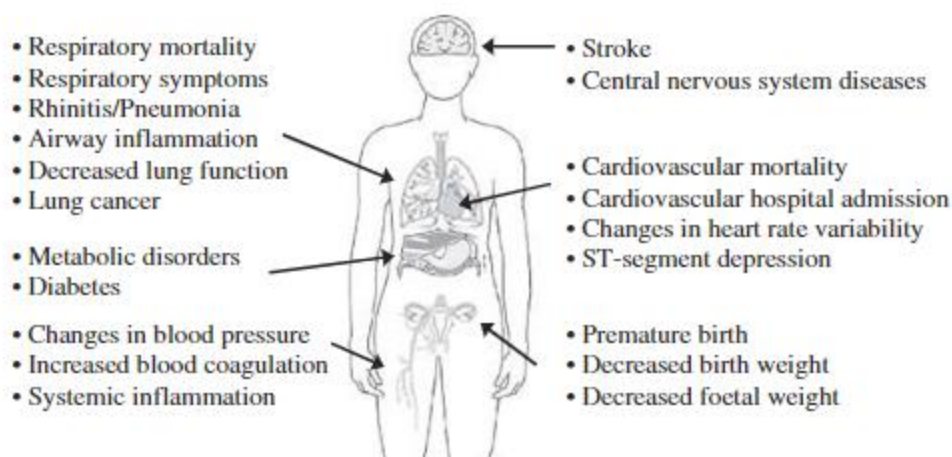
Figure 5: Health outcomes related to air pollution (Costa et al., 2014).

The resistance of human's respiratory system against the airborne particles depends on their size. The bigger particles are restrained by the body's defense mechanisms, such as nose hair or its mucus. Particulate matter with diameter between 0.5 to 10 μm can be found in the lungs and precipitate due to their size. Most of the particles which precipitate are between 2 and 4 μm. So, existing respiratory and heart diseases may get worse and new lung tissue damages may be caused. Coarse particles, including crustal material, are linked with respiratory (*Chen R et al., 2011*), cardiovascular effects (*Atkinson et al., 2010; Chen R et al.,2011; Malig, B.J. and Ostro, B.D., 2009; Mallone et al., 2011*) and premature mortality (*Meister et al., 2012; Tobías et al., 2011*). European countries were forced to decrease the limits of $PM_{2.5}$ concentration, from the annual limit value of 25 $\frac{ug}{m^3}$ to 20 $\frac{ug}{m^3}$ until 2020 (*Directive 2008/50/EC*).

In addition, black carbon can be related to cardiovascular health effects and premature mortality, for short-term (*Janssen et al., 2012, Delfino et al., 2010a; Ito et al., 2011; Kim et al., 2012; Son et al., 2012; Zanobetti et al., 2009*) – and long-term exposures (*Ostro et al., 2010*).

As far as the toxicity of components of particulate mass, sulphur is considered as the most harmful for peoples' health. Sulphur ions can interfere with lung process for particles removal. Several trace metals react to create hydroxyl radicals. Hydroxyl radicals are toxic for body tissues. Coarse particles have intense activity through the hydroxyl radicals. Also, PM_{10} fraction emit amounts of Fe^{+3} in pH equal to 7.2, the same pH value of lungs surfaces (*Gilmour et al. 1996*).

In 2020, 238,000 premature deaths were caused by exposure to concentrations of fine particulate matter above the World Health Organization (WHO) guideline level. In addition,

49,000 premature deaths were related to exposure to nitrogen dioxide above the respective level and 24,000 premature deaths related to acute exposure to ozone. These numbers are reduced by 45% compared to the premature deaths in 2005. Morbidity is also caused by air pollution. For example, in 2019, exposure to fine particulate matter led to 175,702 years lived with disability (YLDs) because of chronic obstructive pulmonary disease in 30 European countries (*EEA, 2022a*).

2.6. Air quality in Europe

The urbanization of world population leads to aggravation of air quality in city centers. EU has defined limit values for the ambient concentrations of two particle fractions, PM_{10} and $PM_{2.5}$, as well as for selected PM_{10} components (*Table 1*). Despite the measures adopted by the different member states in order to meet these limit values, and the obtained reduction of emissions, according to EEA, in 2020, 96% of the European's urban population was exposed to concentrations of $PM_{2.5}$ above the 2021 WHO annual guideline of 5 $\frac{ug}{m^3}$, as shown in *Figure 6* (*EEA, 2022b*).

Table 1: EU limit values for particulate pollution (Directives 2008/50/EC and 2004/107/EC).

Pollutant	Annual limit value	24 hr limit value
PM10	40 ug/m3	50 ug/m3 (not to be exceeded more than 35 days per year)
PM2.5	25 ug/m3	-
Pb	0.5 ug/m3	-
As	6 ng/m3	-
Cd	5 ng/m3	-
Ni	20 ng/m3	-
Benzo(a)pyrene	1 ng/m3	-
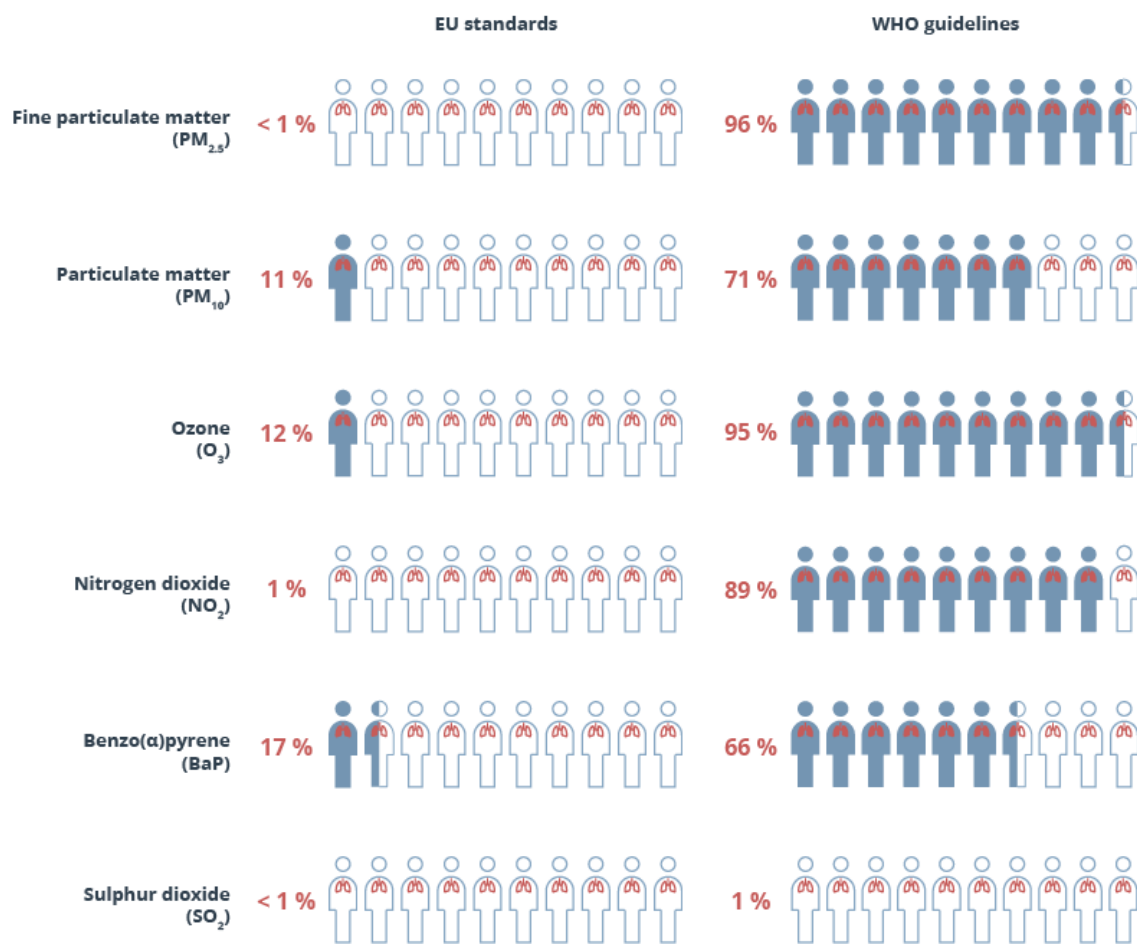
Figure 6: Share of the EU urban population exposed to air pollutant concentrations above EU standards and WHO guidelines in 2020 (EEA, 2022b).

In addition, in 2020, the highest fine particulate matter concentrations were seen in northern Italy and in some eastern European countries. High density of anthropogenic emissions and meteorological and geographical conditions in northern Italy cause the high PM concentrations. In eastern Europe, the use of solid fuels and older vehicle is the main reason for increased PM concentration levels. This situation can be seen in the *Figure 7*.

Figure 8 shows fine particulate matter concentrations in 2020 by European country in relation to the European annual limit value and the WHO annual guideline. Only 2% of monitoring stations register concentrations of $PM_{2.5}$ above the annual limit value of 25 $\frac{\text{ug}}{\text{m}^3}$. 69% of these stations were urban and 21% suburban.
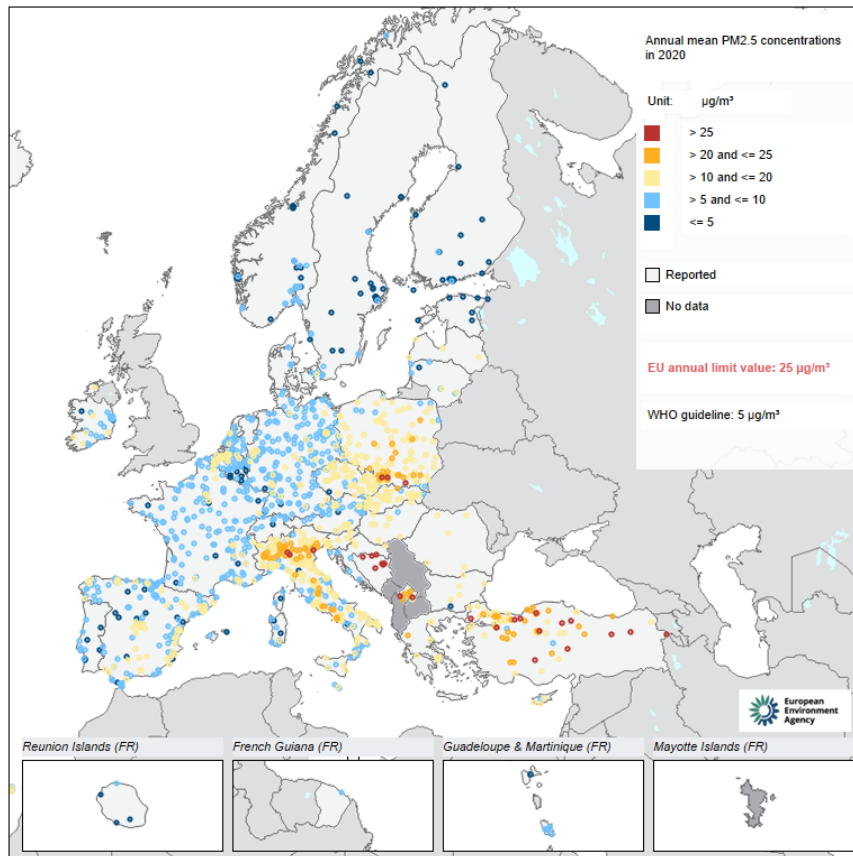
Figure 7: Concentrations of $PM_{2.5}$ in 2020 in relation to the EU annual limit value and the WHO annual guideline (EEA, 2022b).
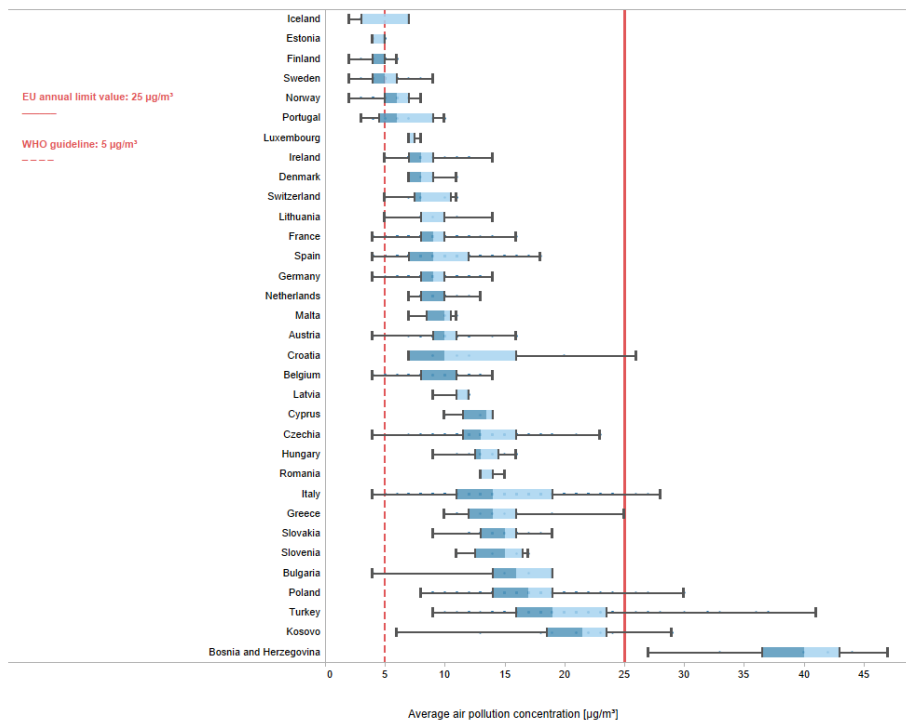
Figure 8: $PM_{2.5}$ concentrations in 2020 by country in relation to the EU annual limit value and the WHO annual guideline (EEA, 2022b).

3. Atmospheric aerosol studies in Greece and Europe

The interest in aerosols has increased in recent decades due to their impact on air quality, human health, and climate change, with efforts focusing on fine particulates (with a diameter of 2.5 um or less), which display more severe impacts. EU member states monitor continuously the ambient concentrations of PM_{10} and $PM_{2.5}$. Given their different natural and anthropogenic origin, and the growing population and industrial activities, it is important to also characterize their chemical composition and perform source apportionment studies. Source apportionment techniques provide the means to identify the major PM sources and to quantify their contribution to the measured PM levels. In this framework, combining data from background and traffic sites can be interesting for determining the primary emission sources in a region with plentiful local sources, understanding the impact of secondary aerosol formation and assessing the variation of source profiles and contributions at the different sites.

Many studies have been conducted in Greece and Europe for emission sources' identification. *Table 2* shows mean $PM_{2.5}$ concentration $\left(\frac{ug}{m^3}\right)$, mean % source contribution to $PM_{2.5}$ and mean source concentration $\left(\frac{ug}{m^3}\right)$ from selected studied performed in Athens and Southern Europe.

Table 2: Mean $PM_{2.5}$ concentration $\left(\frac{ug}{m^3}\right)$, mean % source contribution to $PM_{2.5}$ and mean source concentration $\left(\frac{ug}{m^3}\right)$ for some recent studies.

Study	City	PM2.5	Mineral dust	Non-exhaust emissions	Exhaust emissions	Heavy oil combustion	Sea salt	Biomass burning	Secondary sulphate	Secondary nitrate	Unaccounted	Local dust	Industrial	Sahara dust
Manousakas et al., 2021 (2013-2014)	Athens, Greece - UB site	11.0	1%-0.1	5%-0.4	8%-0.7	8%-0.7	3%-0.3	9%-0.8	66%-5.9	-	-	-	-	-
	Athens, Greece - UT site	19.5	4%-0.9	7%-1.4	19%-4.1	6%-1.2	2%-0.49	20%-4.1	30%-6.1	-	-	-	-	-
Diapouli et al., 2017 (2011-2012)	Athens, Greece - UB site	18.0	2%-0.3	4%-0.7	16%-2.7	6%-1.0	2%-0.4	46%-7.9	25%-4.4	-	-	-	-	-
	Athens, Greece - SUB site	12.4	7%-0.8	1%-0.1	9%-1.0	4%-0.5	1%-0.1	23%-2.6	55%-6.4	-	-	-	-	-
	Thessaloniki, Greece - UB site	25.9	2%-0.4	2%-0.6	5%-1.2	-	2%-0.5	36%-8.7	33%-8.1	20%-4.9	-	-	-	-
	Thessaloniki, Greece - UT site	33.3	2%-0.7	3%-1.1	34%-10.6	-	2%-0.6	22%-7.6	18%-5.6	18%-5.6	-	-	-	-
Diapouli et al., 2022 (2016-2017)	Athens, Greece - UB site	10.5	6%-0.6	3%-0.3	12%-1.3	26%-2.8	3%-0.3	44%-4.6		-	-	6%-0.6	-	-
Amato et al., 2015 (2013-2014)	Barcelona, Spain - UB site	15.0	-	1%-0.2	19%-2.9	5%-0.7	3%-0.4	-	38%-5.7	13%-1.9	5%-0.7	7%-1.0	9%-1.3	-
	Florence, Italy - UB site	13.2	-	2%-0.3	18%-2.5	6%-0.8	2%-0.3	20%-2.8	30%-4.2	14%-1.9	5%-0.7	2%-0.3	-	1%-0.2
	Milan, Italy - UB site	30.1	5%-1.5	8%-2.5	6%-1.8	19%-5.6 *	1%-0.4	17%-5.1	-	30%-8.9	9%-2.6	-	5%-1.4	-
	Athens, Greece - SUB site	11.0	-	5%-0.6	15%-1.7	7%-0.8	1%-0.1	10%-1.2	33%-3.8	6%-0.7	11%-1.3	6%-0.7	-	6%-0.7
	Porto, Portugal - UT site	26.7	15%-3.8	5%-1.3	32%-8.1	13%-3.3 *	4%-1.1	17%-4.4	-	5%-1.4	4%-0.9	-	5%-1.3	-

*including secondary sulphate factor

** UB → urban background, UT → urban traffic, SUB → suburban

As shown in *Table 2*, mean $PM_{2.5}$ concentration is decreased through years. The highest concentration was recorded at traffic sites, due to increased vehicle traffic and anthropogenic activities. Biomass burning and secondary sulphate emissions are the major sources in urban background sites. In traffic sites, vehicle exhaust is the major emission source. Sea salt

contributes similarly among the different Athens sites, as expected given its natural origin and the geography of the Attica peninsula.

In a recent study conducted at an urban background site in Athens (Greece), Diapouli et al. (2022) found that a significant portion of $PM_{2.5}$ consisted of carbonaceous aerosols, but there was a slight decrease in the total carbon (TC) concentrations, with TC accounting for 24% of $PM_{2.5}$ in 2016-2017, compared to 27-30% during the years 2011-2013. The decrease in TC was due to a reduction in organic carbon (OC) rather than elemental carbon (EC), which resulted in a decrease in the OC/EC ratio (on average equal to 5.4). The potassium (K) concentration levels were also lower and the levels during the warm period were higher than those during the cold period. These findings indicate that residential biomass burning was less prevalent during 2016-2017 compared to previous years. Source apportionment analysis revealed that the major source contributing to $PM_{2.5}$ concentration levels (by 44%) was a mixed source related to secondary aerosol formation and biomass burning. This source contained a high concentration of sulphur (S) and organics, suggesting it may be linked to regional pollution. The seasonal variability of OC/EC ratio and K concentrations (higher during specific periods in the warm season) indicated that the biomass burning emissions during the study period were mainly caused by the movement of smoke plumes from wildfires, instead of residential heating.

Manousakas et al. (2021) performed a source apportionment study at an urban background and an urban traffic site in Athens, during 2013-2014. The aim of this work was to assess the variability in source contributions and profiles between the two sites. Mineral dust, biomass burning, fresh sea salt, secondary sulphates and heavy oil combustion profiles displayed high correlation between the sites. Non-exhaust emissions and secondary nitrates profiles presented low/no correlation. The source profiles with the higher correlation were related to natural sources and/or sources originating outside the urban agglomeration.

Diapouli et al. (2017) studied the long-term variability (between 2011-2012 and 2002) of emission sources in urban background and suburban locations in Athens. Biomass burning and secondary inorganic aerosol were the major emission sources at urban background and suburban sites. All anthropogenic sources displayed increased contributions at the urban background site in comparison to the suburban, by a factor of 1.3 (for Vehicle non-exhaust) to 2.7 (for Biomass burning) in PM_{10} and 1.9 (for Oil combustion) to 4.4 (for Vehicle non-exhaust) in $PM_{2.5}$. Only Secondary sulphate contribution was similar at the two sites, indicating the regional character of this source. Assessment of the long-term variability of source contributions revealed significant increase in Biomass burning, from 5-7% in 2002 to 29-36% for 2011-2012. All other anthropogenic sources (Traffic, Oil combustion, Secondary aerosol formation) were significantly lower during 2011-2012, reflecting the impact of the environmental policies during the past decade, but also of the financial crisis and decreased economic activity during this period.

Amato et al. (2015) combined data from five Southern European cities (Athens, Milan, Florence, Barcelona, and Porto) in order to assess the major sources contributing to PM_{10} and $PM_{2.5}$ levels measured at urban traffic, urban background and suburban locations. Secondary sulphate was the major source at urban and suburban background sites. In traffic site, traffic exhaust was, as expected, the most significant contributing source for both size fractions. At the Atlantic site, Porto, sea salt contribution was the highest, followed by the two Mediterranean coastal sites, Barcelona, and Athens. Biomass burning was the second most important source in Milan and Porto and the third in Florence and Athens. The difference is

the contribution of this source among cities may be caused by different penetration of wood as fuel for residential heating. The most interesting is that during high pollution days, the sources contributing most to $PM_{2.5}$ levels were vehicular exhaust emissions in Barcelona and Porto, biomass burning in Florence and Milan and Sahara dust long-range transport in Athens.

In the present work, the concentration levels of $PM_{2.5}$ and related chemical components in Athens (Greece) were assessed in two sites, displaying different level of urbanization and traffic density. Moreover, the major PM sources were identified and their contribution to the observed PM levels was quantified. A traffic site and an urban-background site in Athens have been selected to be compared. The main goal was to characterize the similarities and heterogeneities in PM sources and contributions between the two sites. By finding the main PM sources and their contribution to the observed PM levels, air quality can be improved through targeted and effective mitigation policies, assisting towards meeting the EU legislation and WHO guidelines.

4. Sampling and chemical speciation

4.1. Sampling sites

In the framework of the study of chemical speciation of atmospheric aerosol, $PM_{2.5}$ samples were collected from two different sites in Athens Metropolitan Area during 2019 - 2020: the NCSR "Demokritos" urban background station and the Aristotelous urban traffic station, belonging to the National Monitoring Network.

The basin of Athens is bounded by four large mountains. The Thriasian plain sprawls to the west and the Saronic gulf lies to the southwest. Athens is located in the north temperate zone. The climate in Athens is Mediterranean which is characterized by alternation between prolonged hot - dry summers and mild - wetter winters with moderate rainfall. Athens is frequently affected by the urban heat island effect due to human activity. Also, a complex mountainous geomorphology causes temperature inversion phenomenon. These factors influence the air pollution of Athens and its climate. The Athens Metropolitan Area sprawls over $2,928.717 \, km^2$ and is the most populated region of Greece, having reached a population of $3,722,544 \, km^2$ according to the 2021 census.

The urban-background site (UB-site, DEM-Athens) is located in a pine covered area inside N.C.S.R. "Demokritos" campus, in Agia Paraskevi, Attiki, Greece, at the north-eastern corner of Athens Metropolitan Area (37◦ 99' 50" N 23◦ 81' 60" E), and at about 12 km distance from the city center (*GAWSiS, 2022*). The DEM–Athens station is located on the hillside of Mount Hymettus, at an altitude of 270 m above sea level. The station is away from direct emission sources, and is partly influenced by the urban area and by incoming air from the northeast representative of regional atmospheric aerosol conditions (*Figure 9*).

The urban traffic site (UT-site) is at the Aristotelous Station of the National Air Quality Monitoring Network, in the Athens commercial center. It is located at the first-floor open balcony of the Ministry of Health, next to a busy street (37.99◦ N 23.72◦ E), at an altitude of 64 m above sea level (*GAWSiS, 2022*). This site is impacted by traffic and human activities (*Figure 9*).
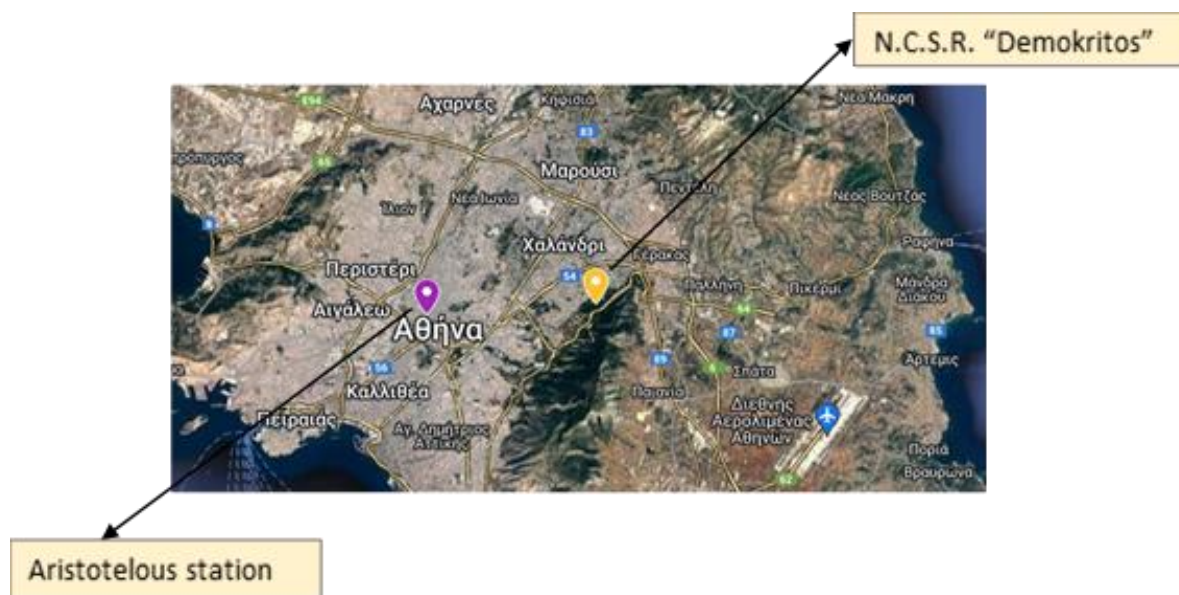
Figure 9: Location of sampling sites in the cities of Athens, Greece.

4.2. Sampling

The sampling campaign lasted for approximately one year, from September 2019 to September 2020. The total number of collected samples in urban-background and traffic station is 79 and 82 respectively. 24h $PM_{2.5}$ samples were collected on Quartz filters by means of low-volume Custom-made sampler in Aristotelous station and on Teflon filters by means of a low-volume Leckel sampler, in Demokritos (*Figure 10*).
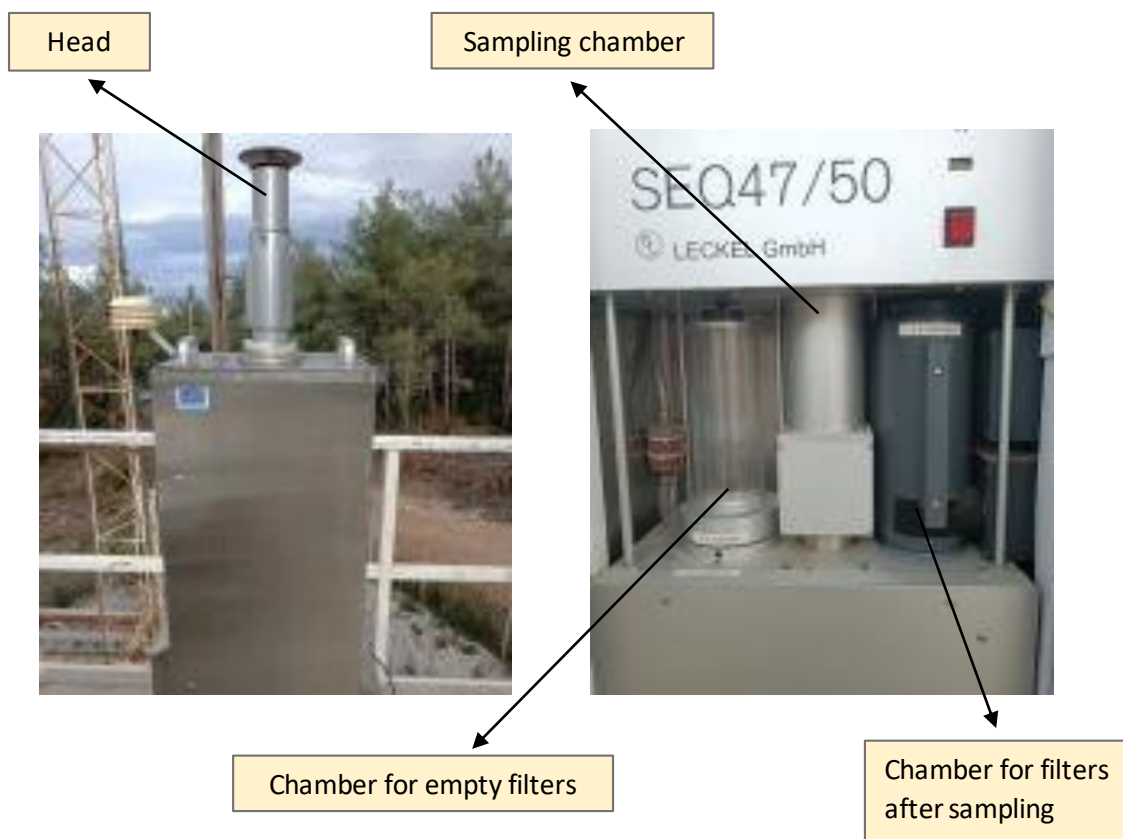
Figure 10: Low-volume Leckel sampler, Demokritos station.

4.3. PM concentration and chemical speciation

PM filters from both sites were weighed before and after sampling, so the total concentration of particulate matter can be measured. After weighing, ½ of the filter was used for multi-elemental analysis. One punch was also cut from the Quartz filters from the Aristotelous station in order to quantify carbonaceous species (*Figure 11*). In Demokritos station, carbonaceous aerosol was measured by a semi-continuous analyzer, as described in detail below. The concentration of carbonaceous species (organic and elemental carbon) was determined through thermal-optical analysis and the elements analysis was performed by X-Ray Fluorescence.
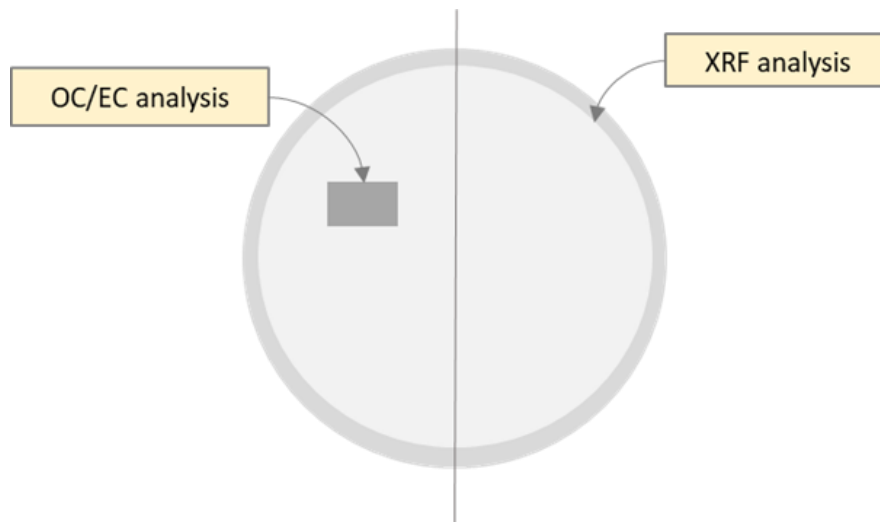
Figure 11: PM Quartz filters from Aristotelous station.

4.3.1. PM mass concentration

$PM_{2.5}$ mass concentration was measured gravimetrically, which is the reference method for the determination of PM mass concentration on air (*EN 12341*). According to EN 12341, all filters are weighed before sampling and after that, following a 48hr period of conditioning in standard temperature and relative humidity conditions (20 ± 1∘C and 45-50% RH). Prior to filter weighing, temperature and relative humidity are checked for the previous 48 hours. In addition, filters are observed in order to identify imperfections and changes in appearance because of sampling or/and transportation. A standard calibrated weight (200 ug) is weighed, so the scale is checked as to its proper functioning. Also, one blank filter, which remains in the weighing chamber and is regularly weighed, is measured. The difference in mass of this test filter should not exceed 40 ug. After that, the samples to be weighed are placed on an ionization system for a few seconds, so that they are grounded. An angular electrode produces ions which equalize the static loads of filter. Two measurements of the filters' mass are conducted (after 48 hours of conditioning and again after 12 additional hours) and the difference between these two values must be less than or equal to 40 ug for clean filters and 60 ug for loaded filters. If this condition is not satisfied, an extra weighing is conducted after a time period greater than 24 hours. If this condition remains unsatisfied, this filter is rejected. This procedure is followed for both clean filters (before sampling) and loaded filters (after sampling).

In the final stage, mean concentration of $PM_{2.5}$ is calculated in the following way,

$$C = \frac{W_2 - W_1}{V} \cdot 10^3 \qquad [\textbf{4.1}]$$

where W_1 is the weight of filter before sampling (mg), W_2 is the weight of filter after sampling (mg), V is the amount of air volume which passed through the filter under ambient conditions (m^3) and C is the concentration ($\mu g/m^3$) ± measurement uncertainty (%).

4.3.2. Organic Carbon and Elemental Carbon – OC/EC

4.3.2.1. General

For the determination of the content of organic (OC) and elemental carbon (EC) the thermal-optical transmittance method was used. The separation and quantification of OC and EC concentrations are performed through the thermal volatilization of OC in inert atmosphere (99.999% by volume Helium) and oxidation of EC in oxidizing atmosphere (He-O_2 mixture at a volume ratio of 98:2) at defined temperature steps. The evolved organic carbon and oxidation products flow through a manganese dioxide (MnO_2) oxidizing oven and all carbon is transformed into carbon dioxide (CO_2), which is then quantitatively estimated. The method's limit of detection is 0.5 µg/cm^2 of carbon. The temperature steps in the inert and oxidizing atmosphere are specified by the thermal protocol used for the analysis. In the framework of this work, the EUSAAR2 thermal protocol was applied, which is the European standard protocol for this type of analysis (*Table 3*). In addition to the elemental carbon present in the sample, elemental carbon can be formed from some charring of organic carbon, as it is pyrolyzed during the initial temperature steps in inert atmosphere. This charring of organic carbon results in an artificially low measurement of the organic carbon and a high measurement for the original elemental carbon if left uncorrected. The thermal-optical transmittance method uses the high light absorbance characteristic of elemental carbon to correct for the pyrolysis-induced error. This is done by passing a laser beam through the sample and monitoring the laser beam transmittance throughout the analysis. Initial transmittance is recorded; as the temperature increases in the inert atmosphere, any charring of the organic carbon results in a decrease in transmittance of the laser. In the oxidizing atmosphere, all of the elemental carbon is oxidized off the sample and the laser transmittance is returned to the background level. The point in the analysis where the laser transmittance equals the initial laser transmittance is the split point between OC and EC (*Figure 12*). Any elemental carbon detected before this point is considered to have been formed pyrolytically by charring of the organic carbon and is this quantified as OC. The remaining elemental carbon is quantified as EC.

Table 3: Temperature steps and steps duration for EUSAAR2 (ELOT EN 16909).

Mode	Step	Temperature (°C)	Duration (s)
He	He1	200	120
	He2	300	150
	He3	450	180
	He4	650	180
He/O₂	He	No heating	30
	He/O₂ 1	500	120
	He/O₂ 2	550	120
	He/O₂ 3	700	70
	He/O₂ 4	850	80

Figure 12: Thermograph of OC/EC analysis for EUSAAR2.

4.3.2.2. Off-line analysis

The quartz fiber filters collected in the Aristotelous station were analyzed by a Lab OC-EC Aerosol Analyzer (Model 5, Sunset Laboratory, Inc., Tigard, OR, U.S.A.), at the Environmental Radioactivity Laboratory of NCSR "Demokritos" (*Figure 13*). A punch of 1x1.5 cm^2 was cut from each filter sample and placed inside the analyzer. The thermal-optical analysis follows the steps described above and the converted CO_2 gas, resulting from the OC thermal evolution and EC oxidation, is quantitatively converted to methane, which is measured by a flame ionization detector (FID) (*OCEC Manual*). The off-line OC/EC analysis was performed following the European Standard EN 16909: 2017, including the Quality Assurance/ Quality Control procedures described below:

I. A "clean oven" run was performed in the beginning of each day of analysis, in order to ensure that no carbon was present inside the instrument's oven.

II. An "Instrument blank" analysis is performed, with a blank filter, in order to verify zero concentrations. This analysis is also used to verify other analytical parameters, such as the pressure, laser signal, heating procedure and the FID signal during the calibration phase of analysis ($FID1_{max}$). The main parameters which should be inspected are the concentration of OC (≤0.2 μg/sq.cm.) and EC (should be zero), the stability of the laser signal, the value of pressure (0.5 -1.0 psig) and $FID1_{max}$ value $(15,000 - 30,000)$.

III. Analysis of a sample containing known amount of OC, in the form of sucrose; a clean punch is spiked, by the use of a pipette, with 10 μl of a solution, containing sucrose dissolved in reagent grade water, in known concentration. The measured OC concentration should be within ±5% of the reference value, while EC concentration

should be zero. These sucrose solutions are also used for the calibration of the analytical system, least once every twelve months.

IV. To check the FID signal, a clean filter is analyzed with the CALGAS protocol. This protocol injects known quantities of methane into the system, without any heating, and the response of the detector is assessed. The Total Carbon (TC) value should be within ±5% of the reference value and the EC/OC value within ±3% of the reference value. The reference EC, OC and TC concentrations are defined as the average values obtained after running 10 repeated CALGAS analyses.

V. To control the long term stability and repeatability of the analyzer, a filter of known concentration is used. This filter is known as "control filter" and has sampled ambient air by a high-volume sampler. The control filter is analyzed 10 times and the average of the OC, EC and TC values obtained are considered as reference values. Given the heterogeneity of the filter, OC and EC values may deviate more in this test and should be within ±10% or ±0.5 $\mu g/cm^2$ (whichever is greater) of the reference value (*OCEC Manual*).

Figure 13: Organic Carbon and Elemental Carbon Laboratory Instrument Model 5, Sunset Laboratory Inc. "Demokritos" station.

4.3.2.3. On-line analysis

For the measurement of the levels of the organic and elemental carbon in the urban-background site, the semi-continuous OCEC field analyzer (Model-4, Sunset Laboratory, Inc., Tigard, OR, U.S.A.) was used. The instrument is operating continuously at the DEM-Athens station, maintained by the Environmental Radioactivity Laboratory, NCSR "Demokritos" (*Figure 14*). It collects ambient aerosol at a sampling flow rate of 8 l/min, on a round 16-mm quartz fiber filter mounted inside the instrument. Its inlet is equipped with a cyclone, to allow for $PM_{2.5}$ sampling, and with an inline parallel carbon denuder, so that the sample is denuded of volatile gases during sampling. The quartz fiber filter is always installed with a second backup filter, mostly to serve as support for the front filter. A collection time of 2.5 hours is

set in the instrument, followed by analysis of the sample by the EUSAAR2 protocol. The converted CO_2 gas, resulting from the OC thermal evolution and EC oxidation, is quantified by a non-dispersive infrared (NDIR) detector. OC and EC concentrations are recorded, thus, near-real time, on a 3 h basis. The 3 h values obtained, were then averaged over the 24 h period corresponding to the Teflon filters collected at the DEM-Athens station (*semi-continuous OCEC*).

Figure 14: Semi-continuous organic and elemental carbon aerosol analyzer, "Demokritos" Laboratory.

4.3.2.4. Semi-continuous Sunset OCEC analyzer Vs Sunset Lab OCEC analyzer

Studies, in which the Semi-Continuous Sunset OCEC analyzer and the Sunset Lab OCEC analyzer are compared, show that the two analyzers' outputs are well correlated, with the OC concentrations displaying slightly better correlations. According to Karanasiou et al. (2020), linear regression of OC concentrations measured by the semi-continuous versus the Lab analyzer produced a correlation coefficient of 0.9, with a slope of 0.93 and a positive intercept of 0.94. As for the EC analysis, correlation coefficient reached 0.6, with a slope of 0.95 and a positive intercept of 0.09. The lower value of the correlation coefficient for EC data relates to the low values of EC concentrations measured.

4.3.3. Multi-elemental analysis

4.3.3.1. Fluorescence Spectroscopy

X-Ray Fluorescence (XRF) is a non-destructive, rapid and safe technique, which is used for characterization of materials. The materials in question can be solid, liquid or gas. XRF may be applied on aerosol filters, providing the concentration of major and trace elements found in

PM. The advantage of this technique is its ability of multi-elemental analysis. In this way, a large number of elements can be analyzed at the same time. The XRF technique is frequently employed for aerosol composition studies, given that only a few minutes are needed in order to detect up to 20 elements of anthropogenic and territorial emissions (*Papagiannis, S., 2022*).

An X-Ray tube generates X-Ray and bombards the sample with a barrage of radiation. The elements of sample emit X-Ray fluorescent radiation with discrete energies. These values are characteristic for each element, so in this way qualitative analysis is achieved. The quantitative analysis is related to intensity of these discrete energies. The mechanisms which take place on microscopic scale of samples are photoelectric interaction and production of characteristic radiation. When a photon with appropriate energy collides with an electron of some atomic layers, this electron will be ionized and will drop out of the atom. The empty position will be covered by an electron from an external atomic layer and the atom will return at ground state. Due to the difference of energy between the two layers, electron transport leads to photon emission. An atom can generate up to one discrete energy because of multiple combinations between empty positions and transfer electron. The energy values are characteristic of an atom and their set constitutes the spectral fingerprint of an element.

4.3.3.2. Epsilon 5 PANalytical

A classic X-Ray fluorescence spectroscope consists of X-Ray tube, sampler and detector. X-Ray fluorescence spectroscopes are divided into two major categories: ED-XRF (Energy Dispersive X-ray Fluorescence) and WD-XRF (Wavelength Dispersive X-ray Fluorescence). The filters from both Aristotelous and Demokritos sites were analyzed by energy dispersive XRF Epsilon 5 (PANalytical), which is operating in the department of Nuclear and Particle Physics in NCSR "Demokritos" (*Figure 15*). The analytical system combines a unique energy dispersive XRF spectrometer with instrument control and analysis software. An ED-XRF spectrometer directly determines the energies of X-Rays in the spectrum and a range of elements, from sodium (Na) to uranium (U) can be analyzed. The elements with higher atomic number have better detection limits.

Figure 15: ED-XRF Epsilon 5 PANalytical, "Demokritos" Laboratory.

ED-XRF technique uses 3D-geometry spectroscope with secondary targets, which emit almost monochrome radiation. The major advantage of Epsilon 5 is the use of these secondary targets between the tube and the sample (*Figures 16 and 17*).
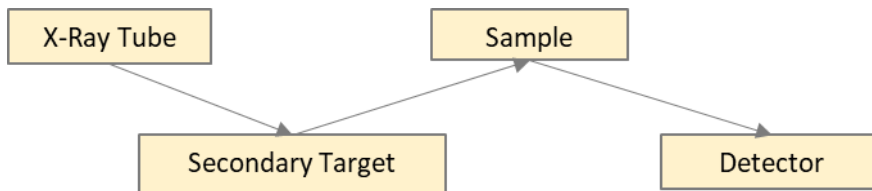
Figure 16: 3D-geometry spectroscope with secondary targets of ED-XRF Epsilon 5 PANalytical.
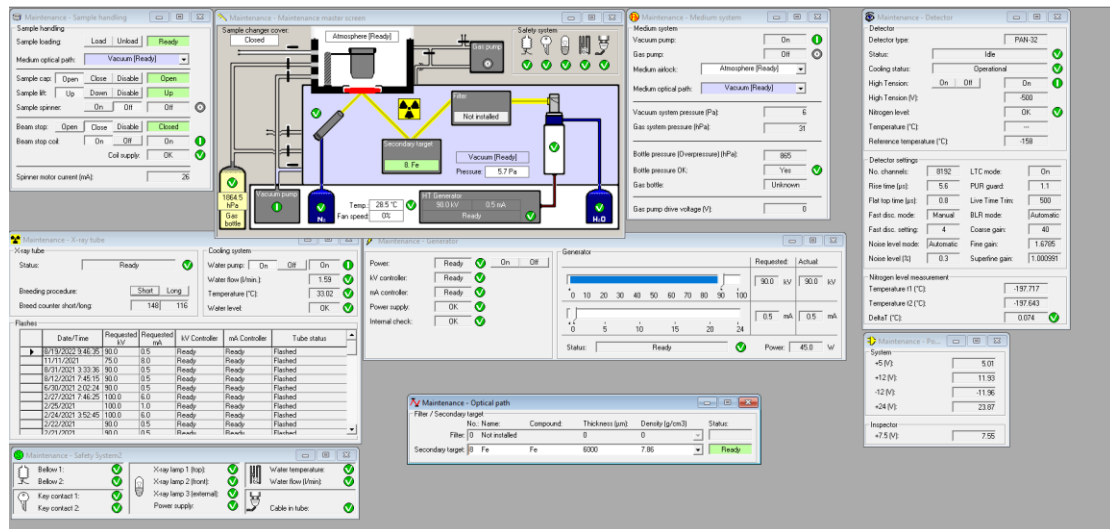
Figure 17: Software of Epsilon 5 PANalytical.

33

The choice of secondary target depends on the materials under study. In most cases, six different secondary targets are used and each of them is selected for the analysis of materials with smaller atomic number. This choice is based on the requested radiation which an electron of the element needs in order to get stimulated. The characteristic X-Ray radiation which is transmitted by the secondary target, facilitates quantitative and qualitative analysis of requested elements compared to X-Ray radiation of tube, due to the elimination of phenomenon Bremsstrahlung, and therefore, secondary targets succeed in decreasing detection limits and providing better observation of elements concentration.

Bremsstrahlung is a phenomenon that occurs when a charged particle (such as an electron) is decelerated or slowed down by the Coulomb field of an atomic nucleus. When this happens, the electron loses energy and emits a photon of X-ray radiation, with a continuous spectrum of energies up to the energy of the original electron. In X-ray physics, Bremsstrahlung radiation can be a significant source of background radiation and can limit the sensitivity and detection limits of X-ray fluorescence (XRF) analysis. When X-rays are used to excite a sample, the primary X-ray beam interacts with the sample and generates fluorescence X-rays that are characteristic of the elements present in the sample. However, some of the primary X-ray photons can interact with the sample and be scattered or absorbed, producing a continuum of background radiation. This background radiation can interfere with the detection of the fluorescence X-rays and increase the noise in the measurement.

Prototype filters are analyzed, for the instrument calibration (F*igures 18 and 19*). In this way, the optimal linear correlation between the intensity of characteristic radiation and concentration of each element is formed. The elemental concentrations are quantified based on these graphs (*Papagiannis, S., 2022*).

Figure 18: Prototype filters for ED-XRF Epsilon 5 PANalytical calibration.
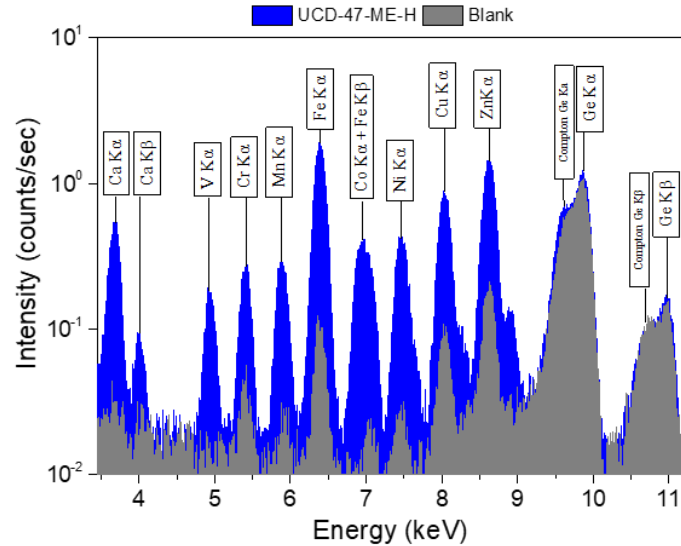
Figure 19: XRF spectrum obtained by the benchtop spectrometer (Epsilon 5) for reference material UCD-47-ME-H using the Ge secondary target (75 kV, 8 mA, 400 s). The blue colored area represents the reference material and the grey the blank Teflon filter (Chatousidou et al., 2022).

The Epsilon 5 mainly includes the following parts:

   I.   X-Ray Tube

An X-Ray tube consists of a metallic filament line (cathode) and a metallic target (anode). The metallic filament line is heated and thermionic electrons are produced. Imposing a potential difference between cathode and anode, electrons are accelerated and are concentrated on the anode. X-Ray emissions are due to the following electrons deceleration. At the same time, atoms of the metallic target are ionized and characteristic X-Ray radiation is emitted. This radiation is used for ionization of the requested elements. An element can emit X-Ray radiation, only if the value of X-Ray photons energy is higher than this of binding energy of atom internal electrons. The high value of voltage which is applied on X-Ray tube of Epsilon 5 facilitates this X-Ray radiation of requested elements. The X-Ray tube is side-scuttles type and liquid-cooled.

   II.   Detector

The intensity of photons is recorded as a function of energy. When a photon enters the detector, it produces an electric pulse proportional to the characteristic radiation of photon. These electric pulses are strengthened and are measured, so the characteristic spectrum is formed. In X-Ray fluorescence spectroscopy, the detectors are solid-state. Epsilon 5 uses a Ge-detector with energy resolution of about 150 eV FWHM. Ge-detector is cooled by liquid nitrogen. The number of electrons which are produced depend on the energy of incoming photon. The higher the energy is, the more electrons can be produced. The outlines of photon detection system are energy resolution, efficiency, velocity response and spatial resolution.

Given the different filter material of the Aristotelous and Demokritos samples (quartz versus Teflon), a different set of elements was detected in each site, with varying detection limits, as shown in *Table 4*.

35

Table 4: A list of all elements measured at each site and the corresponding detection limit.

Element	Teflon Filters UB site	Quartz Filters UT site
	LODs (ug/m3)	LODs (ug/m3)
Na	0.010	0.017
Mg	0.004	0.009
Al	0.006	0.074
Si	0.006	0.020
P	0.002	0.004
S	0.001	0.002
Cl	0.001	0.001
K	0.001	0.001
Ca	0.001	0.003
Ti	0.001	0.002
V	0.000	0.001
Cr	0.000	0.001
Mn	0.001	0.002
Fe	0.001	0.002
Co	0.001	0.002
Ni	0.000	0.001
Cu	0.001	0.001
Zn	0.001	0.002

Element	Teflon Filters UB site	Quartz Filters UT site
	LODs (ug/m3)	LODs (ug/m3)
Ga	0.001	0.001
Ge	0.001	0.001
As	0.000	0.001
Br	0.001	0.003
Rb	0.001	0.002
Sr	0.001	0.002
Ag	0.005	0.011
Cd	0.005	0.012
Sn	0.003	0.005
Sb	0.004	0.007
Cs	0.012	0.026
Ba	0.014	0.030
Ce	0.018	0.037
Pt	0.002	0.005
Au	0.002	0.004
Hg	0.005	0.010
Pb	0.002	0.005

5. Source apportionment (Positive Matrix Factorization –PMF)

5.1. General

Source apportionment is the identification of major emissions sources of a pollutant – for example particulate matter – and the quantification of their contribution to the total measured concentration. Many source apportionment techniques have been developed, but receptor modelling is one of the most common. Receptors models are mathematical approaches which quantify the contribution of emissions sources based on the chemical composition or fingerprints of sources. The database can be shown as a matrix X of i by j dimensions, in which there are i number of samples and j number of measured chemical species. Receptor models aim to solve the chemical mass balance equation between concentrations of chemical components and source profiles, as shown below:

$$x_{ij} = \sum_{k=1}^{N} g_{ik} f_{kj} + e_{ij} \qquad [5.1]$$

where N is the assumed number of sources, x_{ij} is the concentration of each PM chemical component in sample i, g_{ik} is the contribution of source k to sample i, f_{kj} is the relative concentration of species j to the chemical profile of source k and e_{ij} is the residual for species j of sample i.

Residuals represent the difference between measured and modelled concentrations for each species j of sample i. Scaled residuals (r_{ij}) is the residuals scaled by uncertainty. For a good fit, a given species should have a normal distribution of scaled residuals between -3 and +3, as it is shown below (*Figure 20*).
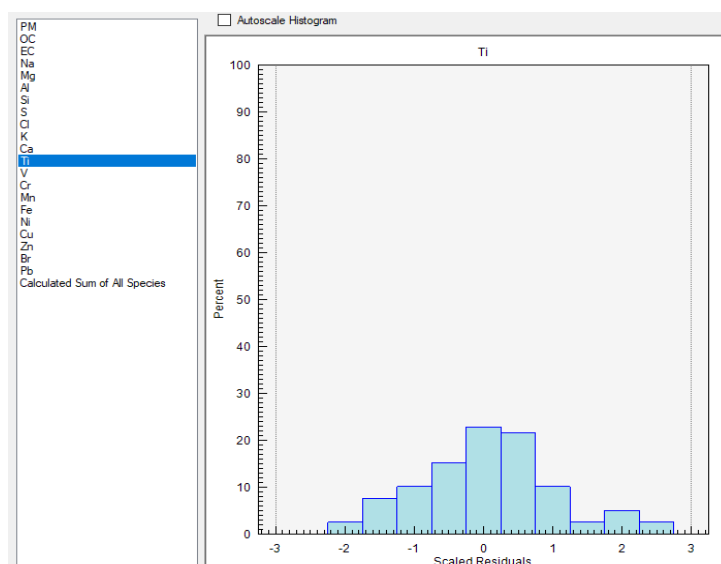
Figure 20: Normal distribution of scaled residuals of Ti.

Also, the variability between solutions which are produced by different runs, is estimated based on scaled residuals. For the control, two parameters are calculated. The sum of the squares of the differences in scaled residuals for each base run pair by species (d_{ij}) and the sum of d across all species for each base run pair (D):

$$d_{ij} = \sum_i d_{jkl} \cdot \left(r_{ijk} \cdot r_{ijl} \right) \qquad [\mathbf{5.2}]$$

$$D_{kl} = \sum_j d_{jkl} \qquad [\mathbf{5.3}]$$

where k and l are two different runs.

Positive matrix factorization (PMF) is a multivariate receptor model which derives factor contributions and profiles of sources minimizing the objective equation Q:

$$Q = \sum_{i=1}^n \sum_{j=1}^m \left(\frac{x_{ij} - \sum_{k=1}^N g_{ik} f_{kj}}{u_{ij}} \right)^2 \qquad [\mathbf{5.4}]$$

where u_{ij} is the uncertainties of species.

PMF decomposes a matrix of sample data into two matrices, factor contributions (G) and factor profiles (F). According to equation [5.4], PMF results are based on a weighted Least Squares fit, where known standard deviations of the input concentrations data are used for measuring the weights of the residuals e_{ij}. PMF solution satisfies the constraints of non-negativity for matrix F and non-significant negativity for matrix G.

Q-value is a critical parameter for PMF analysis, and two versions are derived for the model runs. The first one is the Q-true which is the goodness-of-fit parameter and is calculated including all data points. The second one is the Q-robust, and is calculated excluding the data points with scaled residual greater than ±4. The difference between these two values of Q is a measure of impact of data points with high scale residuals and can be related with peak impacts from sources that are occasionally present during the sampling period (*Diapouli, E., 2016*). Also, a theoretical or expected Q-value is calculated as the number of points in the data matrix minus the total number of elements in the factor matrix:

$$Q - theoritical = n \cdot m - N \cdot (m + n) \qquad [\mathbf{5.5}]$$

where n is the number of samples, m is the number of species and N is the number of obtained factors.

5.2. EPA PMF 5.0

One of the most common PMF models is the EPA PMF; in its latest version (EPA PMF 5), two additional error estimation methods and application of constraints in source contributions and profiles have been added.

The determination of the optimal PMF solution requires multiple iterations of the underlying Multilinear Engine (*Figure 21*). According to Multilinear Engine algorithm, it starts the search for the factor profiles with a randomly generated factor profile. For each factor, the optimal path to the best-fit solution is achieved by using the conjugate gradient approach. In detail, a multidimensional space is contracted by observations and then the model using the conjugate gradient approach, reaches its final destination of the best solution along this path. The lowest value of Q-robust along the path is related to the best solution. This value corresponds to a deep point in the multidimensional space. But it is not certain that point is the deepest (global minimum), because of the random nature of the starting point and the dictated path. So, the model should be run 20 times developing a solution and 100 times for the final solution each time with a different starting point. In this way the chance of reaching the global minimum is maximized (*Brown, St. and Bai, S., 2014*).
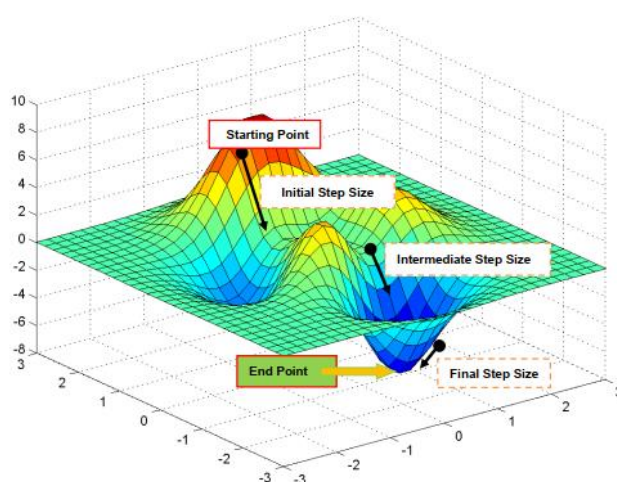
Figure 21: Conjugate Gradient Method – underpinnings of PMF solution search (Brown, St. and Bai, S., 2014).

In addition, the variability of Q-robust values among different runs is related to the variability of the initial base run results due to the random seed used to start the gradient algorithm in different locations. So, in the case that starting point and space influence the path to the minimum, the Q-robust values will vary. Three methods are used to estimate the variability of PMF results.

- The first one is the Bootstrap (BS) analysis and is used to determine the relevance between a small set of observations and the final solution. Random errors and partial effects of rotational ambiguity constitute the bootstrap error intervals. Rotational ambiguity is due to the development of infinite solutions which are similar to the solutions of PMF runs. Bootstrap errors are not influenced by the sample uncertainties which are specified by the users.

- The second one is the Displacement (DISP) analysis and includes the selected solution and its sensitivity to small variations. Only rotational ambiguity affects the

displacement error intervals, and they can be directly influenced by data uncertainties. For this reason, the intervals for down-weighted species may be large.

- The last one is the Bootstrap-Displacement (BS-DISP) analysis and includes both effects of random errors and rotational ambiguity.

Effects of rotational ambiguity of the solution can be assessed by G-space plots. These plots compare the contribution between two different factors and a possible relationship of them (*Figure 22*).
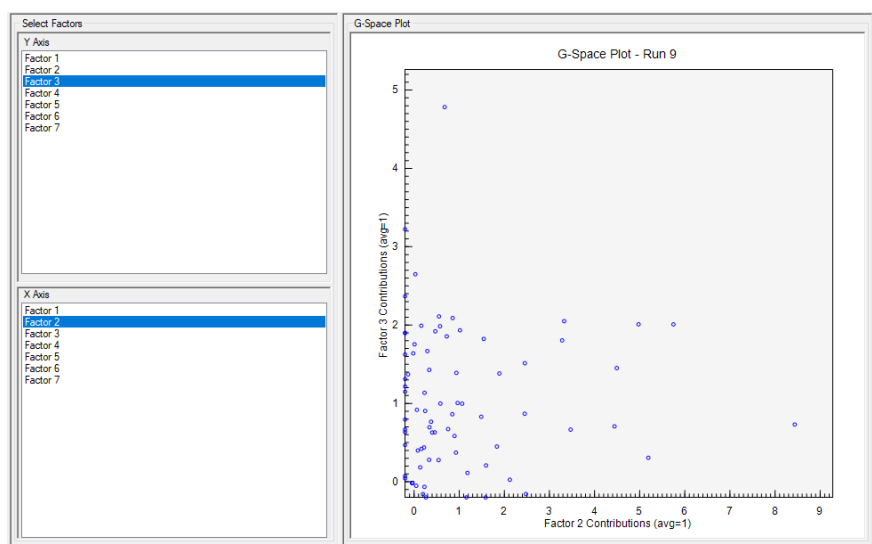
Figure 22: G-space plots of two different factors without a possible relationship between them.

F-peak is a useful tool to examine different rotations of the solution. The solution is considered as the "real" solution when matrices of profiles (matrix F) and contributions (matrix G) display a significant number of zero values. In the case that F-peak values are positive, the matrix F is sharpened and the matrix G is smeared, because the solution shows many near zero values in the matrix F and as many as possible large values. Correspondingly, negative F-peak values force towards solution with a sharpened matrix G and a smeared matrix F.

5.3. Preparation of input data
The input data in the PMF model are the concentration values of $PM_{2.5}$ and chemical components, as well as their uncertainties. The expanded uncertainty (including sampling and analytical uncertainties) was calculated for all input data.

5.3.1. Outliers and missing values
Extreme or missing values are examined as a preliminary analysis, so a correct database will be formed. High values of $PM_{2.5}$ concentration may result either from measurement or analysis error or a real event. Some of these extreme conditions could be related to large-scale forest fires, volcano eruptions or intense dust events. In this study, high concentration values were examined for possible association with dust events. In addition, missing or invalid values of $PM_{2.5}$ and chemical components concentration were replaced by the seasonal

median for each site. The uncertainty for these values was set as 4 times the concentration. The missing values increase the uncertainty of source apportionment solution (*Diapouli, E., 2016*).

5.3.2. Below detection limit values

Below detection limit values may correspond to zero or near zero values of concentration. In the case of uncertainties, zero or negative values should be substituted, because they have no physical meaning. A commonly used practice is to replace the below detection limit values with $^1/_2$ of the detection limit and uncertainties with $^5/_6$ of the detection limit (*Polissar, A.V., 1998*). A species is excluded by the PMF analysis, if it has a large fraction of below detection limit values, since it does not display real variability and cannot provide useful information on sources.

5.3.3. $PM_{2.5}$ chemical components and mass balance

As most of the major PM components have been quantified, a comparison between PM mass and the sum of masses of compounds was attempted. This mass balance approach can be considered as a preliminary source apportionment: The PM mass is distributed to categories depending on types of species or relevant sources. The major categories are carbonaceous component, mineral mass, sea salt, secondary inorganic species and trace metals. The mass balance analysis was conducted for each site separately, and both for the whole measurement period, as well as separately for cold and warm period of the year (*Diapouli, E., 2016*).

5.3.3.1. Carbonaceous component

$PM_{2.5}$ consist of a significant fraction of carbonaceous aerosol. The total amount of carbonaceous content is divided into an organic carbon and an elemental carbon fraction. As organic and elemental carbon play a key role in climate and human health effects of aerosol, the knowledge of their origin is important. Elemental carbon can be emitted from the burning of carbonaceous matter and is mainly divided into the amount emitted by fossil fuel combustion (EC_{ff}) and by biomass burning (EC_{bb}). Most of EC_{ff} emissions are due to road transport, so its concentration is high near the urban sites. EC_{bb} emissions are mainly recorded in winter in rural or residential sites and during wild fire events. On the other hand, organic carbon has both primary and secondary origin. It can be emitted directly in the atmosphere as particles (primary origin) or formed from gas-to-particle conversion processes in the atmosphere (secondary origin). Primary organic carbon is emitted from fossil fuel combustion (OC_{ff}), biomass burning (OC_{bb}) and/or represent biological particles or plant debris (OC_{bio}).

For the mass balance calculation, the sum of concentration of organic and elemental carbon is used. Organic carbon is found in the atmosphere in the form of a great variety of organic compounds. In order to account for the mass of the remaining elements in organic compounds (e.g. hydrogen, oxygen, nitrogen), OC is multiplied by an empirical coefficient factor, to be converted to organic mass (OM). This factor estimates the organic molecular weight per carbon weight. It can range between 1.3 to 2.1, based on the type of site and/or aerosol. For this analysis, the value of coefficient $\left(\frac{OM}{OC}\right)$ was set to 1.7 from the urban-background site and

1.3 from the traffic site (*Salameh et al., 2015 and Diapouli et al., 2017*). The lower the value of this coefficient is, the more immediate and less oxidized are the emissions of organic carbon in this site. The amount of carbonaceous component was calculated as shown below (*Diapouli, E., 2016*).

$$\text{Carbonaceous components} = \frac{\text{OM}}{\text{OC}} \cdot \text{OC} + \text{EC} \qquad [\textbf{5.6}]$$

5.3.3.2. Mineral mass

The mineral mass is mainly found in coarse mode, but it influences $PM_{2.5}$ too. Mineral elements are found mainly in the form of their oxides, so the missing mass should be again taken into consideration through compensating factors. The missing mass of oxygen is found through stoichiometry. For the urban-background station, the following equations are used for the calculation of mineral mass based on sea salt (ss) and no sea salt (nss) concentration of several elements (*Diapouli, E., 2016*).

$$\text{Mineral mass} = 1.35 \cdot [\text{nssNa}] + 1.66 \cdot [\text{Mg} - \text{ssMg}] + 1.89 \cdot [\text{Al}] + 2.14 \cdot [\text{Si}] + 1.2 \\ \cdot [\text{K} - \text{ssK}] + 1.95 \cdot [\text{Ca} - \text{ssCa}] + 1.67 \cdot [\text{Ti}] + 1.43 \cdot [\text{Fe}] \qquad [\textbf{5.7a}]$$

$$[\text{nssNa}] = 0.348 \cdot [\text{Al}] \qquad [\textbf{5.7b}]$$

$$[\text{ssMg}] = 0.119 \cdot [\text{ssNa}] \qquad [\textbf{5.7c}]$$

$$[\text{ssK}] = 0.037 \cdot [\text{ssNa}] \qquad [\textbf{5.7d}]$$

$$[\text{ssCa}] = 0.038 \cdot [\text{ssNa}] \qquad [\textbf{5.7e}]$$

where nssNa is referred to non-sea salt Na concentration and ssMg, ssK, and ssCa are referred to sea salt concentration of Mg, K, and Ca correspondingly.

In the case of the urban-traffic station, Al and Si could not be measured due to the use of quartz filters; so the above equations were modified, through the use of $\frac{\text{Ti}}{\text{Al}}$ and $\frac{\text{Si}}{\text{Ti}}$ ratios found in the literature for the composition of Earth's crust (*Masson 1966*):

$$\text{Mineral mass} = 1.35 \cdot [\text{nssNa}] + 1.66 \cdot [\text{Mg} - \text{ssMg}] + 1.89 \cdot \frac{[\text{Ti}]}{0.054} + 2.14 \cdot 63.15 \cdot [\text{Ti}] \\ + 1.2 \cdot [\text{K} - \text{ssK}] + 1.95 \cdot [\text{Ca} - \text{ssCa}] + 1.67 \cdot [\text{Ti}] + 1.43 \\ \cdot [\text{Fe}] \qquad [\textbf{5.8a}]$$

$$[\text{nssNa}] = 0.348 \cdot \frac{[\text{Ti}]}{0.054} \qquad [\textbf{5.8b}]$$

and [ssMg], [ssK] and [ssCa] calculated as shown above in equations [5.7c] – [5.7e].

5.3.3.3. Sea salt

The contribution of sea salt to the total aerosol mass depends on the distance between the sampling site and the sea. Sea salt is found mainly in the coarse mode (*Pérez et al., 2008*). Sea salt contribution is calculated based on standard sea water concentration. It is considered that the total amount of chlorine comes exclusively from sea salt. Sea salt Na (ssNa) concentration is calculated through the non-sea salt fraction, which corresponds to Na found in the mineral dust. Non-sea salt Na (nssNa) can be estimated using typical ratios between Na and mineral components, found in the literature for the Earth's crust. In this study, the crustal ratio which is used is Na/Al = 0.348. The sea salt mass occurs as the following condition in excel for Demokritos and Aristotelous site respectively:

$$[ssNa] = if\ ([Na] < 0.348 \cdot [Al];\ 0\ ;[Na] - 0.348 \cdot [Al]) \qquad [\mathbf{5.9a}]$$

$$[ssNa] = if\ \left([Na] < 0.348 \cdot \frac{[Ti]}{0.054};\ 0\ ;[Na] - 0.348 \cdot \frac{[Ti]}{0.054}\right) \qquad [\mathbf{5.9b}]$$

In addition to this, sea salt mass has further contributions from Mg, K, Ca and SO_4^{2-}, which are calculated based on typical sea-water ratios of these species with ssNa. So, the total concentration is calculated through the following equation (*Diapouli, E., 2016*).

$$Sea\ salt = [ssNa] +\ [Cl] + [ssMg] + [ssK] + [ssCa] + [ssSO_4^{2-}] \qquad [\mathbf{5.10a}]$$

$$[ssSO_4^{2-}] = 0.253 \cdot [ssNa] \qquad [\mathbf{5.10b}]$$

and [ssMg], [ssK] and [ssCa] calculated as shown above in equations [5.7c] – [5.7e].

5.3.3.4. Secondary inorganic aerosol

The total secondary inorganic mass contains contributions from $nssSO_4^{2-}, NO_3^-, NH_4^+$. Since ion analysis was not conducted in this study, the only available contribution in secondary inorganic aerosol is $nssSO_4^{2-}$. The equation used to quantify $nssSO_4^{2-}$ is shown below:

$$[nssSO_4^{2-}] = [S] \cdot \frac{MB_{SO_4^{2-}}}{MB_S} - 0.253 \cdot [ssNa] \qquad [\mathbf{5.11}]$$

5.3.3.5. Trace elements

Trace elements mass includes the remaining metals, which contribute to PM mass. The values of V and Ni are mostly related to fuel oil combustion, while the levels of Mn, Ba, Cu, Zn, Sb and Sn may be related to non-exhaust traffic emissions (e.g., brake and tire wear). Elements

associated with high temperature industrial processes – such as As, Cd and Pb – and those which are emitted from fuel oil combustion exist in very fine mode. In the coarse fraction tend to contribute materials which is related to road dust, constructions, and demolition – such as crustal components – or associated with road traffic abrasion products – such as Sb, Cu, Mn, Cr, Co, Sn, Ba, Bi, Se and Zn (Pérez et al., 2008).

5.3.3.6. Unaccounted mass

It is known that the sum of masses of all previous fractions is lower than PM mass. The unaccounted mass is related to the uncertainties concerning the estimation of organic and mineral fraction through respective measured concentrations. Furthermore, the samples absorb water and include ions, which are not quantified by available in the present study chemical analyses.

5.3.4. Final selected conditions

The missing species or species with concentrations below detection limit values for less than 50% of total samples, are included in the PMF analysis. The signal-to-noise (S/N) ratio was used to identify species that add uncertainty to the solution and need to be down-weighted (defined as "weak" species). S/N ratio is defined as the desired signal power to the background noise power. This calculation intends to address the artificially low S/N ratio because of high uncertainty values or slightly negative concentration values. So, data with concentration above uncertainty have non-negative signal, whereas data with concentration below uncertainties is considered that have no signal. This value of signal (d_{ij}) depends on x_{ij} (the concentration of species j of sample i) and u_{ij} (the corresponding uncertainty), as shown below (*Diapouli, E., 2016*).

$$d_{ij} = \frac{x_{ij} - u_{ij}}{u_{ij}} \qquad [\mathbf{5.12}]$$

So, the S/N ratio is calculated through the following equation:

$$\left(S/N\right)_j = \frac{\sum_{i=1}^{n} d_{ij}}{n} \qquad [\mathbf{5.13}]$$

Based on S/N ratio, a species is characterized as "weak" when $0.5 \leq S/N < 1$ and as "bad" when $S/N < 0.5$. The "weak" species are used in the analysis, but it is necessary to be down-weighted. The "bad" species are not taken account into PMF analysis. During this choice, the number of samples with missing or below detection limit values and the importance of some species as source tracers should be taken into account.

Also, the sum of the squares of the differences in scaled residuals for each base run pair by species (d) and the sum of d's across all species for each base run pair (D) are two important factors, resulting from residual scaled analysis. The first matrix should have as many as possible near zero elements. If this is not satisfied for some run pairs, the elements with more influence on these run pairs are examined through the D matrix. These elements are selected as "weak" species and their influence on the matrix d is recorded. An example of the influence of elements on matrix d is shown below (*Figure 23*).

(a)

(b)

Figure 23: A part of scaled residual analysis during PMF analysis. (a) The matrix d has no near negative elements and the strong influence of some elements is shown on the matrix D. (b) In matrix d, only six runs are problematic and none of the elements influence the matrix D.

In addition, constraints in the factor profiles or contributions are used, so the solution better represents the "real sources" (*Figure 23b*). For each selected constraint, a limit of change in the Q-value is permitted. This limit of % dQ is defined equal to 0.5. The constraint solution is controlled through error estimation – DISP, BS and DISP-BS – similar to the Base Run solution.

In this study, the EPA PMF 5.0 model was execute for the combined database of traffic and urban background sites, in order to allow for a direct comparison of the different source contributions to $PM_{2.5}$ levels observed at the two sites. In addition, the model was run separately for the traffic and urban background site. This analysis was used in order to explore the impact of the input data in the PMF solution and assess the differences and similarities in the source profiles obtained for the traffic and urban background site. In all cases, the model was initially run for a different number of sources/factors (varying between 4 and 10 factors). An extra modeling uncertainty of 5 % was added in all runs, because of the variation of source profiles in time and chemical transformations from source to receptor.

The best solution was identified through the use of key performance indicators, including the lowest Q values, distribution of scaled residuals, and fit of measured PM concentrations, as well as by assessing the physical meaning of the obtained source profiles and contributions. An additional statistical tool was used in order to support our choice, based on the scaled residual matrix of the solutions. The selection of the number of sources is crucial in PMF analysis, since using too few factors will combine different emission sources together, while using too many factors will lead to dissociation of a real factor into two or more non-existing sources. The ambiguity of random judgment is reduced using the scaled residual matrix (R). Each element in a matrix R is:

$$r_{ij} = \frac{e_{ij}}{s_{ij}} \qquad [\mathbf{5.14}]$$

where s_{ij} is the standard deviation and e_{ij} is the residual for sample i of species j.

Each column in matrix R represents the quality of the fitting of each species to the product of matrix GxF. The maximum individual column mean (IM) and the maximum individual column standard deviation (IS) are two parameters of matrix R, which may be calculated for each number of factors, as it is shown below (*Lee et al., 1999*):

$$IM = \max_{j=1....m} \left(\frac{1}{n} \sum_{i=1}^{n} r_{ij} \right) \qquad [\mathbf{5.15}]$$

$$IS = \max_{j=1....m} \left(\sqrt{\frac{1}{n-1} \sum_{i=1}^{n} (r_{ij} - \bar{r}_j)^2} \right) \qquad [\mathbf{5.16}]$$

These indicators drop drastically at the same time, when the number of factors increases to a critical value. This method constitutes an approach of the "real" solution, reducing the influence of a manual choice.

In the current study, the number of sources was identified based on parameters IM and IS, taking into account also the physical meaning of the obtained sources/factors. For example, as it is shown in *Figure 24*, at the urban background site, the drop in IM value points towards a solution with at least 6 factors, while IS drops at 7 factors and more drastically at 9 factors. By examining the source profiles of the obtained solutions for 7, 8 and 9 factors, we concluded that the 7-factor solution provided better defined source profiles, in terms of the physical meaning of these factors.
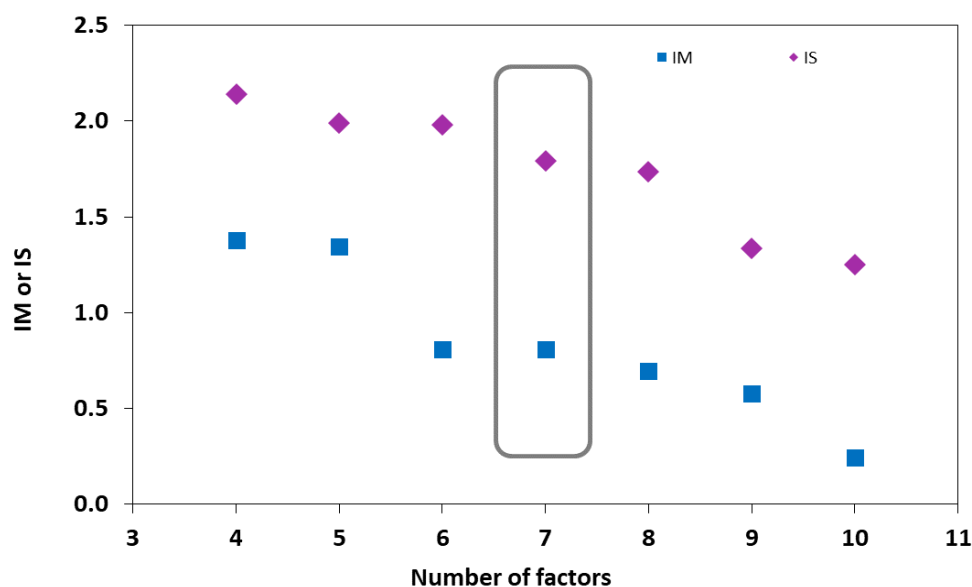
Figure 24: Determination of the number of factors by: (a) maximum individual column mean (IM) and (b) standard deviation (IS) of standardized residuals.

The final solutions were based on 100 runs, while the uncertainty of the solutions was assessed by implementing the bootstrapping and displacement error estimation tools provided by EPA PMF 5.0. The final selected input data and constraints options for the analysis of the two different sites separately and for the combined database are shown in the following *Table 5*.

Table 5: The total selected parameters for the PMF analysis of two sites together and of each site separately (dQ must be smaller than 0.5 for each constraint).

UT – UB sites	
Number of factors: 7	
Species	Category
PM	Strong
OC	Strong
EC	Strong
Na	Strong
Mg	Strong
S	Strong
Cl	Strong
K	Strong
Ca	Strong
Ti	Strong
V	Weak
Cr	Strong
Mn	Strong
Fe	Strong
Ni	Strong
Cu	Strong
Zn	Strong
Br	Strong
Sn	Bad
Sb	Bad
Ba	Strong
Pb	Strong

Constraints		
Factor	Element	Type
Secondary	Na	Pull Down Maximally
Secondary	K	Pull Down Maximally
dQ		0.291

(a)

UT site	
Number of factors: 7	
Species	**Category**
PM	Strong
OC	Strong
EC	Strong
Na	Strong
Mg	Strong
S	Weak
Cl	Weak
K	Strong
Ca	Strong
Ti	Strong
V	Weak
Cr	Strong
Mn	Strong
Fe	Strong
Ni	Strong
Cu	Strong
Zn	Strong
Br	Strong
Sr	Strong
Sn	Bad
Sb	Bad
Ba	Strong
Pb	Strong

Constraints		
Factor	**Element**	**Type**
Sea salt	Na	Pull Up Maximally
Sea salt	Cl	Pull Up Maximally
Biomass burning	Cl	Pull Down Maximally
dQ		0.691

(b)

UB site	
Number of factors: 7	
Species	**Category**
PM	Strong
OC	Weak
EC	Strong
Na	Strong
Mg	Strong
Al	Strong
Si	Strong
S	Strong
Cl	Weak
K	Strong
Ca	Strong
V	Strong
Cr	Strong
Mn	Strong
Fe	Strong
Ni	Strong
Cu	Strong
Zn	Strong
Br	Strong
Sn	Bad
Sb	Bad
Ba	Strong
Pb	Strong

Constraints		
Factor	**Element**	**Type**
Secondary	EC	Set to zero
Soil	EC	Set to zero
dQ		0.141

(c)

6. Results and discussion

6.1. PM mass and chemical composition

The daily variation of particulate mass concentration at the Athens' urban background (UB) and traffic site (UT) for the period of sampling is shown in the *Figure 25*. The measured mean values of PM concentration are 10.5 ± 6.2 $\frac{\text{ug}}{\text{m}^3}$ and 22.9 ± 11.6 $\frac{\text{ug}}{\text{m}^3}$ at urban background and traffic site respectively. The average $PM_{2.5}$ mass concentration levels measured at Demokritos site are in agreement with the results reported for the same site by Taghvaee et al. (2019) (11.4 ± 4.4 $\frac{\text{ug}}{\text{m}^3}$ during 06-09/2017 and 02-03/2018) and by Vasilatou et al. (2017) (16 ± 6 $\frac{\text{ug}}{\text{m}^3}$ during 01-06/2008). In addition, the average $PM_{2.5}$ mass concentration at Aristotelous site is slightly lower than those of previous studies conducted at traffic sites (37.7 ± 15.7 $\frac{\text{ug}}{\text{m}^3}$ in Thessaloniki during June 2011 to May 2012 and 39.7 $\frac{\text{ug}}{\text{m}^3}$ in Athens during 06/1999-05/2001) (*Tolis et al., 2015; Chaloulakou et al., 2005)*. The mean annual $PM_{2.5}$ concentrations measured at the two sites are both lower than the respective EU annual limit value (25 $\frac{\text{ug}}{\text{m}^3}$). The highest values of $PM_{2.5}$ concentrations are observed at urban traffic site during cold period (*Figure 25*). Given the distinct character of the two sites, it is expected that they are influenced on a different scale by emission sources, which is also reflected in the variability of the PM concentration (*Figure 26).* In addition, mean 24 h $PM_{2.5}$ concentrations in urban-background site are compared with those in traffic site (*Figure 27).* The increased particulate matter concentration at the traffic site can be related to intense road traffic and emissions of residential heating from the densely populated city center. On the other hand, at the urban background site, the levels are lower, due to decreased anthropogenic activities.
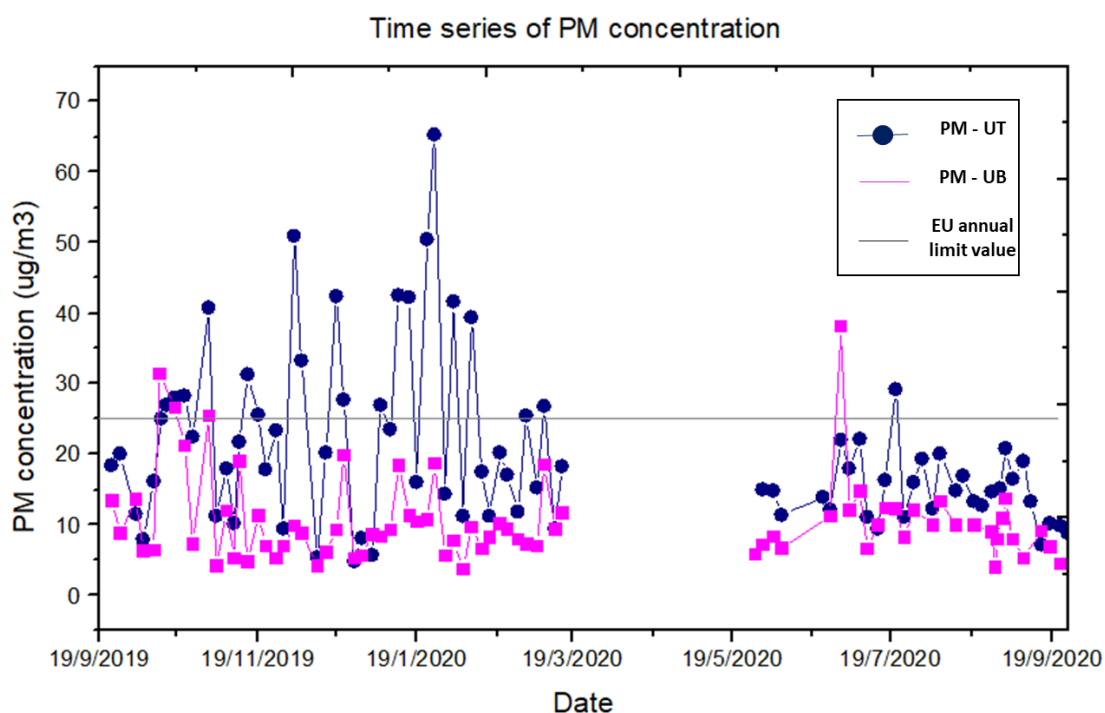
Figure 25: Time series of $PM_{2.5}$ concentration $\left(\frac{ug}{m_3}\right)$ in UT and UB sites. The EU annual limit value is 25 $\frac{ug}{m^3}$.
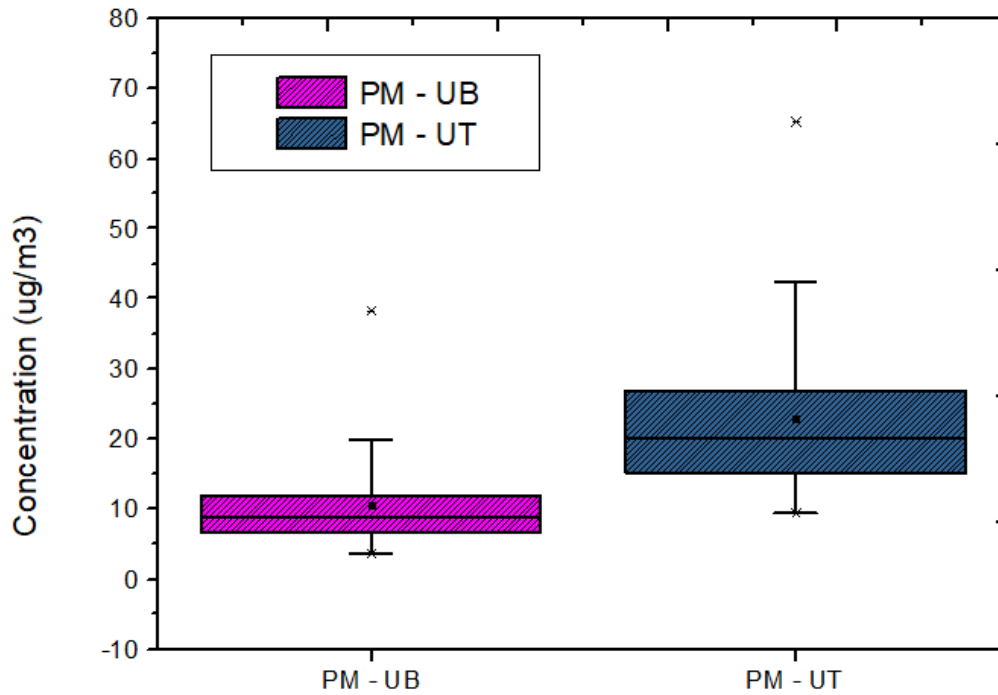
Figure 26: Box plots of $PM_{2.5}$ concentration $\left(\frac{ug}{m_3}\right)$ in UT and UB sites.

PM2.5

$y = 0.18x + 6.80$
$R^2 = 0.11$
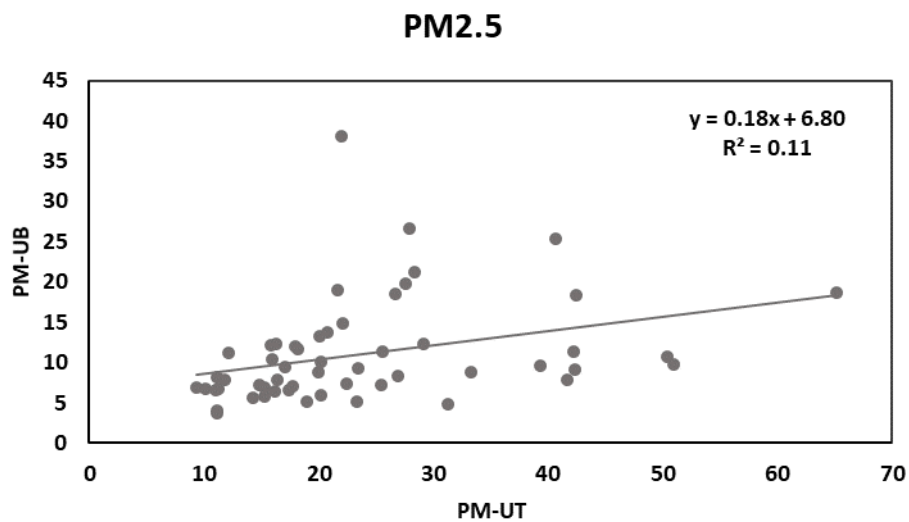
Figure 27: Comparison between the mean 24 h $PM_{2.5}$ concentration $\left(\frac{ug}{m_3}\right)$ measured at the two sites.

The concentration levels of organic (OC) and elemental carbon (EC) measured at the two sites are shown in *Figure 28*. OC is both of primary and secondary origin. Organic carbon can be derived from biomass burning, fossil fuel combustion, formed from gas-to-particle conversion processes in the atmosphere or represent biological particles and plant debris, whereas elemental carbon relates only to primary emissions from different combustion processes (such as biomass burning and road transport). As it is shown in *Figure 28,* the levels of carbon

mass concentration are increased at the traffic site due to the presence of more intense anthropogenic sources. The measured organic carbon mass concentration is found at 7.3 ± 3.0 $\frac{ug}{m^3}$ and $2.1 \pm 0.9 \frac{ug}{m^3}$, whereas elemental carbon mass concentration is equal to $1.9 \pm 1.4 \frac{ug}{m^3}$ and $0.3 \pm 0.1 \frac{ug}{m^3}$, in traffic and urban background site respectively. In a study which was conducted in the city center of Thessaloniki, Greece in 2011-2012, the average organic carbon mass concentration was $6.6 \frac{ug}{m^3}$ and the respective elemental carbon mass concentration was $1.3 \frac{ug}{m^3}$ (*Tolis et al., 2015*). Also, at the urban background site, the observed carbon levels are similar to the results reported in a recent study at the National Observatory of Athens, Greece, in which the corresponding carbon levels were $2.1 \pm 1.3 \frac{ug}{m^3}$ and $0.5 \pm 0.4 \frac{ug}{m^3}$ (*Paraskevopoulou et al., 2014*). As it is shown in *Table 6*, OC and EC concentrations are higher during the cold period at UT site. The UB site displays significantly higher values during the cold period only for EC concentrations. In the wintertime, an additional carbon source is the residential heating. Moreover, we should consider that most of the warm period corresponds to months when the COVID-19 pandemic was already underway, and the mitigation measures adopted by the government against the spread of the disease may have impacted the intensity of anthropogenic activities, including vehicular traffic. OC concentrations do not display significantly different values between the two seasons in the UB site, which may be due to the intensification of the atmospheric oxidation processes, due to increased solar radiation; secondary aerosol formation is known to affect significantly PM levels at this site, especially in the base of fine particle concentrations (*Manousakas et al., 2021*).

.
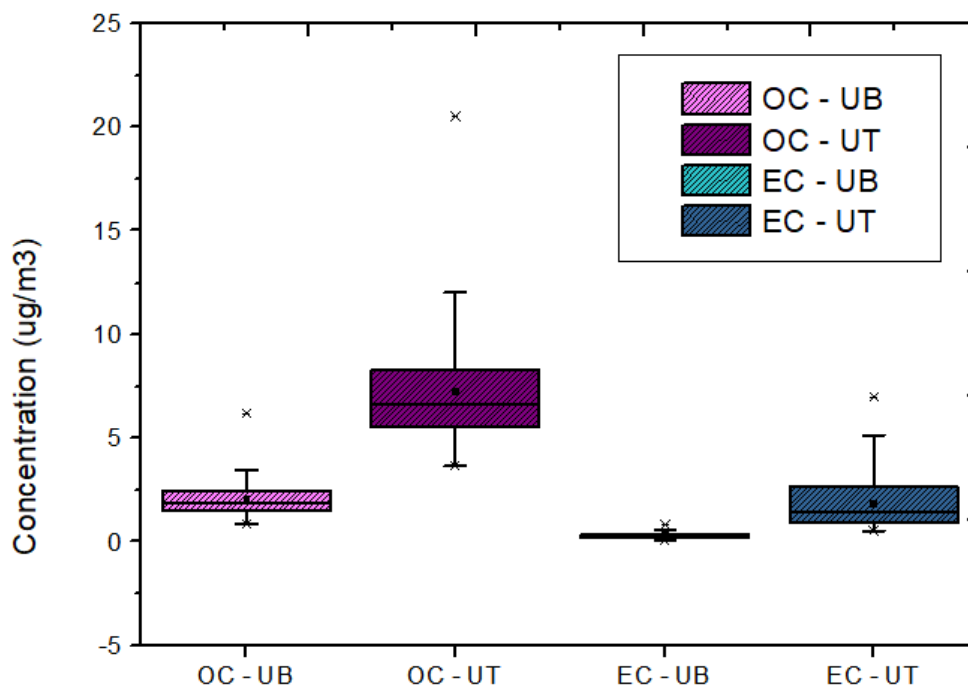
Figure 28: Box plots of OC and EC concentration $\left(\frac{ug}{m_3}\right)$ in UT and UB sites.

Organic carbon to elemental carbon (OC/EC) ratio is used to determine the origins of carbonaceous matter. It depends on pollution sources and vary among different sites. Several factors influence the value of this ratio, such as changes in emission sources, aerosol aging and the presence of secondary organic aerosol. An increased OC/EC ratio may indicate enrichment of the organic carbon fraction from biomass burning sources and/or contribution of secondary organic carbon and condensation of semi-volatile organic compounds in low temperatures (*Salameh et al., 2015*).

The OC/EC ratio was calculated in the two different sites and the highest values of the ratio were found in the UB site (*Figure 29*) during all seasons. The UB site, being less impacted by direct emissions, may be more influenced by secondary processes, which lead to increased OC/EC ratios. Biogenic compounds may also contribute to this difference. Biogenic aerosol is mostly found in the coarse mode but may be also contained in $PM_{2.5}$, to a lesser extent. The location of the UB site, inside the NCSR "Demokritos" campus, in a vegetated area, explains the presence of primary and secondary biogenic aerosol, which may further increase the OC/EC ratio. Furthermore, the seasonal highest values of the ratio were observed during summer period because the atmospheric oxidation processes are more intense than cold periods. Hence, the contribution of secondary organic carbon to PM mass is stronger in summer months. Also, the high proportion of gasoline and diesel-powered vehicles in Greece influence the OC/EC ratio. The reported values of the mean OC/EC ratio for vehicular emissions are in the range of 0.5-0.8 for heavy-duty diesel vehicles and 1.7-2.3 for light-duty gasoline vehicles (*Pio et al., 2011*) On the other hand, the high values of the ratios during cold period mainly depend on biomass burning sources and the use of fireplaces and wood stoves. OC/EC ratio from residential heating vary from low to high values (from 2.8-7.5 to 26-119 by *Zhang et al., 2013*), whereas forest fire is shown relatively high values (14.5 by *Na et al., 2004*). At the urban background, the mean OC/EC value found is 8.7 ± 4.6, which is very close to the corresponding value at urban sites in Thessaloniki (8.1) and Prague (8.7), that were related to wood combustion (*Samara et al., 2014*). On the other hand, the mean OC/EC value at the traffic site was estimated equal to 4.9 ± 2.0, indicative of the increased impact from primary anthropogenic emissions.
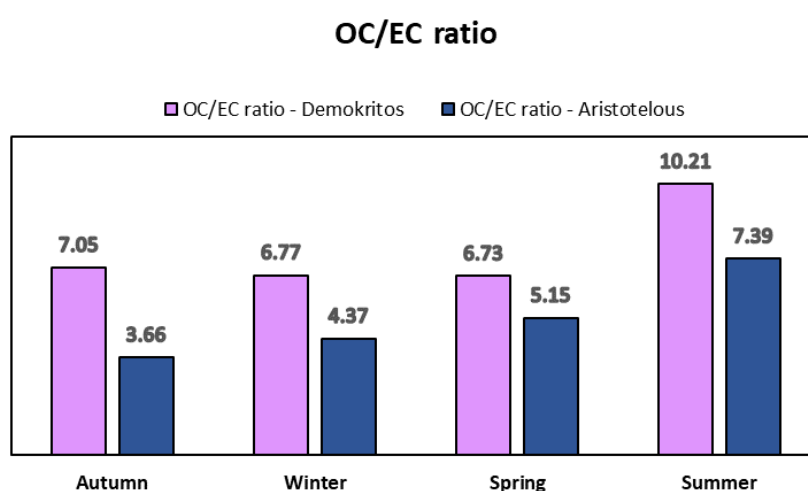
OC/EC ratio

Figure 29: Seasonal variability of the OC/EC ratios in UB and UT sites.

Descriptive statistics of the measured elemental concentrations at the two sites are shown in *Figure 30*. XRF has high detection limits for the lighter elements (Na and Mg, and to a lower extent S and Cl), while the method's performance is worse in the case of Quartz fiber filters, due to the higher thickness of these filters in comparison to Teflon filters. This should be taken into account when comparing the elemental concentration of the light elements between the two sites. In addition, Quartz fiber filters are composed of silicon dioxide, resulting in a very high background for both Si and Al, so these elements are not included in the analysis (*Figure 30b*). The highest contribution to $PM_{2.5}$ mass is observed for S, followed by crustal elements (Fe, Ca, Al, Si), K (which may be related both with soil dust and biomass burning) and Na only in the case of the UB site (related mostly to sea salt). Ni and Pb mean annual concentrations were found at both sites much below the respective EU limit values set by Directives 2004/107/EC and 2008/50/EC (20 ng/m³ for Ni and 500 ng/m³ for Pb).
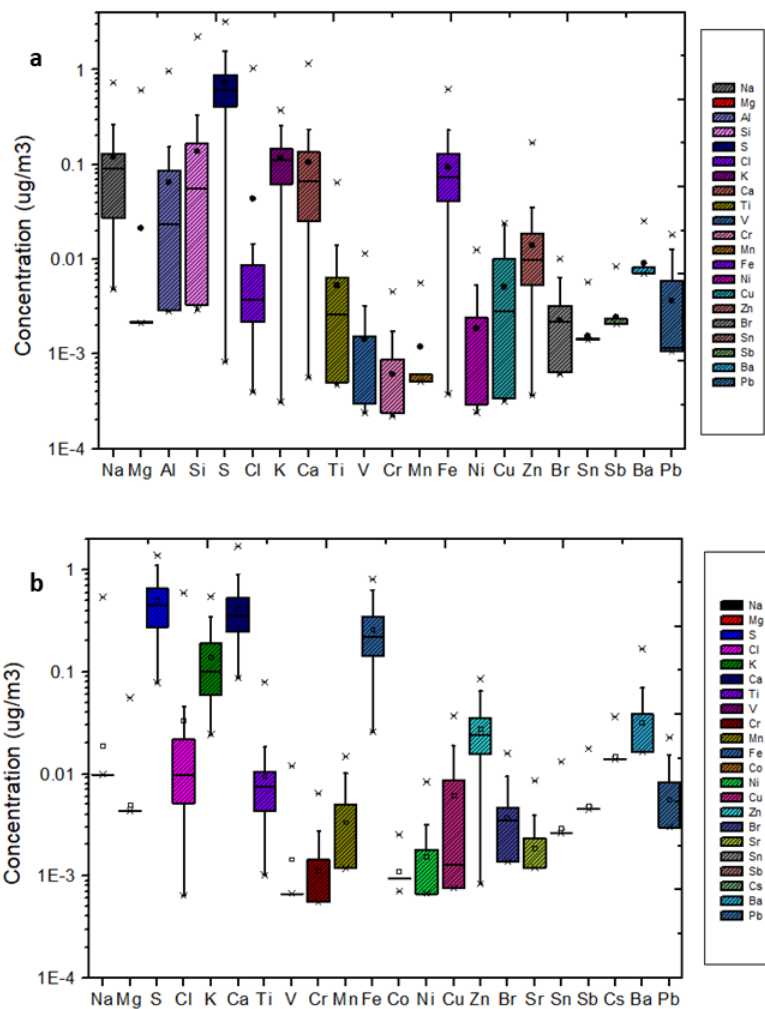
Figure 30: Box plots of elements concentration $\left(\frac{ug}{m_3}\right)$ in (a) UB site and (b) UT site.

The mean seasonal concentrations of $PM_{2.5}$ and chemical components at the two sampling sites are shown in *Table 6.* A t-test analysis (at p=0.01) was conducted, in order to assess whether there is statistically significant seasonal variation. The concentration values displayed

in bold in the *Table 6* correspond to species demonstrating significant seasonal variation. The seasonal variation of K at both sites indicates the influence of biomass burning during winter, which points towards residential heating. In addition, Zn displays significantly higher values during the cold period at the UT site. This metal is linked with vehicular emissions (both exhaust and non-exhaust) and may point towards increased traffic in comparison to the warm period, as discussed also above for carbonaceous species. Most of the warm period data correspond to summer and autumn of 2020. This time of year, people have just returned to their ordinary life after the first lockdown, so they are more careful and avoided unnecessary movements.

Table 6: The mean seasonal concentrations of $PM_{2.5}$ and chemical components measured at the traffic and urban background sites. A t-test analysis was conducted for each site; numbers in bold correspond to concentrations displaying statistically significant difference between seasons (at p = 0.01).

	Mean ± St. deviation (ng/m3)			
	Aristotelous site		**Demokritos site**	
	Cold period	**Warm period**	**Cold period**	**Warm period**
PM	**26952 ± 13250**	**17240 ± 5054**	10315 ± 5728	10696 ± 6918
OC	**7982 ± 3763**	**6441 ± 1417**	2233 ± 1088	1988 ± 601
EC	**2347 ± 1541**	**1347 ± 943**	**344 ± 158**	**229 ± 98**
Na	26 ± 83	10 ± 0	152 ± 161	82 ± 105
Mg	6 ± 8	4 ± 0	33 ± 107	7 ± 29
Al	-	-	71 ± 177	56 ± 46
Si	-	-	153 ± 394	117 ± 112
S	453 ± 301	558 ± 250	756 ± 676	713 ± 419
Cl	**58 ± 116**	**6 ± 3**	66 ± 188	17 ± 78
K	**174 ± 126**	**100 ± 67**	**156 ± 76**	**72 ± 49**
Ca	450 ± 306	371 ± 168	96 ± 197	116 ± 81
Ti	9 ± 15	9 ± 5	6 ± 12	4 ± 4
V	1 ± 2	2 ± 2	1 ± 3	1 ± 2
Cr	1 ± 1	1 ± 1	1 ± 1	0 ± 1
Mn	3 ± 3	3 ± 3	1 ± 1	1 ± 1
Fe	293 ± 182	228 ± 121	101 ± 112	87 ± 57
Co	1 ± 0	1 ± 0	-	-
Ni	2 ± 2	2 ± 1	2 ± 3	1 ± 2
Cu	6 ± 7	6 ± 9	5 ± 6	5 ± 5
Zn	**36 ± 19**	**18 ± 11**	18 ± 26	9 ± 9
Br	4 ± 2	3 ± 2	**3 ± 2**	**2 ± 1**
Sr	2 ± 2	1 ± 1	-	-
Sn	3 ± 2	3 ± 1	2 ± 1	2 ± 1
Sb	5 ± 2	5 ± 2	2 ± 1	3 ± 1
Cs	14 ± 0	16 ± 5	-	-
Ba	**41 ± 29**	**21 ± 15**	10 ± 6	8 ± 1
Pb	6 ± 5	5 ± 4	**2 ± 2**	**5 ± 6**

6.2. Chemical mass closure

Mass closure analysis was conducted separately for the two sites, for both the entire year and warm-cold period, as it is shown in *Figure 31*. Carbonaceous matter is the most abundant component for both sites. The relative contribution of carbonaceous matter to total $PM_{2.5}$ is relatively stable for each site. Higher contribution is observed at the traffic site (55%) than in urban-background site (36%). This can be related to increased traffic emissions in the Aristotelous site. Furthermore, the highest contribution of carbonaceous species is observed during summer in the traffic site (62%). The corresponding concentrations of OC and EC are lower in warm in comparison to cold period; nevertheless, the lower $PM_{2.5}$ concentrations during warm period results in a higher contribution of carbonaceous aerosol during this period. At the urban background site, the carbonaceous species' contribution does not display much variability.

Secondary inorganic aerosol (SIA) accounts in the study only for particulate SO_4^{2-}, and is related to secondary aerosol formation in the atmosphere from the photochemical oxidation of gaseous sulphur oxides emitted mainly from combustion of fossil fuel. The production of particulate SO_4^{2-} from SO_2 is a relatively slow reaction, so its concentration is often related to emissions far away from the sampling site (regional pollution). At the urban-background site, SIA displays the second highest contribution to $PM_{2.5}$ (21%) and this can be explained by reduced influence of other local sources. On the other hand, at the traffic site, the contribution of SIA is lower, due to the increased influence of other emission sources. Generally, the levels of secondary sulphate are relatively stable, given their regional character.

Soil contribution is found higher in the traffic site (15%) than in the urban-background site (9%). Given that the UB site is closer to open soil surfaces, this results may be mostly related to increased soil dust resuspension from the road, due to intense traffic observed at the Aristotelous site.

Sea salt concentration is found higher in the Demokritos site, whereas in the Aristotelous site it is negligible. The high detection limits of the XRF method in the case of Na and Mg, when Quartz fiber filters are used in the analysis, results in the inefficient quantification of these species, which are key components of sea salt.

In addition, several trace elements were found in both sites. V, Cr, Ni, Cu, Zn, Br, Pb, Sn, Sb and Ba are the main elements which had a detectable concentration in the fine fraction. All these can be related to anthropogenic activities, thus their higher concentration in the traffic site is expected.

Unaccounted mass consists of major PM species not measured in this study (mainly NO_3^- and NH_4^+) and H_2O present on the particles and on the filter material, which is not quantified during the different chemical analyses. NO_3^- are produced by the atmospheric transformation of gaseous NO_x emitted through combustion processes, such as vehicular traffic. They are usually found in the form of NH_4NO_3 and their formation is favored during wet and cold conditions. This may explain that, during the cold period in the traffic site, the percentage of unaccounted mass is higher (*Figure 31*). On the other hand, this percentage is relatively stable in the urban-background site. This may be explained by NO_x atmospheric reaction with $NaCl$ to $NaNO_3$, which displays greater stability in the atmosphere and is less impacted by environmental conditions.
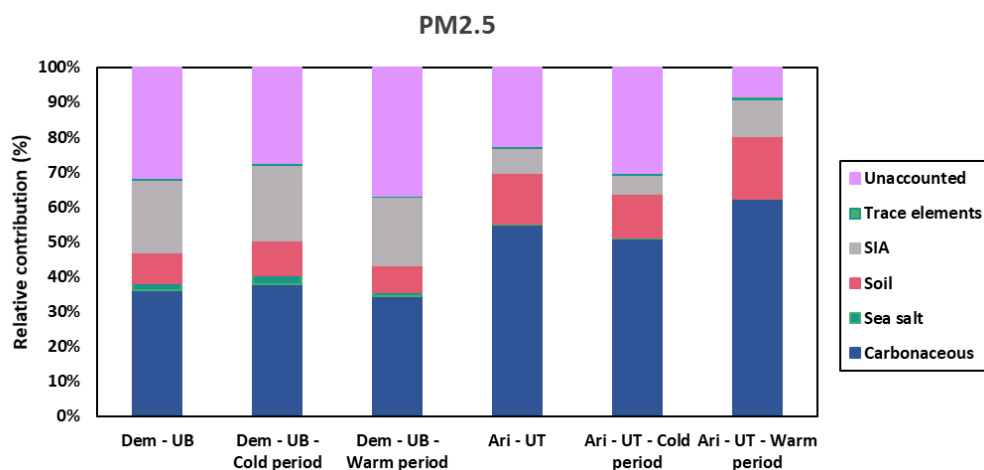
PM2.5

Figure 31: Relative contribution of PM components to total PM$_{2.5}$ mass.

6.3. Source contribution and chemical profiles obtained by PMF

PMF analysis was performed simultaneously for the datasets from both sites as a combined base, thereby expanding the database and facilitating convergence towards a more statistically robust solution. PMF analysis of the two sites together is possible because they are in the same metropolitan area and therefore the expected source profiles are similar, with some differences in their contributions. The source profiles for 2019 – 2020 datasets are shown *in Figure 32.* The identification of sources resulted in 7 PM sources, including traffic non-exhaust emissions, secondary sulphates & organics, mineral dust, traffic exhaust emissions, heavy oil combustion, sea salt and biomass burning. The relative mass of species (%) apportioned to each source is presented in *Figure 33.* The sources' relative contribution (%) for the urban background and the traffic site are shown in *Figure 34. Figure 35* shows the seasonal contribution of each source at each site.

The uncertainty of the final solution was assessed by using the DISP and BS functions in EPA PMF 5.0. With respect to displacement (DISP), no factor swaps occurred at the lowest dQmax level (dQmax = 4), indicating that the solution is well-defined. Boot-strapping (BS) was performed for 100 runs and the initial solution indicated high rotational ambiguity. Two constraints were added (as shown in *Table 5*), resulting in very good factor mapping (above 88 % for all factors) for the final constrained solution.

Sea salt profile was identified by the high contribution of Na, Cl and Mg. Fresh sea salt is mostly found in the coarse fraction (*Eleftheriadis et al., 2014*). The relative contribution of the different species in the sea salt profile, when compared to the corresponding values in sea water, may provide an indication of whether the sea salt aerosol is fresh or aged. In the current study, Cl/Na and Mg/Na ratios in the sea salt profile are equal to 1.9 and 0.08 respectively, and are in good agreement with sea water composition (Cl^-/Na^+ equal to 1.8 and Mg^{+2}/Na^+ equal to 0.12) (Diapouli et al., 2017). Sea salt contributed 0.5% in urban background site and 2.9% in traffic site (*Figure 34*).
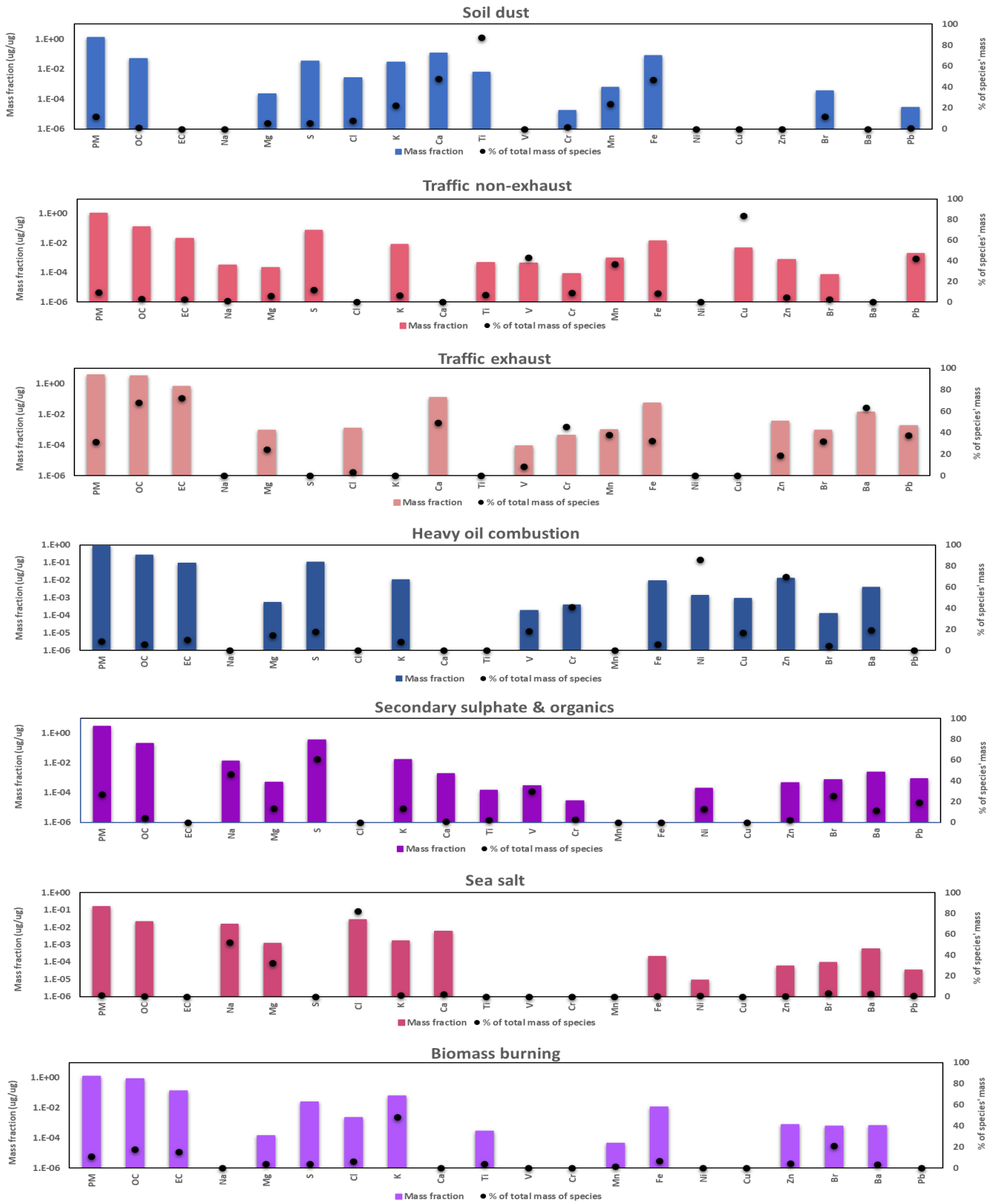
Figure 32: Chemical profiles of sources identified for the 2019-2020 $PM_{2.5}$ Athens dataset.
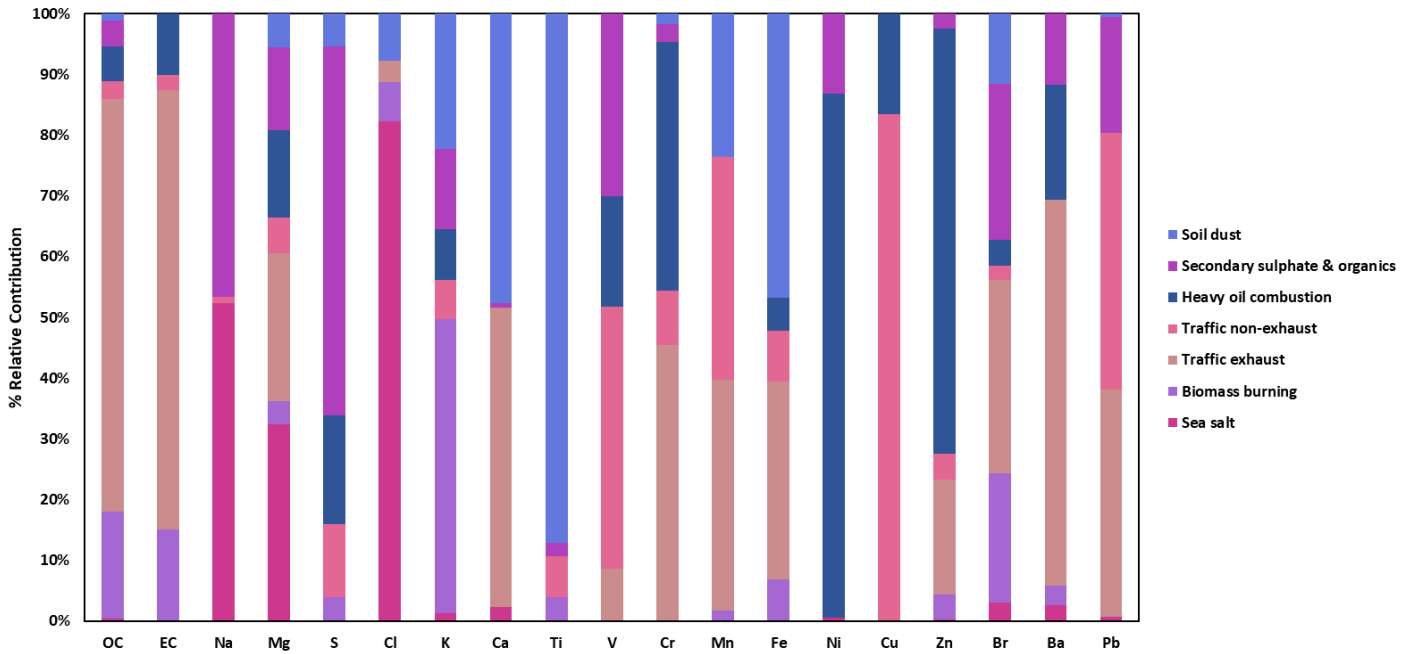
Figure 33: Relative mass of species (%) apportioned to each factor/source identified for the 2019-2020 $PM_{2.5}$ Athens dataset.
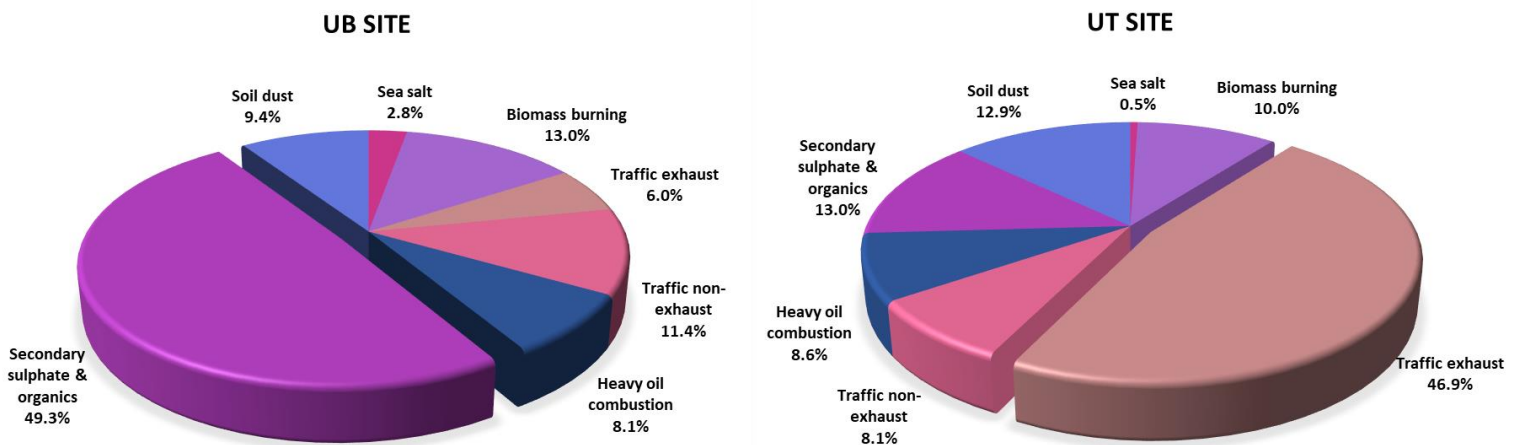
Figure 34: Relative contribution (%) to total $PM_{2.5}$ of PM sources identified by PMF, for the 2019-2020 Athens dataset.
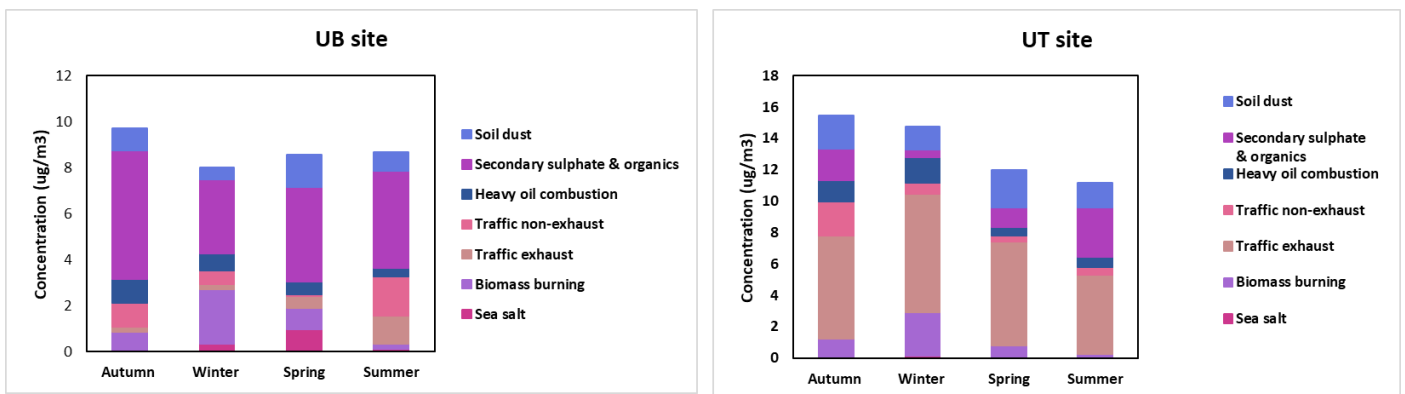
Figure 35: Mean source contribution to PM by season, for the $PM_{2.5}$ Athens dataset during 2019-2020.

The mineral dust factor can be considered as a mixture of several sources, including soil resuspension, regional mineral dust, long range transport of African dust and also dust generated from urban works (e.g. building and demolition) (*Athanasopoulos et al., 2010*). The mineral dust profile is identified by high loadings of crustal species, such as Al, Si, Ca, Fe, Ti and Mn. Aluminum and silicon were not used in PMF analysis, due to the use of quartz filters in UT site. Therefore, the major element for identification of the soil dust factor was Ti. This profile accounted for more than 87% of the total mass of Ti and 46 - 47% of Fe and Ca (*Figure 33*). The Mineral dust profile displayed a higher contribution of Ca in comparison to typical composition of earth's crust, which is compatible with the enrichment in Ca reported for the Athens soil (*Argyraki and Kelepertzis, 2014*). Mineral dust contributed 9.43% in urban background site and 12.90% in traffic site (*Figure 34*).

The mean 24 h contributions of the mineral dust source displayed some distinct peak concentrations (*Figures 36a and 36b*). Back-trajectory analysis was performed for these days in order to identify potential African dust-transport events at each site. The long-range transport of African dust was studied using 5-day backward air mass trajectories obtained every 12 hours and at three heights (500, 1000, and 1500m above sea level) by the Hybrid Single Particle Lagrangian Integrated Trajectory (HYSPLIT) Model. *Figures 37* and *38* show the validated dust events in the urban-background and urban traffic sites, respectively. As seen in *Figures 14a and b*, the same events were identified for both sites. The highest contribution of soil dust was observed on 7/11/2019, 22/12/2019, and 08/03/2020 for both sampling sites (*Figures 37a, 37c, 37d, 38a, 38c, 38d*). By examining the height of the air masses when passing above Africa, before reaching our sites, one can observe that during these events air masses were at low (below 1000 m) or medium (1500 2000 m) heights. The contribution is higher when the incoming airflows are closer to the surface of the Sahara Desert in the days prior, allowing for more soil dust to be transported. Conversely, on 12/11/2019, the contribution of soil dust was lower due to airflow movements at higher altitudes (above 2500 m) in the preceding days (*Figures 37b and 38b*).

The UT site displayed slightly higher soil dust contributions in comparison to the UB site, although the DEM-Athens station is located in a vegetated area and is surrounded by open soil surfaces. These increased contributions were mostly found during the warm period and are associated with local dust resuspension, promoted by the warm and dry environmental

60

conditions, and enhanced by intense vehicular traffic at the UT site. This observation is further supported by the relatively low contribution from non-exhaust emissions in the UT site (again in comparison to the UB site), suggesting that the resuspension of soil dust from the roads was apportioned to the Mineral dust source rather than the Traffic non-exhaust source in the UT site.
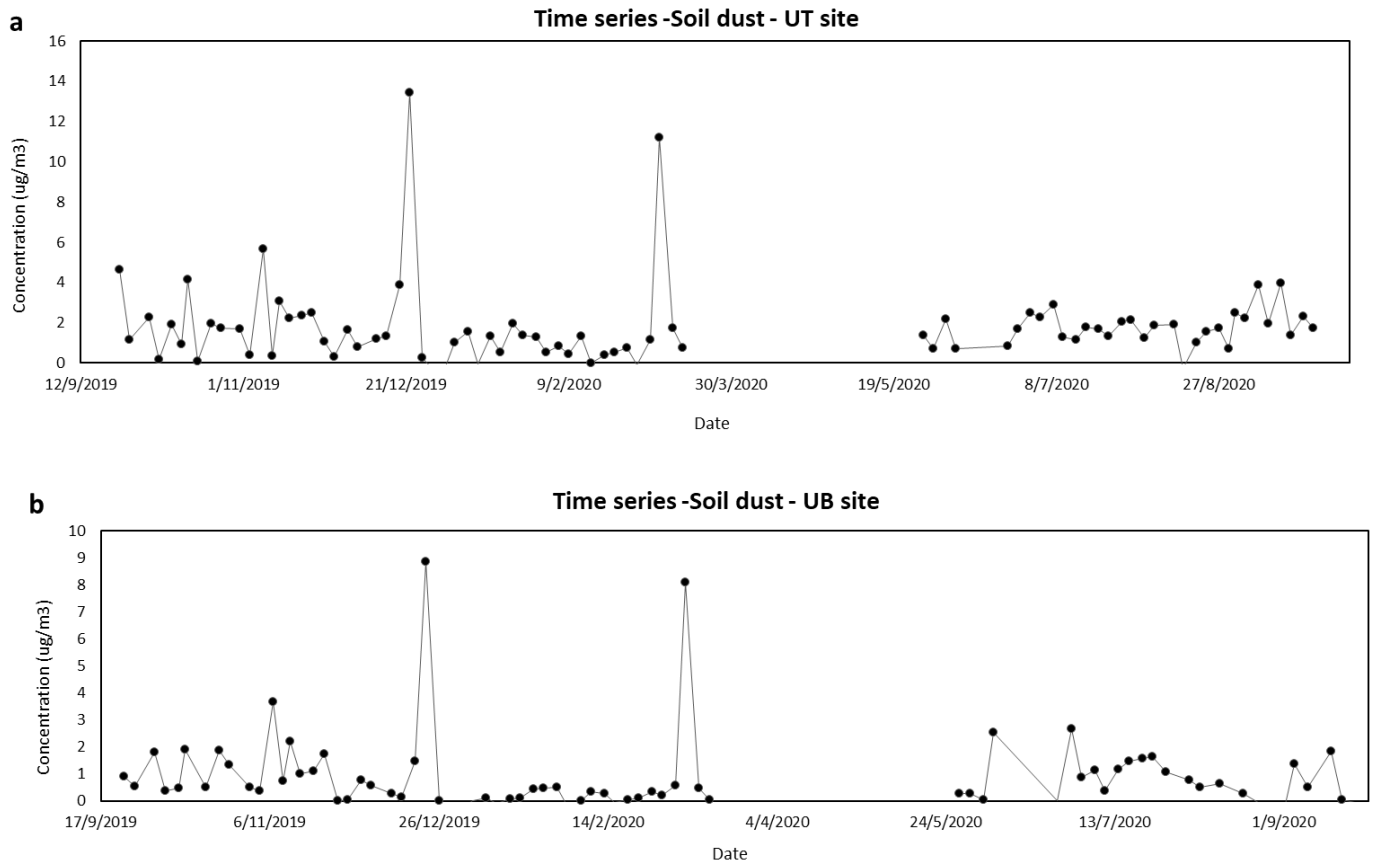
Figure 36: Time series of contribution of soil dust source (in ug/m³) to the total $PM_{2.5}$ mass for (a) UT site and (b) UB site.

NOAA HYSPLIT MODEL
Backward trajectories ending at 1200 UTC 07 Nov 19
CDC1 Meteorological Data

NOAA HYSPLIT MODEL
Backward trajectories ending at 1200 UTC 12 Nov 19
CDC1 Meteorological Data

Job ID: 167188   Job Start: Wed Jan 25 09:14:24 UTC 2023
Source 1 lat.: 37.994999 lon.: 23.816000 hgts: 500, 1000, 1500 m AGL

Trajectory Direction: Backward   Duration: 120 hrs
Vertical Motion Calculation Method: Model Vertical Velocity
Meteorology: 0000Z 1 Nov 2019 - reanalysis

Job ID: 167191   Job Start: Wed Jan 25 09:16:07 UTC 2023
Source 1 lat.: 37.994999 lon.: 23.816000 hgts: 500, 1000, 1500 m AGL

Trajectory Direction: Backward   Duration: 120 hrs
Vertical Motion Calculation Method: Model Vertical Velocity
Meteorology: 0000Z 1 Nov 2019 - reanalysis

NOAA HYSPLIT MODEL
Backward trajectories ending at 1200 UTC 22 Dec 19
CDC1 Meteorological Data

NOAA HYSPLIT MODEL
Backward trajectories ending at 1200 UTC 08 Mar 20
CDC1 Meteorological Data

Job ID: 166976   Job Start: Wed Jan 25 09:02:18 UTC 2023
Source 1 lat.: 37.994999 lon.: 23.816000 hgts: 500, 1000, 1500 m AGL

Trajectory Direction: Backward   Duration: 120 hrs
Vertical Motion Calculation Method: Model Vertical Velocity
Meteorology: 0000Z 1 Dec 2019 - reanalysis

Job ID: 167068   Job Start: Wed Jan 25 09:06:06 UTC 2023
Source 1 lat.: 37.994999 lon.: 23.816000 hgts: 500, 1000, 1500 m AGL

Trajectory Direction: Backward   Duration: 120 hrs
Vertical Motion Calculation Method: Model Vertical Velocity
Meteorology: 0000Z 1 Mar 2020 - reanalysis

Figure 37: Back trajectory analysis in UB site for (a) 7/11/2019, (b) 12/11/2019, (c) 22/12/2019, (d) 08/03/2020.
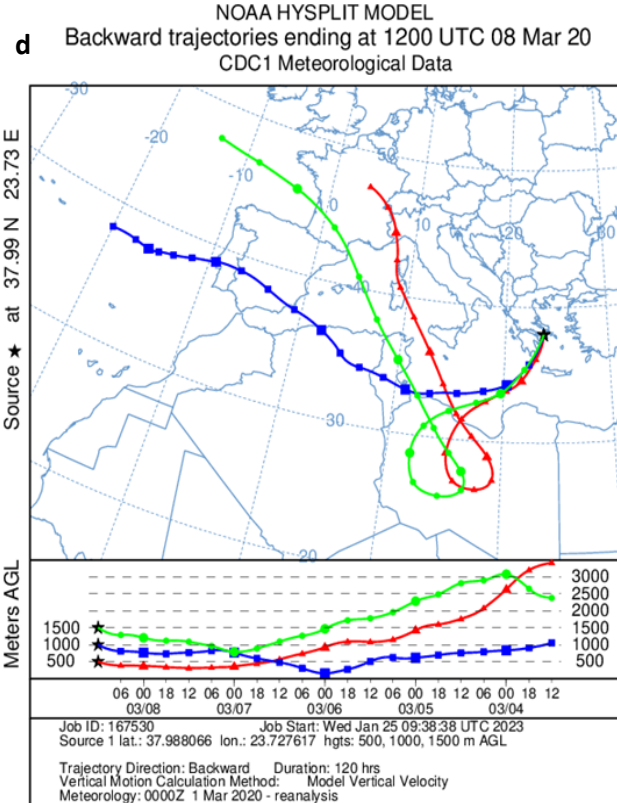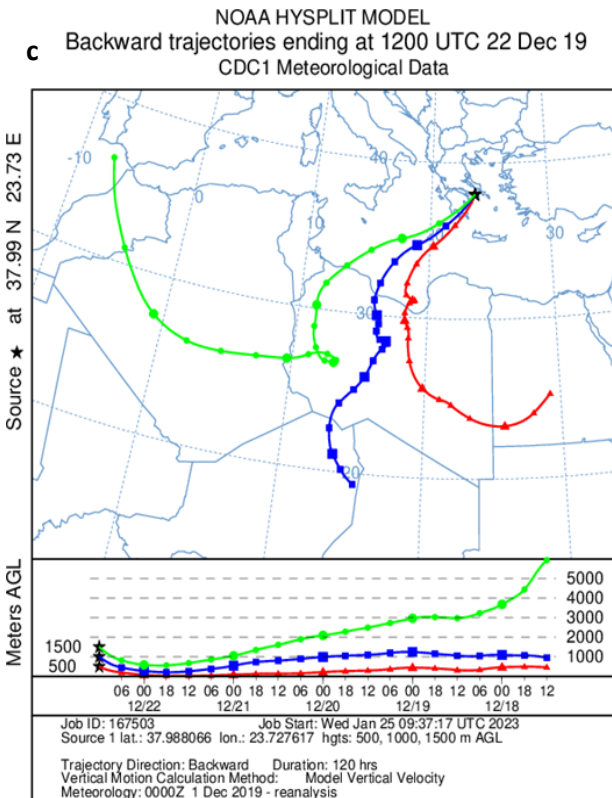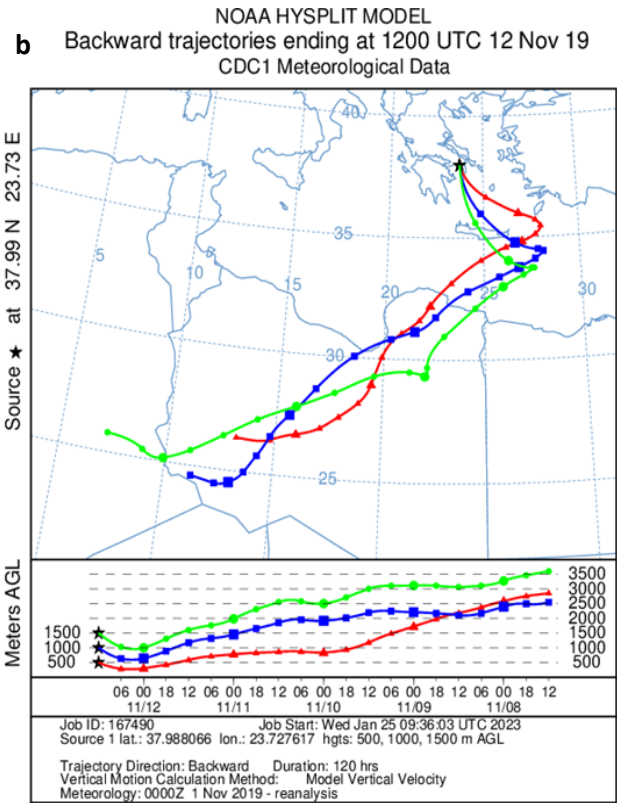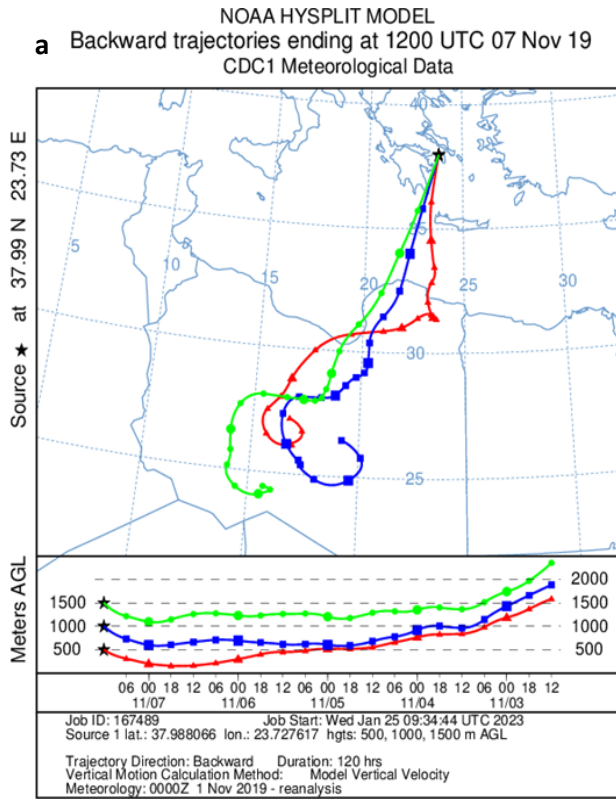
Figure 38: Back trajectory analysis in UT site for (a) 7/11/2019, (b) 12/11/2019, (c) 22/12/2019, (d) 08/03/2020.

The Traffic non-exhaust (or Road dust) source was traced by metals that originate both from brake, tire and vehicle body wear (Cu, Zn, Fe, Mn, Pb) and from road surface and asphalt wear (Fe, Ti, Pb). The Vehicle non-exhaust profile accounted for more than 83% of the total mass of Cu, 36% of Mn and 42% of Pb (*Figure 33*). This profile displays also significant contributions from other species (such as OC, EC, S and K) but the percentage of the mass of these species apportioned to this source is negligible. Non-exhaust emissions relate to the resuspension by vehicular traffic of particles that have been deposited on the road surface; for this reason, the road dust profiles often contain species commonly found in high concentration in urban aerosols (*Diapouli et al., 2017*). Traffic non-exhaust contributed 11.4% in urban background site and 8.1% in traffic site (*Figure 34*).

The traffic exhaust profile accounted for most of the carbonaceous species' mass, approximately 68% of OC and 72% of EC (*Figure 32*). Elemental carbon is a known tracer for traffic emissions, and organic carbon has been associated with combustion sources, including traffic, as emissions from these sources are rich in semi-volatile organic compounds (*Diapouli et al., 2017*). In addition, Zn, Ca and Fe contributed to the traffic exhaust profile. These metals can be originating from vehicle body wear (Zn, Fe) or emitted from the combustion of lubricating oil (Zn, Ca). Zn may be also emitted from galvanized materials, tire wear and the use of zinc compounds in rubber production (*Diapouli et al., 2017*). Other elements contributing to this profile were V and Cr, which are related to fuel combustion. As shown in *Figures 34* and *35*, the traffic exhaust emission source accounted for the highest contribution, both relative (46.9%) and in terms of absolute concentrations, tin the traffic site. Argyropoulos et al. (2016) report OC/EC ratio equal to 8.9 for gasoline catalytic car exhaust source profile emissions, and 0.7 - 1.0 for diesel car source profile emissions. The obtained ratio in the traffic exhaust profile falls within this range and is indicative of the relative share of gasoline and diesel vehicles in the city of Athens. Traffic exhaust contributed 6.0% in urban background site and 46.9% in traffic site (*Figure 34*).

The heavy oil combustion profile was identified by the presence of V and Ni. 86 % of Ni and 18 % of V was apportioned to this profile. It also included carbonaceous species and S, Fe, Zn and K. Heavy oil combustion emissions have a lower percentage of organic carbon in relation to elemental carbon, in comparison to vehicular emissions; the obtained OC/EC ratio in this profile (OC/EC equal to 3) is in agreement with what was expected. Other elements contributing to the heavy oil combustion profile are Cr, Mg and Ba. The oil combustion source may be originating from shipping emissions from the Aegean shipping routes in the area surrounding the Attica peninsula and beyond, as well as petrochemical activities west of Athens Metropolitan Area (*Diapouli et al., 2017*). The high contribution of S verify that heavy oil combustion source may be related to regional emissions. In addition, the *Figures 34* and *35* show that oil combustion contributed equally both urban background and traffic sites. Heavy oil combustion contributed 8.1% in urban background site and 8.6% in traffic site (*Figure 34*).

During PMF analysis, some profiles are not easily identified as coming from a specific source; for this reason, a European repository of PM source profiles has been built (Specieurope database), following the development of the U.S. source profiles' repository (Speciate database). These databases may serve as a reference point when assessing our PMF solution and assigning specific sources to the obtained factor profiles (*Pernigotti et al., 2016*). In the current study, traffic exhaust and heavy oil combustion profiles were tested against relevant profiles included in the Specieurope database. The traffic exhaust profile was compared with

a single "average" profile, which consisted of emissions from various types of vehicles. Since this average profile does not accurately represent traffic exhaust emissions, the standard deviation of the relative contribution of the different species to the profile was used to account for the variability. The heavy oil combustion profile was compared to the two profiles available in the database, corresponding to the burning of fuel oil and to oil refinery emissions. The results of the analysis showed that the traffic exhaust profile was well-aligned, according to the average traffic profile obtained from different European studies, as shown in *Figure 39*. Furthermore, comparison of the heavy oil combustion profile with the two Specieurope profiles indicated similarities in the relative contribution of major species (OC, EC and S), and presence of other relevant species (V, Cr, Fe, Zn, Ni, Cu, and Ba), as shown in *Figure 40*.
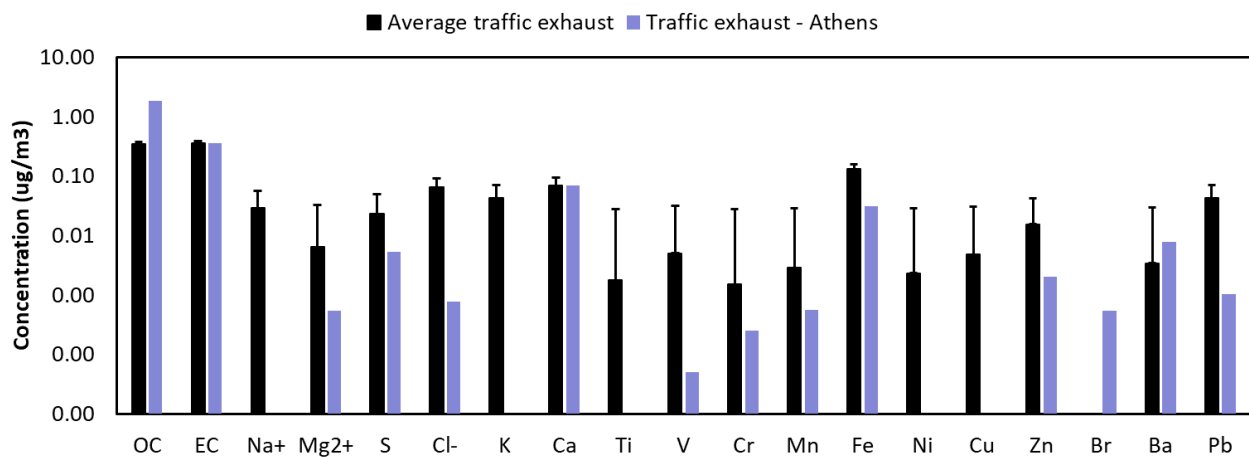
Figure 39: Comparison of the Specieurope traffic exhaust profiles with the corresponding profile obtained for Athens in this study.
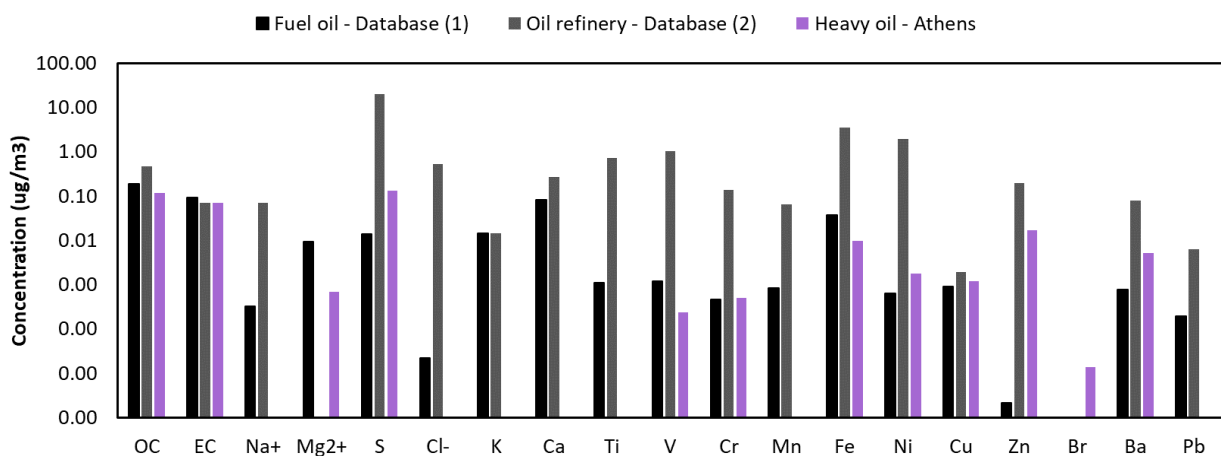
Figure 40: Comparison of the Specieurope heavy oil combustion profiles with the corresponding profile obtained for Athens in this study.

65

Secondary inorganic aerosols are formed by the reaction of H_2SO_4 (g) and HNO_3 (g) with NH_3, giving $(NH_4)2SO_4$ and NH_4NO_3, respectively (*Manousakas et al. 2017*). Due to the absence of NH_4^+ and NO_3^-, the contribution of secondary inorganic aerosols profile was underestimated. The identified profile is related to SO_4^{2-} and OC. This factor relates to the photochemical oxidation of gaseous sulphur oxides and volatile organic compounds (VOCs). The contribution of other elements (Na, K, Mg and V) to this profile may be related to the long-range transport of natural (such as sea salt) and anthropogenic pollutants together with secondary aerosol. Because of the slow oxidation of SO_2 to SO_4^{2-}, sulphates are found in aged air masses and so this factor can be more related regional than local pollution (*Querol et al., 1998*). It is known that Greece is influenced by long-range transport phenomena (*Manousakas et al. 2017*). The high contribution of secondary sulphate and organics factor was clearly shown in the urban background site, where the relative contribution of the other, primary, sources was not very high due to the nature of the UB site (*Figure 34*). Secondary sulphates & organics contributed 49.3% in urban background site and 13.0% in traffic site (*Figure 34*).

Biomass burning profile was traced by OC, EC and K. The OC/EC ratio was calculated equal to 6.2, being in the range of typical biomass burning values (*Diapouli et al., 2014*). In this factor, a lower contribution of Cl is also observed, and may be attributed to K being in the form of KCl in fresh smoke. In addition, in fires, plastic waste is burned with the biomass, so Cl is released (*Manousakas et al., 2017*). The presence of S in this profile is related to photo-oxidation of biomass burning emissions during transport (*Diapouli et al., 2017*). *Figure 35* shows that the contribution of the biomass burning source is higher during cold period, but also is significant in summertime. Because of the economic crisis and increased prices of diesel, which is widely used as the most common means of domestic heating in Greece, biomass burning is used for cheaper domestic heating (*Manousakas et al., 2017*). In addition, during warm period forest fires occur, so the biomass burning emissions are strengthened. Biomass burning contributed 13.0% in urban background site and 10.0% in traffic site (*Figure 34*).

6.4. Assessment of source profiles' variability

In addition to the PMF analysis presented above, the model was also run for each sampling site separately. This analysis assisted towards better understanding of the impact of input data in the PMF solution; moreover, it provided the opportunity to compare the source profiles obtained for the urban background and traffic sites and assess how the characteristics of each site affect these profiles (*Figure 41*).

The Soil dust profiles obtained in the three solutions are very similar. In the UB-run, Al and Si (typical soil dust tracers) contribute to the total mass of mineral dust. Due to usage of quartz filters in the traffic site, these elements cannot be quantified and presented in the other two runs. The availability of several soil dust tracers in the UB-run resulted in a "cleaner" soil dust profile, including significant contributions only from crustal elements.

Traffic exhaust

Heavy oil combustion

Secondary sulphates & organics

Sea salt

Biomass burning
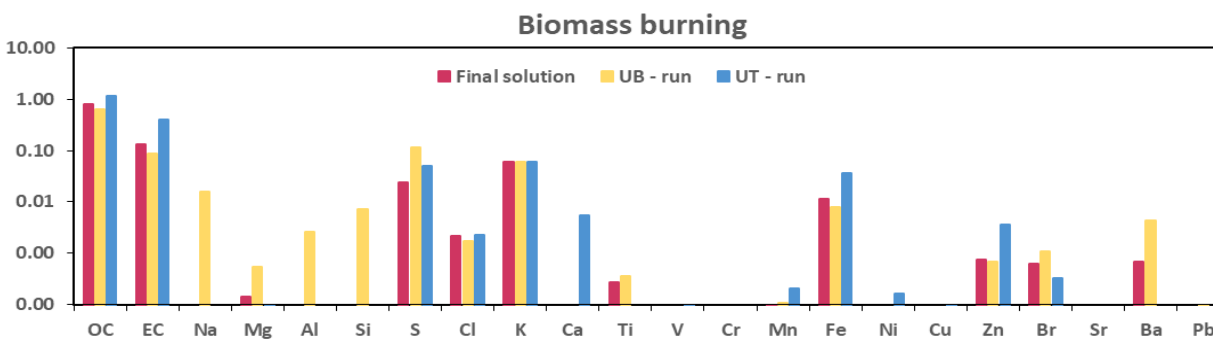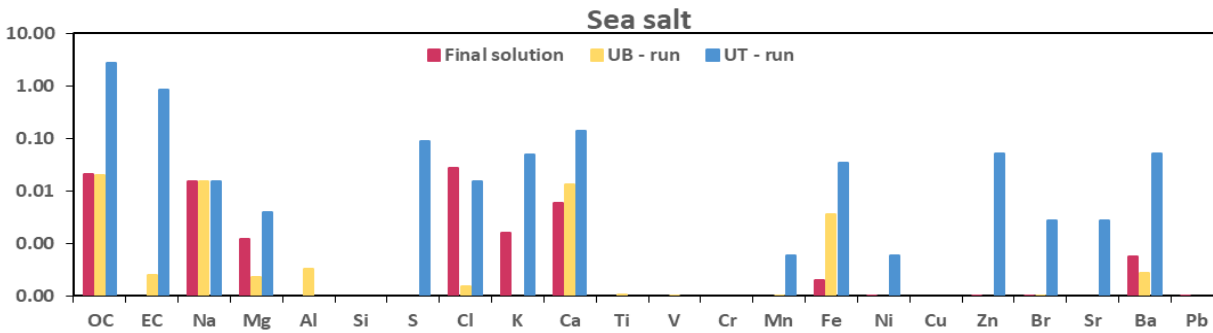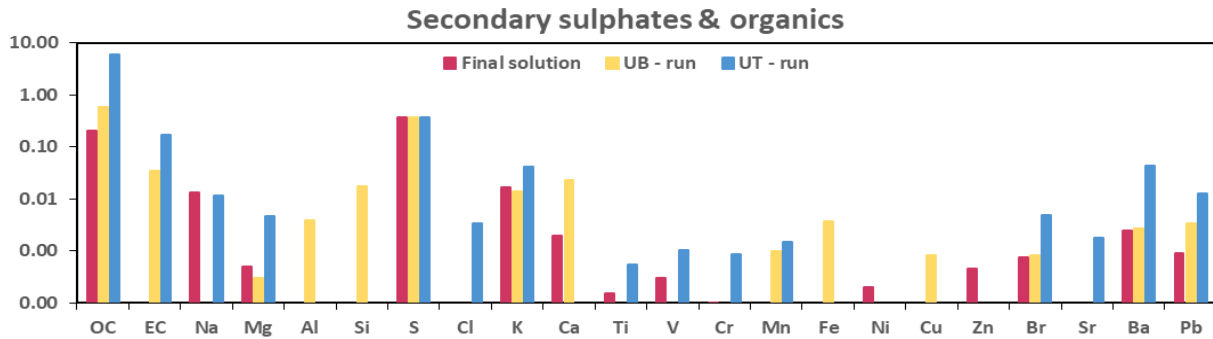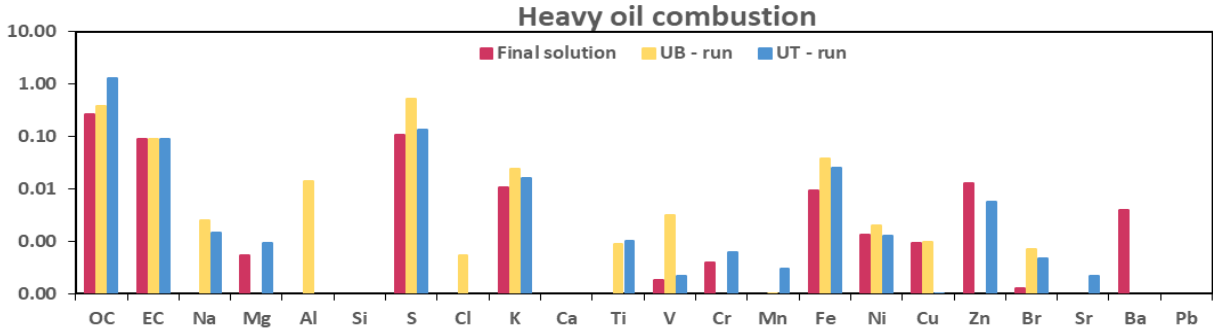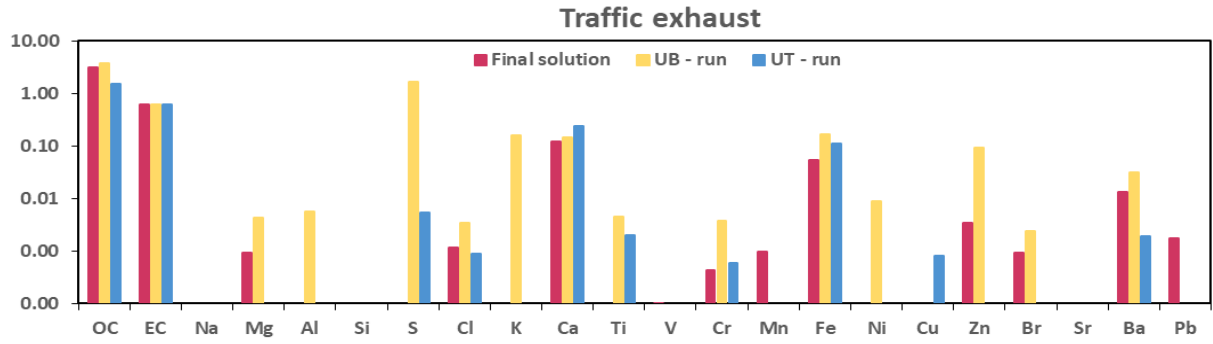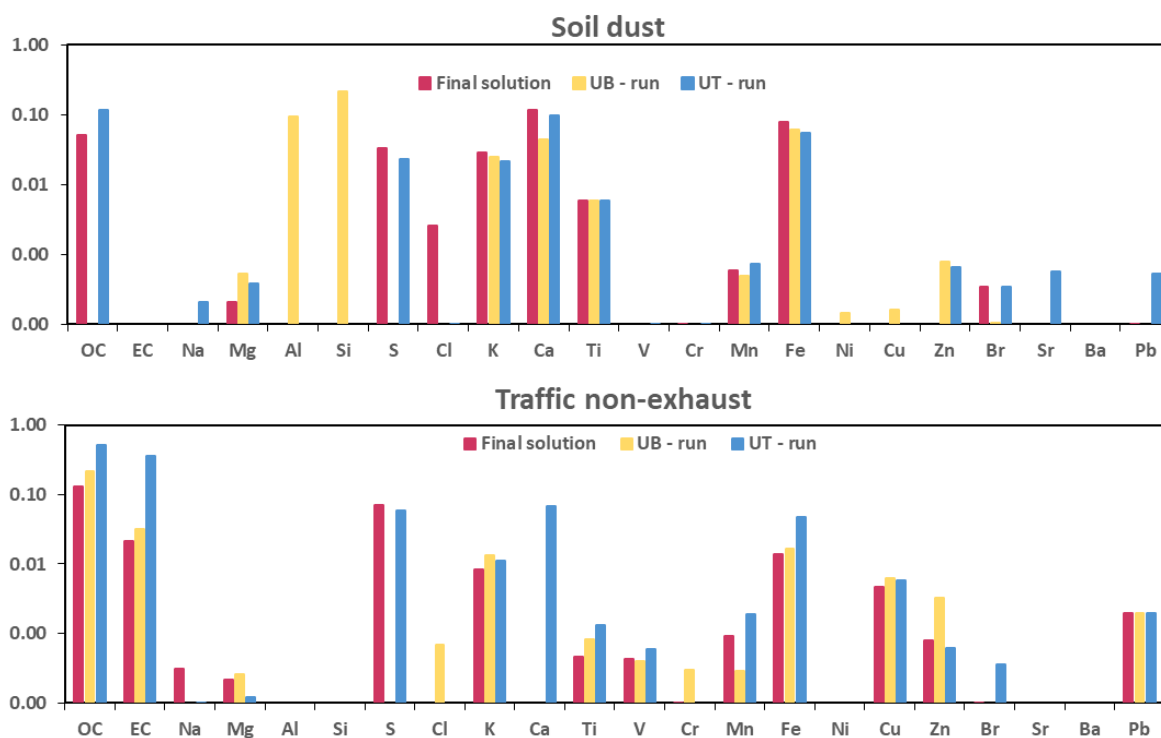
Figure 41: Chemical profiles of sources identified for the combined 2019-2020 Athens dataset (final solution) and for the two solutions obtained when data from each site is run separately.

The sea salt profiles displayed significant difference between runs, with the UB-run providing a sea salt profile that could be considered as representative for an aged sea salt. This is demonstrated by the very low Cl/Na ratio (equal to 0.01), suggesting Cl deficit, due to the conversion of NaCl to $NaNO_3$, in the presence of NOx emissions, with the subsequent release of Cl in gaseous form (*Diapouli et al., 2017*). The combined database solution points towards fresh sea salt aerosol (due to the impact of the traffic site data). On the other hand, the traffic site data alone cannot provide a well-defined sea salt profile, because of increased uncertainties in the quantification of the key sea salt species Na and Mg, due to the use of quartz fiber filters in this site.

Secondary inorganic aerosol and organics compounds source was difficult to identify, due to the absence of NH_4^+ and NO_3^-. In this case, the only characteristic tracers were S and OC. S measurement displays a higher uncertainty in quartz filters in comparison to Teflon. Because of these reasons, the obtained sources profiles in all runs were not very "clean", with this limitation being more pronounced in the UT-run.

Regarding the traffic non-exhaust profiles, a higher contribution of soil elements can be seen in the UT-run. This may be caused by stronger soil dust resuspension due to traffic, since the available open soil surfaces in the city center are fewer. In addition, in the traffic site, the dust on the road was enriched in OC an EC because of the various local anthropogenic activities (including intense vehicular traffic).

The traffic exhaust profiles obtained by the three solutions are very similar. The profile obtained by the UT-run is characterized as more fresh, due to the lower OC/EC ratio (2.4), in

comparison to the urban background site (5.9). The significant contribution from sulphur in the UB profile further support the hypothesis that the traffic exhaust emissions reaching the site are rather aged. It should be noted that the urban background site is inside the NCSR "Demokritos" campus, away from local sources, including traffic.

The heavy oil combustion profiles were also very similar between runs. The major differentiation among runs was the contribution of secondary compounds. In the UB-run profile, more secondary inorganic compounds were observed (S), whereas in UT-run the contribution of OC was enhanced and may be related to secondary organic aerosol forming during the transport of emissions to the receptor site.

With respect to the biomass burning source, the three runs have provided comparable profiles. The most prominent difference is the obtained OC/EC ratio in the profiles. While in the UB-run the ratio was equal to 7.4 (close to the one obtained by the combined dataset), in the in traffic site the ratio was calculated equal to 2.8. This value is very low for biomass burning emissions and suggests that this profile is not well-defined and other combustion sources (such as vehicular traffic) may contribute to this source.

7. Conclusions and future research

In this work, a yearly measurement campaign (09-2019 – 09/2020) performed at two sites in the Athens metropolitan area, representative of different levels of urbanization and traffic density (urban traffic and urban background locations), was exploited in order to assess particulate pollution in the city and to identify the major sources responsible. The annual measured $PM_{2.5}$ concentration was lower than the EU annual limit value of $25\frac{ug}{m^3}$. However, 24h $PM_{2.5}$ concentration, especially in traffic site, was higher than the WHO guidelines, which recommend a 24h limit value of $15\frac{ug}{m^3}$. Carbonaceous aerosol contributed significantly to total $PM_{2.5}$. The OC/EC ratio was found equal to 8.7 and 4.9 for the urban background and traffic sites, respectively. The increased ratio in the urban background site is characteristic of the background character of the site, away from direct emissions and significantly impacted by secondary aerosol generation. K concentration levels were higher during winter due to increased biomass burning for residential heating, whereas increased concentration of EC and Zn during cold period was related to more intense vehicular traffic in the pre-covid cold period.

The combined chemical speciation database from the two sites was used for the application of the EPA PMF 5.0 model, for the source apportionment of atmospheric $PM_{2.5}$. Seven sources were identified, including soil dust, traffic non-exhaust emissions, traffic exhaust emissions, heavy oil combustion, secondary sulphates & organics, sea salt and biomass burning.

The contribution from vehicular traffic (exhaust and non-exhaust emissions) was found equal to $1.5 \frac{ug}{m^3}$ and $7.6 \frac{ug}{m^3}$ for the urban background and traffic site respectively. The increased contribution of this source to $PM_{2.5}$ at the traffic site dataset is expected, due to intense vehicle traffic observed in this area. The contribution found for the urban background site was in agreement with a recent study conducted at the same site (*Diapouli et al., 2022*). The Heavy oil combustion emission source contributed by $0.7\frac{ug}{m^3}$ and $1.2 \frac{ug}{m^3}$ at the urban background and traffic site, respectively. This source was related to shipping and industrial activities (oil refineries in the West of the Athens metropolitan area). Biomass burning contribution was found lower (9-14%) for both sites in comparison to the contributions reported for DEM-Athens station and another urban background site during 2011-2012 (29-36%) (*Diapouli et al., 2017*); this result reflects the improvement of the financial situation in Greece, during these last years. The highest biomass burning concentrations were recorded during wintertime, due to residential heating. The influence of this factor was higher in the traffic site, which is a densely populated region. Secondary sulphates and organics source contributed by 49.3% and 13.0% at the traffic and urban background sites, respectively. The higher contribution of this source at the urban background site reflected the lower impact from local primary emissions.

The contribution of natural sources (sea salt and soil dust) was 10-15% for both sites; fine particles are known to originate mainly from anthropogenic sources. Nevertheless, during dust events, total $PM_{2.5}$ concentration was significantly influenced by natural sources. The long-range transport of African dust was studied using 5-day backward air mass trajectories. The verified dust events were observed during cold period and resulted in increased $PM_{2.5}$ concentrations.

The PMF model was also applied to the database of each site separately. This analysis assisted towards better understanding the impact of input data in the PMF solution and provided the opportunity to compare the source profiles obtained from for the urban background and traffic sites and assess how the characteristics of each site affect these profiles. The

comparison of the three distinct PMF runs (combined database and UB and UT databases) revealed similarities in the profiles of soil dust, traffic exhaust, heavy oil combustion and biomass burning, although the UB site displayed more aged profiles. The analysis also highlighted the difficulty in obtaining well-defined profiles when key source tracers are not measured with high accuracy (such as the case of Na and Mg, tracers for sea salt, in the traffic site) or are not measured at all (such as NH_4^+ and NO_3^-, tracers of secondary aerosol).

The results of source apportionment analysis in recent and past years demonstrate the effects of control measures and technological developments allowing for cleaner energy and reduced emissions from traffic sources. In addition, they reflect the effects of the bad financial situation in Greece during last years. Because of this, economic activities were decreased and household practices (e.g. usage of wood combustion for residential heating) contributing to poor air quality were increased in an effort of reduced living costs. Other types of crises may also influence air quality, such as the COVID-19 pandemic, which led to mitigation measures against the spread of the disease and resulted in decreased anthropogenic emissions during the lockdown periods and after. This impact was also visible in this study, during the warm period campaign which was mostly during 2020, when the pandemic was already underway.

As this study has been completed, several ideas for future research could be proposed. The first one is the simultaneously source apportionment analysis in multiple cities in order to understand the impact of traffic emissions across the country and in different urban areas, not just in Athens. It is important to investigate whether the same behavior is observed in larger, more congested roads compared to smaller ones.

The second one is about multi-elemental analysis. In future research, the analysis of the elements in the filters could be performed using the Particle Induced X-Ray Emission (PIXE) method. PIXE is the measurement of X-rays emitted from a sample due to high-energy ion bombardment. This method has better sensitivities than XRF analysis and requires much less measurement time per filter (about 2 minutes) compared to XRF (about 50 minutes).

The last one is the installation of online XRF instruments, so a real time source apportionment could be conducted. The elemental composition can be measured by an Xact Ambient Metals Monitor, which takes measurement every half hour. By doing so, we can observe how much each source contributes during the day, which is referred to as High-Time-Resolution Source Apportionment (*Rai et al., 2020*). The High-Time-Resolution Source Apportionment refers to the process of determining the contribution of each pollution source during different times of the day, by taking measurements at frequent intervals. This can provide valuable information for developing effective air pollution control strategies.

8. References

Akagi, S. K., Yokelson, R. J., Wiedinmyer, C., Alvarado, M. J., Reid, J. S., Karl, T., Crounse, J. D., and Wennberg, P. O., 2011. Emission factors for open and domestic biomass burning for use in atmospheric models, Atmos. Chem. Phys., 11, 4039–4072.

Alves, C., Vicente, A., Nunes, T., Gonçalves, C., Fernandes, A.P., Mirante, F., Tarelho, L., Sánchez De La Campa, A.M., Querol, X., Caseiro, A., Monteiro, C., Evtyugina, M., Pio, C., 2011b. Summer 2009 wildfires in Portugal: emission of trace gases and aerosol composition. Atmos. Environ. 45, 641–649.

Ambient air. Measurement of elemental carbon (EC) and organic carbon (OC) collected on filters. 2017. Hellenic Standard. ELOT EN 16909.

Argyraki, A., Kelepertzis, E., 2014. Urban soil geochemistry in Athens, Greece: The importance of local geology in controlling the distribution of potentially harmful trace elements. Sci. Total Environ. 1, 482-483, 366-77.

Athanasopoulou, E., Tombrou, M., Russell, A.G., Karanasiou, A., Eleftheriadis, K., Dandou A., 2010. Implementation of road and soil dust emission parameterizations in the aerosol model CAMx: Applications over the greater Athens urban area affected by natural sources. JOURNAL OF GEOPHYSICAL REASERCH. Atmosphere. 115.

Atkinson, R., Arey, J., 2003. Gas-phase tropospheric chemistry of biogenic volatile organic compounds: a review. Atmos. Environ. 37 (Suppl. 2), 197–219

Atkinson, RW., Fuller, GW., Anderson, HR., Harrison, RM., Armstrong, B., 2010. Urban ambient particle metrics and health: a time-series analysis. Epidemiology. 21, 501-11.

Badarinath, K.V.S., Latha, K.M., Chand, T.R.K., Gupta, P.K., 2009. Impact of biomass burning on aerosol properties over tropical wet evergreen forests of Arunachal Pradesh, India. Atmos. Res. 91, 87–93.

Bowen H.J.M., 1966. Trace elements ib biochemistry, Academic press, New-York.

Brown, St., Bai, S., 2014. Sonoma Technology, Inc. Petaluma, CA 94954EPA. Positive Matrix Factorization (PMF) 5.0. Fundamentals and User Guide. U.S. Environmental Protection Agency. Office of Research and Development. Washington, DC 20460.

Calvo, A. I., C. Alves, A. Castro, V. Pont, A. M. Vicente, and R. Fraile. 2013. Research on aerosol sources and chemical composition: Past, current and emerging issues. Atmos. Research. 120-121, 1-28.

Chaloulakou, A., Kassomenos, P., Grivas, G., Spyrellis, N., 2005. Particulate matter and black smoke concentration levels in central Athens, Greece. Environment International. 31, 5, 651-659.

Chatoutsidou S.E., Papagiannis, S., Anagnostopoulos, D.F., Eleftheriadis, K., Lazaridis, M., Karydas, A.G., 2022. Application of a handheld X-ray fluorescence analyzer for the quantification of air particulate matter on Teflon filters, Spectrochimica Acta Part B: Atomic Spectroscopy. 196, 106517

chemical composition in five European Mediterranean cities: A 1-year study. Atmospheric Research. 155, 102-117.

Chen, R., Li, Y., Ma, Y., Pan, G., Zeng, G., Xu, X., Chen, B., Kan, H., 2011. Coarse particles and mortality in three Chinese cities: the China Air Pollution and Health Effects Study (CAPES). Sci Total Environ. 409, 4934-8.

Chin, M., Jacob, D.J., 1996. Anthropogenic and natural contributions to tropospheric sulfate: a global model analysis. J. Geophys. Res. 101, 18691–18699.

Corbett, J.J., Fischbeck, P., 1997. Emissions from ships. Science 278, 823.

Costa, S., Ferreira, J., Silveira, C., Costa, C., Lopes, D., Relvas, H., Borrego, C., Roebeling, P., Miranda, AI., Teixeira, JP., 2014. Integrating health on air quality assessment --review report on health risks of two major European outdoor air pollutants: PM and NO$_2$. J. Toxicol. Environ. Health. B. Crit. Rev. 17, 307-340.

Delfino, RJ., Tjoa, T., Gillen, DL., Staimer, N., Polidori, A., Arhami, M., Jamner, L., Sioutas, C., Longhurst, J., 2010. Traffic-related air pollution and blood pressure in elderly subjects with coronary artery disease. Epidemiology. 21, 396-404.

Diapouli, E., 2016. USER GUIDE FOR THE APPLICATION OF THE EPA PMF 5.0 SOFTWARE PACKAGE FOR SOURCE APPORTIONMENT ANALYSIS. N.C.S.R "DEMOKRITOS"

Diapouli, E., Fetfatzis, P., Panteliadis, P., Spitieri, C., Gini, M.I., Papagiannis, S., Vasilatou, V., Eleftheriadis, K., 2022. PM2.5 Source Apportionment and Implications for Particle Hygroscopicity at an Urban Background Site in Athens, Greece. Atmosphere. 13, 1685.

Diapouli, E., Manousakas, M., Vratolis, S., Vasilatou, V., Maggos, Th., Saraga, D., Grigoratos, Th., Argyropoulos, G., Voutsa, D., Samara, C., Eleftheriadis, K., 2017. Evolution of air pollution source contributions over one decade, derived by

Diapouli, E., Manousakas, M., Vratolis, S., Vasilatou, V., Maggos, Th., Saraga, D., Grigoratos, Th., Argyropoulos, G., Voutsa, D., Samara, C., Eleftheriadis, K., 2017. Evolution of air pollution source contributions over one decade, derived by PM10 and PM2.5 source apportionment in two metropolitan urban areas in Greece. Atmos. Environ. 164, 416-430.

Diapouli, E., Manousakas, M., Vratolis, S., Vasilatou, V., Maggos, Th., Saraga, D., Grigoratos, Th., Argyropoulos, G., Voutsa, D., Samara, C., Eleftheriadis, K., 2017. Evolution of air pollution source contributions over one decade, derived by PM10 and PM2.5 source apportionment in two metropolitan urban areas in Greece. Atmos. Environ. 164, 416-430.

Diapouli, E., Popovicheva, O., Kistler, M., Vratolis, S., Persiantseva, N., Timofeev, M., Kasper-Giebl, A., Eleftheriadis, K., 2014. Physicochemical characterization of aged biomass burning aerosol after long-range transport to Greece from large scale wildfires in Russia and surrounding regions, Summer 2010. Atmos. Environ. 96, 393-404.

Directive 2008/50/EC of the European Parliament and of the Council of 21 May 2008 on ambient air quality and cleaner air for Europe. OJ L 152, 11.6.2008, p. 1–44 (BG, ES, CS, DA, DE, ET, EL, EN, FR, IT, LV, LT, HU, MT, NL, PL, PT, RO, SK, SL, FI, SV). Special edition in Croatian: Chapter 15 Volume 029 P. 169 - 212

EC, 2004. Second Position Paper on Particulate Matter. European Commission.

Eleftheriadis, K., Ochsenkuhn, K.M., Lymperopoulou, Th., Karanasiou, A., Razos, P., Ochsenkuhn-Petropoulou, M., 2014. Influence of local and regional sources on the observed spatial and temporal variability of size resolved atmospheric aerosol mass concentrations and water-soluble species in the Athens metropolitan area. Atmos. Environ. 97, 252-261.

European Environment Agency (EEA), Europe's air quality status, 2022b, Web Report. (https://www.eea.europa.eu/publications/status-of-air-quality-in-Europe-2022/europes-air-quality-status-2022)

European Environment Agency (EEA), Health impacts of air pollution in Europe, 2022a, Web Report. (https://www.eea.europa.eu/publications/air-quality-in-europe-2022/health-impacts-of-air-pollution)

Formenti, P., Elbert, W., Maenhaut, W., Haywood, J., Osborne, S., Andreae, M.O., 2003. Inorganic and carbonaceous aerosols during the Southern African Regional Science Initiative (SAFARI 2000) experiment: chemical characteristics, physical properties, and emission data for smoke from African biomass burning. J. Geophys. Res. 108, 8488.

Gao, C., Oman, L., Robock, A., Stenchikov, G.L., 2007. Atmospheric volcanic loading derived from bipolar ice cores: accounting for the spatial distribution of volcanic deposition. J. Geophys. Res. 112, D09109.

Gilbert M. Masters, Wendell P. Ela, 2018. Introduction to environmental engineering and science. Klidarithmos.

Gilmour, P.S., Brown, D.M., Lindsay, T.G., Beswick, P.H., MacNee, W., Donaldson, K., 1996. Adverse Health Effects of PM10 Particles: Involvement of Iron in Generation of Hydroxyl Radical. Occupational and Environmental Medicine. 53, 817-825.

Ito, K., Mathes, R., Ross, Z., Nádas, A., Thurston, G., Matte, T., 2011. Fine particulate matter constituents associated with cardiovascular hospitalizations and mortality in New York City. Environ. Health Perspect. 119, 467-73.

Janssen, N.AH., Gerlofs-Nijland, M.E., Lanki, T., Salonen, R.O., Cassee, F., Hoek, G., Fischer, P., Brunekreef, B., Krzyzanowski M., 2012. Health effects of black carbon. Copenhagen, WHO Regional Office for Europe

Karanasiou, A., Panteliadis, P., Perez, N., Minguillón, M.C., Pandolfi, M., Titos, G., Viana, M., Moreno, T., Querol, X., Alastuey, A., 2020. Evaluation of the Semi-Continuous OCEC analyzer performance with the EUSAAR2 protocol. Science of The Total Environment. 747, 141266.

Kim, SY., Peel, JL., Hannigan, MP., Dutton, SJ., Sheppard, L., Clark, ML., Vedal, S., 2012. The temporal lag structure of short-term associations of fine particulate matter chemical constituents and cardiovascular and respiratory hospitalizations. Environ. Health Perspect. 120, 1094-9.

Kittelson, D.B., 1998. Engines and nanoparticles: a review. J. Aerosol Sci. 29, 575–588.

Koçak, M., Mihalopoulos, N., Kubilay, N., 2007. Chemical composition of the fine and coarse fraction of aerosols in the northeastern Mediterranean, Atmos. Environ. 41, 34, 7351-7368.

Koulouri, E., Saarikoski, S., Theodosi, C., Markaki, Z., Gerasopoulos, E., Kouvarakis, G., Mäkelä, T., Hillamo, R., Mihalopoulos, N., 2008. Chemical composition and sources of fine and coarse aerosol particles in the Eastern Mediterranean. Atmos. Environ. 42, 26, 6542-6550.

Lee, E., Chan, Ch.K., Paatero, P., 1999. Application of positive matrix factorization in source apportionment of particulate pollutants in Hong Kong. Atmos. Environ. 33, 19, 3201-3212.

Liu, G., Niu, Z., Van Niekerk, D., Xue, J., Zheng, L., 2008. Polycyclic aromatic hydrocarbons (PAHs) from coal combustion: emissions, analysis, and toxicology. Rev. Environ. Contam. Toxicol. 192, 1–28.

Lorenzo, R., Kaegi, R., Gehrig, R., Grobéty, B., 2006. Particle emissions of a railway line determined by detailed single particle analysis. Atmos. Environ. 40, 7831–7841

Mahowald, N.M., Kloster, S., Engelstaedter, S., Moore, J.K., Mukhopadhyay, S., Mcconnell, J.R., Albani, S., Doney, S.C., Bhattacharya, A., Curran, M.a.J., Flanner, M.G., Hoffman, F.M., Lawrence, D.M., Lindsay, K., Mayewski, P.A., Neff, J., Rothenberg, D., Thomas, E., Thornton, P.E., Zender, C.S., 2010. Observed 20th century desert dust variability: impact on climate and biogeochemistry. Atmos. Chem. Phys. 10, 10875–10893

Malig, B.J., Ostro, B.D., 2009. Coarse particles and mortality: evidence from a multi-city study in California. Occup Environ Med. 66, 832-9.

Mallone, S., Stafoggia, M., Faustini, A., Gobbi, GP., Marconi, A., Forastiere, F., 2011. Saharan dust and associations between particulate matter and daily mortality in Rome, Italy. Environ. Health Perspect. 119, 1409-14.

Manousakas, M., Diapouli, E., Belis, C.A., Vasilatou, V., Gini, M., Lucarelli, F., Querol, X., Eleftheriadis, K., 2021. Quantitative assessment of the variability in chemical profiles from source apportionment analysis of PM10 and PM2.5 at different sites within a large metropolitan area. Environmental Research. 192, 110257.

Manousakas, M., Papaefthymiou, H., Diapouli, E., Migliori, A., Karydas, A.G., Bogdanovic-Radovic, I., Eleftheriadis, K., 2017. Assessment of PM2.5 sources and their corresponding level of uncertainty in a coastal urban area using EPA PMF 5.0 enhanced diagnostics. Science of The Total Environment. 574, 155-164.

Mason, B., 1996. Principles of Geochemistry, 3rd ed., Wiley, New York.

Meister, K., Johansson, C., Forsberg, B., 2012. Estimated short-term effects of coarse particles on daily mortality in Stockholm, Sweden. Environ. Health Perspect. 120, 431-6.

Mohr, C., Huffman, J.A., Cubison, M.J., Aiken, A.C., Docherty, K.S., Kimmel, J.R., Ulbrich, I.M., Hannigan, M., Jimenez, J.L., 2009. Characterization of primary organic aerosol emissions from meat cooking, trash burning, and motor vehicles with high-resolution aerosol mass spectrometry and comparison with ambient and chamber observations. Environ. Sci. Technol. 43, 2443–2449.

Na K, Sawant AA, Song C, Cocker DR (2004) Primary and secondary carbonaceous species in the atmosphere of Western Riverside County, California. Atmos. Environ. 38:1345–1355.

NIWA Taihoro Nukurangi. Educational Resources. Science topics. Layers of the atmosphere. (https://niwa.co.nz/education-and-training/schools/students/layers)

O'Dowd, C.D., Langmann, B., Varghese, S., Scannell, C., Ceburnis, D., Facchini, M.C., 2008. A combined organic–inorganic sea-spray source function. Geophys. Res. Lett. 35, L01801.

Organic Carbon/ Elemental Carbon (OCEC). Laboratory Instrument Manual. Sunset Laboratory Inc. Model 5. Revision 8.03.

Ostro, B., Lipsett, M., Reynolds, P., Goldberg, D., Hertz, A., Garcia, C., Henderson, KD., Bernstein, L., 2010. Long-term exposure to constituents of fine particulate air pollution and mortality: results from the California Teachers Study. Environ. Health Perspect. 118, 363-9.

Papagiannis, S., 2022. Calibra. Research Infrastructure for Ion Accelerators. MIS 5002799. Technical manual for the use of analytical experimental setups for elemental analysis of air using ionic techniques and X-ray fluorescence for external users. P1.7.1.

Paraskevopoulou, D., Liakakou, E., Gerasopoulos, E., Theodosi, C., and Mihalopoulos, N., 2014. Long-term characterization of organic and elemental carbon in the PM2.5 fraction: the case of Athens, Greece. Atmos. Chem. Phys. 14, 13313–13325

Pérez, N., Pey, J., Querol, X., Alastuey, A., López, J.M., Viana, M., 2008. Partitioning of major and trace components in PM10–PM2.5–PM1 at an urban site in Southern Europe. Atmos. Environ. 42, 8, 1677-1691.

Pernigotti, D., Belis, C.A., Spanò, L., 2016. SPECIEUROPE: The European data base for PM source profiles. Atmospheric Pollution Research. 7, 2, 307-314.

Pio CA, Cerqueira M, Harrison RM, Nunes T, Mirante F, Alves C et al (2011) OC/EC ratio observations in Europe: Re-thinking the approach for apportionment between primary and secondary organic carbon. Atmos. Environ. 45:6121–6132.

Pirrone, N., Cinnirella, S., Feng, X., Finkelman, R.B., Friedli, H.R., Leaner, J., Mason, R., Mukherjee, A.B., Stracher, G.B., Streets, D.G., Telmer, K., 2010. Global mercury emissions to the atmosphere from anthropogenic and natural sources. Atmos. Chem. Phys. 10, 5951–5964.

Polissar, A.V., Hopke, Ph.K., Malm, W.C., Sisler, J.F., 1998. Atmospheric aerosol over Alaska: 1. Spatial and seasonal variability. Papers on Atmospheric Chemistry. JOURNAL OF GEOPHYSICA; RESEARCH. Atmospheres.

Pöschl, U., 2005. Atmospheric Aerosols: Composition, Transformation, Climate and Health Effects. 44, 46, 1433-7851. Angewandte Chemie International Edition.

Prospero, J.M., Nees, R.T., Uematsu, M. (1987). Deposition rate of particulate and dissolved aluminium derived from Saharan dust in precipitation at Miami, Florida. Journal of Geophysical Research, 92, 14723-14731.

Querol, X., Alastuey, A., Puicercus, J., Mantilla, E., Ruiz, C.R., Lopez-Soler, A., Plana, F., Juan, R., 1998. Seasonal evolution of suspended particles around a large coal-fired power station: Chemical characterization. Atmos. Environ. 32, 4, 719-731.

Rai, P., Furger, M., Haddad, I.E., Kumar, V., Wang, L., Singh, A., Dixit, K., Bhattu, D., Petit, J.E., Ganguly, D., Rastogi, N., Baltensperger, U., Tripathi, S.N., Slowik, J.G., Prévôt, A.S.H., 2020. Real-time measurement and source apportionment of elements in Delhi's atmosphere. Science of The Total Environment. 742, 140332.

Reid, J.S., Koppmann, R., Eck, T.F., Eleuterio, D.P., 2005b. A review of biomass burning emissions part II: intensive physical properties of biomass burning particles. Atmos. Chem. Phys. 5, 799–825.

Salameh, D., Detournay, A., Pey, J., Pérez, N., Liguori, Fr., Saraga, D., Bove, M.Ch., Brotto, P., Cassola, F., Massabò, D., Latella, A., Pillon, S., Formenton, G., Patti, S., Armengaud, A., Piga, D., Jaffrezo, J.L., Bartzis, J., Tolis, E., Prati, P., Querol, X., Wortham, H., Marchand, N., 2015.

Salameh, D., Detournay, A., Pey, J., Pérez, N., Liguori, Fr., Saraga, D., Bove, M.Ch., Brotto, P., Cassola, F., Massabò, D., Latella, A., Pillon, S., Formenton, G., Patti, S., Armengaud, A., Piga, D., Jaffrezo, J.L., Bartzis, J., Tolis, E., Prati, P., Querol, X., Wortham, H., Marchand, N., 2015. PM2.5 chemical composition in five European Mediterranean cities: A 1-year study. Atmos. Research. 155, 102-117.

Samara, C., Voutsa, D., Kouras, A., Eleftheriadis, K., Maggos, T., Saraga, D., Petrakakis, M., 2014. Organic and elemental carbon associated to PM10 and PM2.5 at urban sites of northern Greece. Environ. Sci. Pollut. Res. Int. 21(3):1769-1785.

See, S.W., Balasubramanian, R., 2008. Chemical characteristics of fine particles emitted from different gas cooking methods. Atmos. Environ. 42, 8852–8862

Seinfeld, J.H., Pandis, SP.N., 2006. Atmospheric Chemistry and Physics: From Air Pollution to Climate Change. 2nd Edition. WILEY-INTERSCIENCE.

Son, JY., Lee, JT., Kim, KH., Jung, K., Bell, ML., 2012. Characterization of fine particulate matter and associations between particulate chemical constituents and mortality in Seoul, Korea. Environ. Health Perspect. 120, 872-8.

Starik, A., 2008. Gaseous and particulate emissions with jet engine exhaust and atmospheric pollution. Advances on Propulsion Technology for High-Speed Aircraft (pp. 15-1–15-22). Educational Notes RTO-EN-AVT- 150, Paper 15. Neuilly-sur-Seine. RTO, France.

Sunset Laboratory Inc. SEMI-CONTINUOUS OCEC. CARBON AEROSOL ANALYZER. A GUIDE TO RUNNING AND MAINTAINING THE SUNSET LABORAORY SEMI-CONTINUOUS OCEC ANALYSER. 10180 SW Nimbus Ave. Suite J-5. Portland, OR 97223.

Taghvaee, S., Sowlat, M.H., Diapouli, E., Manousakas, M.I., Vasilatou, V., Eleftheriadis, K., Sioutas, C., 2019. Source apportionment of the oxidative potential of fine ambient particulate matter (PM2.5) in Athens, Greece. Science of The Total Environment. 653, 1407-1416.

Tobías, A., Pérez, L., Díaz, J., Linares, C., Pey, J., Alastruey, A., Querol, X., 2011. Short-term effects of particulate matter on total mortality during Saharan dust outbreaks: a case-crossover analysis in Madrid (Spain). Sci. Total Environ. 15, 412-413, 386-9.

Tohka, A., Karvosenoja, N., 2006. Fine Particle Emissions and Emission Reduction Potential in Finnish Industrial Processes. Reports of Finnish Environment Institute.

Tolis, E.I., Saraga, D.E, Lytra, M.K., Papathanasiou, A.Ch., Bougaidis, P.N., Prekas-Patronakis, O.E., Ioannidis, I.I., Bartzis, J.G., 2015. Concentration and chemical composition of PM2.5 for a one-year period at Thessaloniki, Greece: A comparison between city and port area. Atmos. Environ. 113, 197-207.

Toshihiko, T., Toru, N., Seita, E., Takashi, Y.N., Teruyuki, N., 2005. Simulation of climate response to aerosol direct and indirect effects with aerosol transport-radiation model. Journal of Geophysical Research: Atmospheres. J. Geophys. Res.110, D2, 0148-0227.

United States Environmental Protection Agency. Particulate Matter Pollution. Health and Environmental Effects of Particulate Matter (PM). (https://www.epa.gov/pm-pollution/health-and-environmental-effects-particulate-matter-pm)

Vasilatou, V., Diapouli, E., Abatzoglou, D., Bakeas, E.B., Scoullos, M., Eleftheriadis, K., 2017. Characterization of PM2.5 chemical composition at the Demokritos suburban station, in Athens Greece. The influence of Saharan dust. Environ. Sci. Pollut. Res 24, 11836–11846.

White, W.H., 2008. Chemical markers for sea salt in IMPROVE aerosol data. Atmos. Environ. 42, 261–274.

Woodcock, A.H., 1972. Smaller salt particles in oceanic air and bubble behavior in the sea. J. Geophys. Res. 77, 5316–5321.

World Meteorological Organization. Environment. Atmospheric composition.2022. (https://public.wmo.int/en/our-mandate/focus-areas/environment/atmospheric-deposition)

Xu, M., Yu, D., Yao, H., Liu, X., Qiao, Y., 2011. Coal combustion-generated aerosols: formation and properties. P. Combust. Inst. 33, 1681–1697

Yuan, T., Remer, L.A., Pickering, K.E., Yu, H., 2011. Observational evidence of aerosol enhancement of lightning activity and convective invigoration. Geophys. Res. Lett. 38, L04701.

Zanobetti, A., Franklin, M., Koutrakis, P., Schwartz, J., 2009. Fine particulate air pollution and its components in association with cause-specific emergency admissions. Environ. Health. 21, 8-58.

Zhang Y, Obrist D, Zielinska B, Gertler A (2013) Particulate emissions from different types of biomass burning. Atmos. Environ. 72:27–35.